Numerical study of non-linear spectroscopy and Four-Wave-Mixing in two and multi-level atoms

by

Meena Patel

Thesis submitted in fulfilment of the requirements for the degree

Master of Engineering: Electrical Engineering

in the Faculty of Engineering

at the Cape Peninsula University of Technology

Supervisor: **Dr. Kessie Govender**
Co-Supervisor: **Prof. Gerhard De Jager** (University of Cape Town)

Bellville
August 2017

Declaration

I, Meena Patel, declare that the content of this thesis represents my own unaided work, and that the thesis has not previously been submitted for academic examination towards any qualification. Furthermore, it represents my own opinions and not necessarily those of the Cape Peninsula University of Technology.

Signed	Date

Abstract

In this research, we undertake a numerical study of the interaction between laser beams and two as well as multi-level atoms. The main aim of this research is to obtain a deeper understanding of laser-atom interactions and non-linear processes such as optical four-wave mixing. This work will supplement experiments to be conducted by other members of the group, who are involved in generating entangled photons via four-wave mixing in cold rubidium atoms.

We begin by performing a basic study of the interaction between laser beams and two-level atoms as an aid to gain knowledge of numerical techniques, as well as an understanding of the physics behind light-atom interactions. We make use of a semi-classical approach to describe the system where the atoms are treated quantum mechanically and the laser beams are treated classically. We study the interaction between atoms and laser beams using the density matrix operator and Maxwell's equations respectively. By solving the optical Bloch equations for two-level atoms we examine the atomic populations and coherences and present plots of the density matrix elements as a function of time. The effects of various parameters such as laser intensity, detuning and laser modulation have been tested. The behaviour of the laser beam as it propagates through the atomic sample is also studied. This is determined by Maxwell's equation where the atomic polarization is estimated from the coherence terms of the density matrix elements.

The research is then extended to include a study of the interaction between multiple laser beams and multi-level atoms - in our case four-wave mixing. Our approach makes use of four levels of an atom in a diamond configuration interacting with co-propagating pump lasers having different wavelengths. The pump lasers stimulate the atoms from the ground state $|\psi_1\rangle$ to an excited state $|\psi_3\rangle$ via an intermediate state $|\psi_2\rangle$. The atoms then return back to the ground state via another intermediate state $|\psi_4\rangle$. This results in the generation of two additional correlated and coherent photon beams. We study the characteristics of these photon beams for various pump beam detunings. We present plots of the intensities of the generated photons as well as of the populations at each level as a function of the pump beam detuning. Our analysis shows that the intensities of the coherent beams are strongly dependent on the detuning of the laser beams. The populations show similar dependence, however there are particular values of detuning that maximises the coherent beam intensities without populating the levels significantly.

Acknowledgements

I would like to thank all the people who have contributed in some way to the work described in this thesis.

Firstly, I would like to thank my supervisor Dr. Kessie Govender from the Department of Electrical Engineering at the Cape Peninsula University of Technology for his guidance during my study. Dr. Govender has spent countless hours teaching me all the necessary background physics I needed such as quantum mechanics, electromagnetic theory, optics and atomic physics to name a few. He has allowed this thesis to be my own work, but steered me in the right direction whenever he thought I needed it, supported my attendance at various conferences and has always demanded a high quality of work. His patience, never-ending enthusiasm and constant motivation are greatly appreciated.

I would like to acknowledge my co-supervisor Prof. Gerhard de Jager from the Department of Electrical Engineering at the University of Cape Town for his support and motivation during my study. He has taken the time to read my thesis and has always given valuable and insightful comments where he deemed necessary.

I would like to thank my fellow lab/classmates for their academic support. They provided a friendly and cooperative atmosphere at work. They

have also provided useful feedback and comments on my work.

Thank you to the French South African Institute of Technology (F'SATI) and the National Research Foundation for the scholarship. The financial assistance of the National Research Foundation towards this research is acknowledged. Opinions expressed in this thesis and the conclusions arrived at, are those of the author, and are not necessarily to be attributed to the National Research Foundation.

I wish to express my sincere gratitude to my family for their unending encouragement, love, prayers, care and support during my study. Thank you to my friends for your thoughts, well-wishes and constant motivation.

My final word of thanks goes to everyone who has supported me directly or indirectly to complete my research.

Research Outputs

1. Patel, M., De Jager, G., Nkosi, Z. and Govender, K. 2016. Nonlinear optical processes and saturated absorption spectroscopy in two and multi-level atoms: a theoretical and numerical study. In: *The* 61^{st} *Annual Conference of the South African Institute of Physics*
   (presented as a poster presentation)

2. Patel, M., De Jager, G., Nkosi, Z., Wyngaard, A. and Govender, K. 2017. On the non-linear spectroscopy including saturated absorption and four-wave mixing in two and multi-level atoms: a computational study. In: *The* 28^{th} *IUPAP Conference on Computational Physics* Journal of Physics: Conference Series
   (presented as an oral presentation)

3. Patel, M., De Jager, G., Mpiana, F. and Govender, K. 2017. A semi-classical and quantum mechanical analysis of four-wave mixing in an ensemble of rubidium atoms. In: *The* 62^{nd} *Annual Conference of the South African Institute of Physics*
   (presented as a poster presentation)

Contents

List of Figures

Chapter 1

Introduction

1.1 Background information

In this thesis we report on the numerical study of non-linear optical processes occurring when one or more laser beams interacts with a gaseous atomic ensemble. Specifically, we examine the interaction of two-level atoms with a laser beam, saturated absorption spectroscopy and four-wave mixing which involves four levels of an atom, four-wave mixing being the ultimate goal. Four-wave mixing is a process where two pump beams interact with four atomic levels generating two correlated/entangled photons in the process.

The motivation for this study is that light-atom interaction (Jakowski and Morokuma, 2009; Glushkov, 2014; Glushkov, Khetselius, Svinarenko,

and Prepelitsa, 2011) is currently an active area of research in the field of quantum computing and communication. This study will also supplement and support experimental work currently being conducted by other members of the Quantum Physics Research Group[1]. There is growing evidence that the next generation of computing and the internet will be quantum based, that is, they will operate using phenomena of quantum physics (Coffey, 2013), such as superposition and entanglement. The technology required for making a commercially viable quantum computer is still in its infancy. There are a variety of platforms (DiVincenzo, 2000) that are being investigated such as spin systems in solids, trapped ions in semiconductors and ultra-cold atoms in optical lattices to name a few (Bloch, 2005).

To understand how quantum computing differs from classical computing we consider the following analogy of navigating through a maze. Classical computers attempt to solve such problems by proceeding on a particular path and choosing one direction at a fork. Should the chosen direction be a dead end, it would return to the fork and try a different direction until the maze is exited. If the maze is large, a classical computer can take eons to examine every route; quantum computers would be able to solve the problem within a reasonable amount of time. This is because classical computers operate using *bits*, either a 1 or a 0, in order to perform tasks. On the other hand, quantum computers operate using *qubits*. Due to the nature of quantum mechanics the qubits can be 1 , 0 or both 1 and 0 simultaneously, in other words a superposition of two states. In superposition one qubit can store/perform two calculations at once; two qubits can store/perform four calculations at once and so on. Referring back to the maze analogy, qubits disperse in all directions at once and, due to the exponential rate at which they multiply, they simultaneously explore every possible route to quickly and efficiently

[1]**Quantum Physics Research Group - CPUT:** `http://www.cput.ac.za/academic/faculties/engineering/research/quantum_physics`

find a solution. The problem with qubits is that any interference, a measurement for example, will cause the quantum state to be destroyed resulting in the loss of information.

Quantum computing and quantum information processing is a technology that utilizes single atoms and photons to accomplish tasks that are difficult to do using conventional technology. Some of these tasks include the secure encryption of data (Gisin, Ribordy, Tittel, and Zbinden, 2002), solving certain mathematical problems and rapid data base searching to name a few. Superposition and entanglement are key phenomena that are exploited in quantum information systems. Quantum systems will also require a means of communication and this cannot be via classical laser pulses.

There are various schemes or platforms, as mentioned above, that are currently being investigated to perform quantum processing of information, but at the Cape Peninsula University of Technology (CPUT) a group of engineers, physicists and mathematicians (Quantum Physics Research Group (QPRG)) are studying cold atoms as a route to quantum computing and information processing (Quantum Physics Research Group). Cold atoms are created by using a system of laser beams interacting with atoms under an ultra low vacuum in a device called a magneto-optical trap (MOT). In order to achieve this goal of creating cold atoms, an apparatus that will cool and trap a group of atoms must be built and tested after which the properties of these cold atoms will be studied.

Once a cloud of cold atoms have been achieved there are a number of research directions that could be pursued, such as statistics of cold atoms, single atom manipulation, light-atom interaction, studies involving Bose-Einstein condensate, etc. The group is examining the light-atom interaction for the purposes of developing components that will facilitate communication

between quantum devices. In particular the group will examine non-linear processes such as four wave mixing in an ensemble of cold atoms (and electromagnetically induced transparency) for the purposes of generating entangled photon pairs and a heralded single photon source for quantum communication.

As alluded to earlier, the main aim of the present project is the study of four-wave mixing with the view to determining the characteristics of the coherent and correlated photons that are generated. In this regard, the next section provides a partial review of published literature on four-wave mixing, including experimental and computational works. This is followed by a statement of the current research problem, aims and objectives and then a thesis outline is given.

1.2 Literature Review

Entangled photons are the most desirable form of communication between quantum systems. Spontaneous parametric down conversion (SPDC) in non-linear crystals is the most conventional method used to generate these entangled photons. Maximum efficiency is achieved when the photon bandwidth matches the absorption profile of the atoms when entanglement is transferred from photons to stationary qubits. The bandwidth of the photons produced by SPDC have magnitudes of Tera-Hertz, which is much higher than the absorption profile of the receiving atoms. These photons also have a short coherence time, normally a few picoseconds, as well as a short coherence length, around 100 μm.

Four wave mixing in atomic rubidium (Rb) ensembles is another method used to generate entangled photons (Brekke, Day, and Walker, 2008; Du, Wen, and Rubin, 2008; Becerra, Willis, Rolston, and Orozco, 2011; Jen and

Chen, 2016; Srivathsan, Gulati, Chng, Maslennikov, Matsukevich, and Kurtsiefer, 2013; de Melo and Vianna, 2014; Gulati, Srivathsan, Chng, Cerè, Matsukevich, and Kurtsiefer, 2014; Gulati, Srivathsan, Chng, Cerè, and Kurtsiefer, 2015). One possible scheme shown in Figure 1.1 is used by Srivathsan et al. (2013), it makes use of four different levels of the atoms as well as two pump beams that excite the atoms from the lower level, $5S_{1/2}$, to an upper level, $5D_{3/2}$, via an intermediate level, $5P_{3/2}$. The atoms will then emit two photons when returning to the lower level, $5S_{1/2}$, via another intermediate level, $5P_{1/2}$. Du et al. (2008) reported that these biphoton sources have properties such as long coherence time, long coherence length, high spectral brightness and high conversion efficiency. The atom is left in the same state it was in before the interaction in the diamond configuration, this is due to the fact that the four photon process conserves energy and momentum. It is possible for the atom to return to the lower level from the upper level via multiple intermediate levels, the final state of any intermediate level however, remains the same.

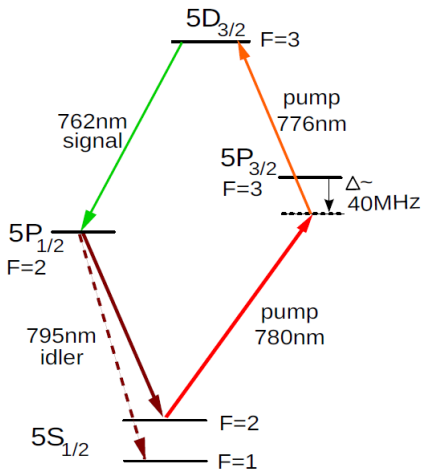

Figure 1.1: ^{87}*Rb cascade level configuration of four-wave mixing (Srivathsan et al., 2013).*

Four wave mixing via intermediate Rydberg[2] states in an ultracold ^{87}Rb atomic ensemble was conducted by Brekke et al. (2008) in order to generate coherent light beams. Up to 25% of the emitted light was emitted in a diffraction limited solid angle for experiments conducted using low atomic densities with a non-collinear arrangement for the pump beams.

A warm ^{87}Rb vapour cell having a length of 1.5 cm was used by Becerra et al. (2011) to measure the time correlation between photons generated by four wave mixing. Having chosen the appropriate levels of the rubidium atom in a diamond configuration, photons in the telecommunication wavelength ($\sim$ 1367 nm) were produced. These values are quite useful because they fall within the telecommunication wavelengths for optical fibres. Quantum beats were observed in the time correlation of two photons when the probabilities of the two decay paths interfere.

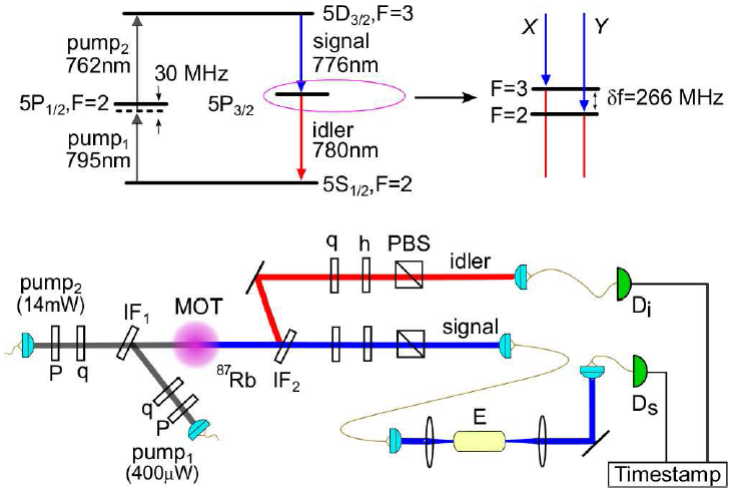

Figure 1.2: *^{87}Rb four-wave mixing level configuration and experimental schematic of Gulati et al. (2015).*

[2]Atomic Rydberg states occur when atoms are electronically excited to very high energy states.

Entangled photons have been generated by Srivathsan et al. (2013), Gulati et al. (2014) and Gulati et al. (2015) by using cold ^{87}Rb atoms. The hyperfine levels of the ground state and the first excited state were used in a diamond configuration by Srivathsan et al. (2013) and Gulati et al. (2014) as shown in Figure 1.1 and the configuration used by Gulati et al. (2015) is shown in Figure 1.2. A magneto-optical trap (MOT) was used to cool the atoms down to an optical density[3] of approximately 32 while the pump beams were collinear having an angular separation of 0.5°. Gulati et al. (2015) have produced polarization entangled photon pairs by making use of the set-up shown in Figure 1.2. Their experiment has also resulted in the observation of quantum beats due to the emitted photons having two decay paths (X and Y in Figure 1.2). Gulati et al. (2014) have made use of homodyne detection to produce heralded single photons. The temporal envelope of the photons have also been measured; an exponentially increasing or decreasing temporal profile has been found depending on the heralding scheme being used.

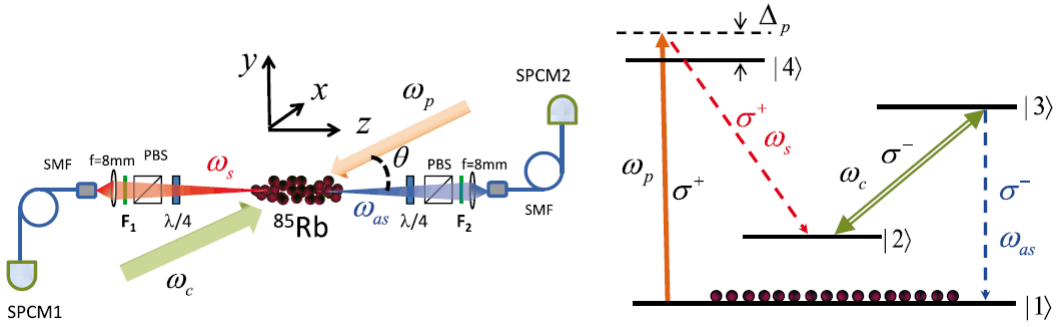

Figure 1.3: *A backward spontaneous four-wave mixing experimental set-up with a 2D MOT and energy level scheme of ^{85}Rb used by Han et al. (2015).*

A double lambda scheme has been used by Han et al. (2015) to generate

[3]Optical density refers to the degree to which a refractive medium slows down transmitted rays of light.

photon pairs in a cold ^{85}Rb atomic cloud having a coherence time of 2.34 μs. A 2D MOT was used to prepare the atoms and the pump beams were arranged to oppose each other, i.e. a backwards geometry, Figure 1.3. This results in the generated photon pairs to be in opposing directions as well. An electromagnetically induced transparency configuration was achieved when various levels of the atom are strategically chosen and used together with a pump beam. In this way the time correlation of the photon pairs is improved. A coherence time of 10 μs can be realised when making use of this configuration. Du et al. (2008) have reported a coherence time of 0.9 μs for frequency entangled photons, Zhao, Guo, Liu, Sun, Loy, and Du (2014) have generated photon pairs with a coherence time exceeding 1 μs and Liao, Yan, He, Du, Zhang, and Zhu (2014) have measured a coherence time of 300 ns.

By shaping the temporal characteristics of interacting photons between two atomic systems, it is possible to improve absorption, emission and storage of the information stored in a photon. Shaping of the temporal quantum waveform of narrow-band biphotons has been demonstrated by Chen, Zhang, Yan, Loy, Wong, and Du (2010) and generated in a cold atomic ensemble via four-wave mixing. Kolchin, Belthangady, Du, Yin, and Harris (2008) have shaped the anti-Stokes photons by making use of an electro-optic modulator and four-wave mixing coupled with an electrically induced transparency (EIT). Stokes photons trigger the modulator which appear sooner than the anti-Stokes photons, they have a delay due to the EIT effect. Four-wave mixing in rubidium using a vapour cell has been done by Dabrowski, Parniak, Pecak, Chrapkiewicz, and Wasilewski (2014) and Kölle (2014) where thermal motion plays a significant role on the coherence.

Parniak and Wasilewski (2015) have made use of a diamond configuration to develop a model that calculates the non-linear polarization in non-degenerate four-wave mixing. The model includes the effects of the hyperfine

structure as well as Doppler broadening. The modelled results were verified against experimental results where the intensity of warm ^{85}Rb vapour was measured as a function of laser frequency. Excellent conformity of theory and experiment has been reported.

1.3 Problem Statement

While there has been a fair amount of work that has been done in studying four-wave mixing, there are still open questions such as: What is the best arrangement of the pump beam? How does laser detuning affect the yield of coherent beams? How does laser detuning affect the populations and hence spontaneous emission?

Aim

The aim of this research was to undertake a numerical study in order to simulate four-wave mixing (FWM) in an ensemble of gaseous atoms and to study the characteristics of the coherent photons that are generated by the FWM process.

Objective/Work-plan

In order to achieve the above aim the following objectives/work-plan was followed:

1. Numerical study of the interaction of a two-level atom with a laser beam to develop the necessary computational skills.
2. Numerical study of saturated absorption spectroscopy to develop a further understanding of the physics involved in laser-atom interactions.
3. Finally, a numerical study of four-wave mixing in an atomic gas using a semi-classical approach for multi-level atoms.

Embedded in the above is the acquisition of the physics necessary to understand light-atom interactions. This study has been limited to a simple scheme which involves four levels of the atom having a diamond configuration. The effects of laser and atomic polarization have not been considered for the time being. These effects can be easily incorporated in a future extension of the present work. The research has been kept simple so that an emphasis is put on the understanding of basic concepts and processes.

1.4 Thesis Outline

The remainder of the thesis is as follows:

- **Chapter 2** : ***Background theory*** - This chapter includes basic concepts in quantum physics and electromagnetism.
- **Chapter 3** : ***Two-level atom interacting with a uniform laser beam*** - A numerical analysis of a two-level atom interacting with a uniform laser beam. A semi-classical approach is used where the laser is treated classically and the atom quantum mechanically. We solve the optical Bloch equations numerically and determine the populations and coherences of the atoms.
- **Chapter 4** : ***Two-level atom interacting with a modulated laser beam*** - In this chapter we conduct a study that is similar to the study in Chapter 3. We make use of the same semi-classical approach except that here we modulate the frequency and vary the level of modulation of the laser beam.
- **Chapter 5** : ***Saturated Absorption Spectroscopy*** - A numerical analysis of saturated absorption spectroscopy in two-level atoms is presented. Here we solve Maxwell's equations numerically to determine

the effects of the atoms on the laser beams. The optical Bloch equations were solved analytically to obtain the atomic polarization which we use in Maxwell's equations. The steady state solution of the Bloch equations can be found in Appendix B.

- **Chapter 6** : ***Four-wave mixing*** - A theoretical and computational analysis of four-wave mixing in multi-level atoms is presented. The atom is treated quantum mechanically and the generated photons are treated classically. The atomic polarization is determined from the third and fourth order density matrix terms which are obtained by making use of perturbation theory. We then make use of Maxwell's equations to find the intensities of the generated photons.

- **Chapter 7** : ***Summary and conclusion*** - This chapter contains the summary and conclusions.

- **Appendices** :

  - **A - *Flowcharts*** - This appendix provides basic flowcharts depicting the computational processes of two-level atoms using the optical Bloch equations and Runge-Kutta method.
  - **B - *Steady state solution of the optical Bloch equations*** - This appendix provides the steady state solution of the optical Bloch equations for a two-level atom and supplements Chapter 5.
  - **C - *Derivation and steady state solution of density matrix elements of four-wave mixing*** - In this appendix we derive the density matrix elements required for four-wave mixing and solve the steady state solution for the same elements. Equations derived in this appendix are used in Chapter 6.

Chapter 2

Background theory

2.1 Introduction

This project requires a sound grasp of certain concepts in quantum physics as well as electromagnetism. Throughout our study we treat the atom quantum mechanically and the laser beams (electromagnetic waves) classically. Since this study is being conducted by us engineers, who have minimal training in quantum systems, it was necessary to learn the basics of these systems.

Some of the basic quantum mechanics concepts are briefly explained in Section 2.2[1] and Section 2.3 covers some basic atomic theory and introduces

[1]Material presented in this chapter is based on the texts by (Liboff, 2002; Arya, 1986)

the possible application of rubidium. Section 2.4 briefly describes the equations required for the electromagnetic field.

2.2 Basic quantum mechanics concepts

At the atomic and subatomic level particles behave like waves or have wave-like properties. These waves are represented by the character $\Psi(\vec{r},t)$, also known as the wave function. Ψ, in general, is a complex function of the position, (x,y,z), and time, t, of the particle. The physical meaning attached to Ψ is that its modulus squared, $|\Psi|^2$, gives the probability of finding the particle at a certain position $\vec{r}$ at any given time t. By this interpretation $\int_{\infty}^{\infty}|\Psi|^2 d^3\vec{r} = 1$. For a particle in a potential $V(x,y,z)$, Ψ is a solution to the time dependent Schrödinger wave equation

$$-\frac{\hbar^2}{2m}\nabla^2\Psi \; + \; V\Psi \; = \; \imath\hbar\frac{\partial\Psi}{\partial t} \tag{2.1}$$

and evolves in time according to

$$\Psi(\vec{r},t) \; = \; \psi^{-\imath Et/\hbar} \tag{2.2}$$

where ψ is the solution to the time independent Schrödinger equation.

The above equation, equation (2.1), can also be written as

$$\hat{H}\Psi \; = \; i\hbar\frac{\partial\Psi}{\partial t}$$

where $\hat{H} \; = \; -\frac{\hbar^2}{2m}\nabla^2 \; + \; V$ is the Hamiltonian of the system and V is the potential energy.

The wave function Ψ contains all the information about the particle or system such as its energy, momentum, position and angular momentum.

These are called observables. Associated with every observable[2] in a physical system is a mathematical operator that is used in conjunction with the wave function. The Hamiltonian above, $\hat{H}$, is an example of an energy operator. Liboff (2002) presents a number of examples of applications of the above theory.

Quantum mechanical calculations can become very complicated; a reduced notation, the Dirac notation[3], is used. The wave function Ψ is then represented by a more general state vector $|\Psi\rangle$ in a Hilbert space[4], which is called the *ket* vector, and the average value of an operator $\hat{A}$ in the state $|\Psi\rangle$ is given by $\langle\Psi|\hat{A}|\Psi\rangle$. This is just an inner product of $\langle\Psi|$ and $\hat{A}|\Psi\rangle$, where $\langle\Psi|$ is called the *bra*.

If $|\Psi_1\rangle, |\Psi_2\rangle, |\Psi_3\rangle, ...$ are energy eigenstates of a certain particle having energy eigenvalues $H|\Psi_i\rangle = E_i|\Psi_i\rangle$, then it is possible for the particle to be in a state denoted by:

$$|\Psi\rangle = a_1|\Psi_1\rangle + a_2|\Psi_2\rangle + a_3|\Psi_3\rangle + ... \tag{2.3}$$

where $|a_i|^2$ indicates the probability that a measurement of the energy would give the value E_i. The state represented by equation (2.3) is called a superposition state.

Another important type of state is an entangled state[5] involving two particles. If $|\Psi_1\rangle$ and $|\Psi_2\rangle$ are the possible state vectors of two particles, A

[2] An observable is a physically measurable parameter.

[3] $\langle\Psi|\hat{A}|\Psi\rangle = \int \Psi^* \hat{A} \Psi d^3\vec{r}$

[4] A Hilbert space is a normed vector space where the norm of a vector is obtained using an inner product. It is a space of square integrable functions, say $f(x)$, on an interval $[a, b]$ such that $\int_a^b |f(x)|^2 dx < \infty$.

[5] Entanglement describes how pairs/groups of particles interact with each other in ways such that the quantum state of each particle is determined by its correlated particle.

and B, then an entangled state is

$$|\Psi\rangle = \alpha\,|\Psi_1^A\rangle\,|\Psi_2^B\rangle + \beta\,|\Psi_2^A\rangle\,|\Psi_1^B\rangle \tag{2.4}$$

where $|\Psi_i^X\rangle$ is the state of particle X in state $|\Psi_i\rangle$. A state is said to be entangled when it cannot be reduced to a product of two states.

A system containing a mixture of atoms in various quantum states is described by a density matrix operator, $\hat{\rho}$. Similar to how Ψ evolves in time according to the Schrödinger equation, $\hat{\rho}$ evolves in time according to the *Liouville-von Neumann* equation[6]

$$i\hbar\frac{\partial\hat{\rho}}{\partial t} \;=\; \left[\hat{H},\hat{\rho}\right] \tag{2.5}$$

and tells us everything we need to know about the system. This equation can also be used to describe the evolution of of the density matrix operator for pure states[7]. The above equation will be crucial in the quantum mechanical analysis of laser-atom interactions. The Hamiltonian then will include an additional term that contains the laser-atom interactions.

Physical problems are usually too complex to be solved exactly, therefore approximate methods are used to solve Schrödinger's equation. We make use of the Hamiltonian in the form $H = H_0 + H'$ where H_0 is the unperturbed Hamiltonian and H' is a perturbation term. We want to solve the following equation

$$(\hat{H}_0 + \lambda\hat{H}')\Psi_n = E_n\Psi_n \tag{2.6}$$

where λ is infinitesimal. We solve the above equation using perturbation techniques as follows: Expanding Ψ_n and E_n as power series of λ, substitut-

[6] $[\hat{H},\hat{\rho}]$ is a commutator. If $\hat{H}\hat{\rho} - \hat{\rho}\hat{H} = 0$, then we say that $\hat{H}$ and $\hat{\rho}$ commute. Operators in QM generally do not commute.

[7] A pure state is described by a well defined point in a Hilbert space.

ing back into Schrödinger's equation and arranging terms according to the power of λ results in a series of simultaneous equations. The zero order is unperturbed. The higher orders contain perturbation and are small compared to the zero order because H' is small compared to H_0. This perturbation technique will be used in Chapter 6 where we examine four-wave mixing.

2.3 Atomic theory

2.3.1 Basic concepts

The solution of Schrödinger's equations for atomic systems tells us that the energy of the electrons in the atom are quantized and it highlights the quantum numbers, n (principal quantum number), l (angular momentum quantum number) and m (magnetic quantum number).

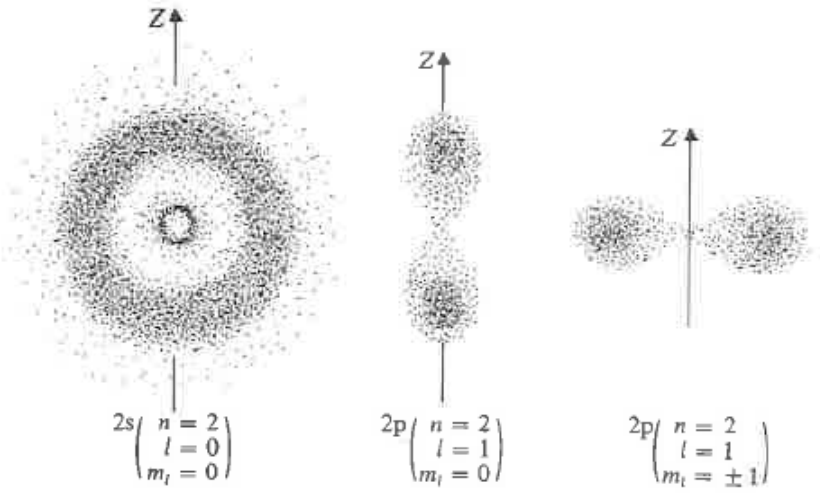

Figure 2.1: *Quantum mechanical model of the atom (Arya, 1986).*

The electron within an atom does not have well defined orbits, all that

can be said about the electron-position is probabilistic in nature. Figure 2.1 illustrates this for the first few orbitals of hydrogen. The density of the dots indicate the probability of finding the electron in a given region. The electron orbits the nucleus at a radius r_n, with energy E_n determined by the quantum number n. The energies are quantized meaning that atoms exist only in certain stationary states[8] which have discrete energies. E_1 refers to the lowest energy level, also called the ground state. $E_2, E_3, ..., E_n$ are called the excited states. Atoms can make transitions between ground and excited states by emitting or absorbing photons. Since atoms are most stable in the ground state, an atom in an excited state will make a transition, via lower energy states, back to the ground state.

Figure 2.2(**A**) represents the energy level diagram when considering an atom having multiple states of ϕ_n with respective energies, E_n. The principal quantum number n has integer values greater than one and determines the energy level. These levels split into sub-levels represented by l, the angular momentum quantum number, and holds integer values from 0 to $(n-1)$. The sub-levels $l = 0, 1, 2, 3, 4, 5...$ are referred to by s, p, d, f, g... respectively. The total angular momentum due to the electron(s) is given by $j = |l - s| \dots l + s$ in steps of 1, where s is the spin angular momentum of the electron and is equal to $\pm 1/2$. The total angular momentum including the nuclear spin is given by $F = |j - I| \dots j + I$ in steps of 1, where I is the nuclear spin. The energy level diagram depicting these sub-levels can be seen in Figure 2.2(**B**) for the hydrogen atom. It is common to represent energy states using spectroscopic notation as follows: nl_j e.g. $5S_{1/2}$, where the sub-level notation has been capitalized.

When an atom is placed in a laser beam an interaction occurs. The

[8] A stationary state is a state which corresponds to an eigenfunction of the Hamiltonian of the system.

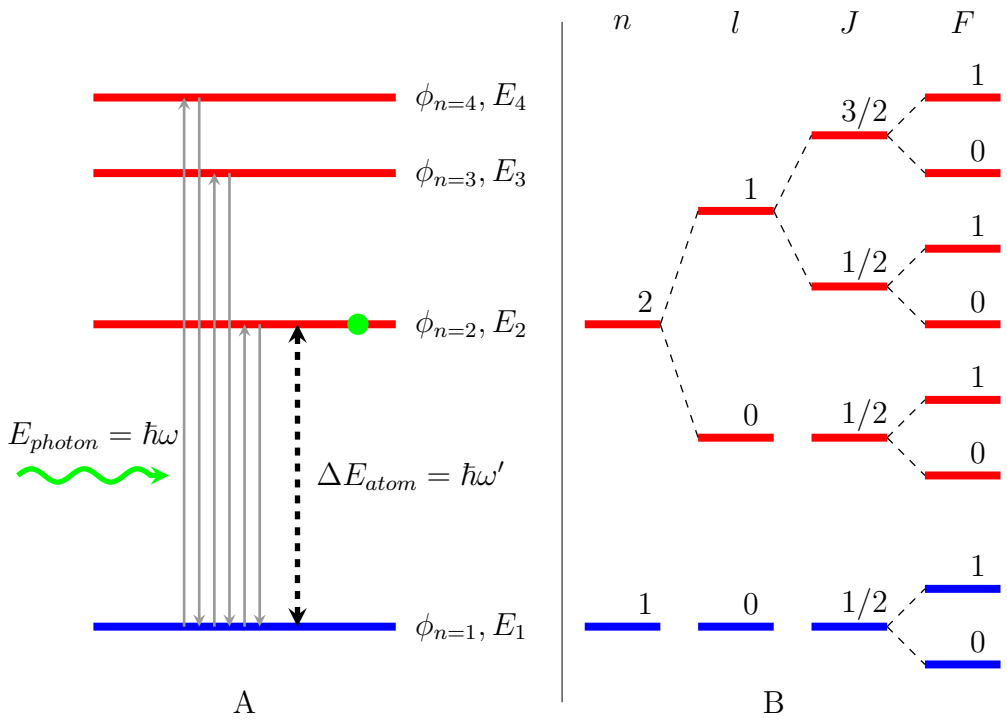

Figure 2.2: ***A*** *- An energy level diagram representing the interaction of a photon from a laser beam with an electron where the blue line, $\phi_{n=1}$, is the ground state and the red lines, $\phi_{n=2,3,4...}$, are excited states.* ***B*** *- Energy level diagram of hydrogen showing the sub-levels for the first two energy levels.*

electric dipole moment, $\vec{\mu}$, of the atom causes it to interact with the electric field of the laser. Since the electric field of the laser is oscillating, it causes the dipole moment to oscillate as well, resulting in an exchange of energy. This interaction is given by $-\vec{\mu}\cdot\vec{E}$. $\Delta E_{atom} = \hbar\omega'$ represents the difference in energy between any two states. $E_{photon} = \hbar\omega$ is the energy of the photon from the laser. If $E_{photon} = \Delta E_{atom}$, the atom will absorb the photon and jump to one of the allowed excited states as it cannot linger between states. Since atoms are most stable in ϕ_1, an atom that has been excited will therefore decay back to ϕ_1 after some time and a photon will be emitted.

2.3.2 Energy level structure of rubidium

Numerical and theoretical work discussed later in the thesis is based partially on rubidium atoms. We therefore provide some basic characteristics of rubidium. The energy levels used can be seen in Figure 2.3 for two isotopes, ^{85}Rb and ^{87}Rb. Rubidium gas is commonly used for laser cooling and Bose–Einstein condensation. Its desirable feature here is that it can be easily excited using readily available diode lasers.

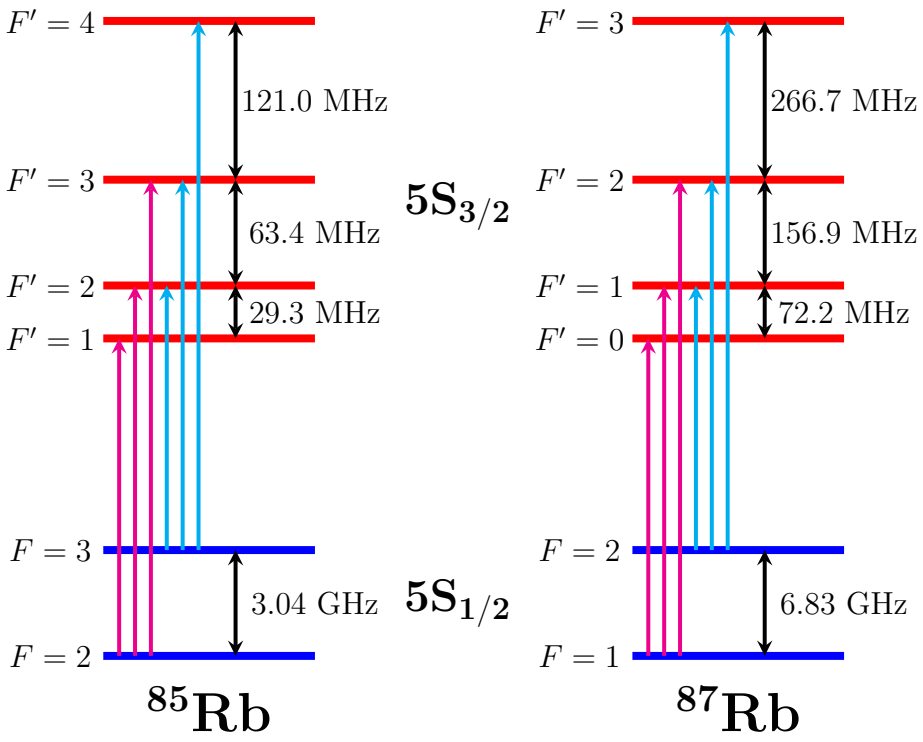

Figure 2.3: *An energy level diagram illustrating the allowed transitions between the $5S_{1/2}$ and $5S_{3/2}$ states of rubidium 85 and 87. The blue lines are representative of ground states and the red lines are of excited states.*

2.4 Basic electromagnetic theory

Since light is an electromagnetic wave, it must satisfy all of Maxwell's equations. We use these equations in the following form where we assume that $\rho_f = 0$ (free charge density) and $J = 0$ (surface current density):

$$\nabla \cdot \vec{E} = \frac{\rho_f}{\epsilon_0} - \frac{1}{\epsilon_0}\nabla \cdot \vec{P} \tag{2.7}$$

$$\nabla \cdot \vec{H} = 0 \tag{2.8}$$

$$\nabla \times \vec{E} = -\mu_0 \frac{\partial \vec{H}}{\partial t} \tag{2.9}$$

$$\nabla \times \vec{H} = J + \epsilon_0 \frac{\partial \vec{E}}{\partial t} + \frac{\partial \vec{P}}{\partial t} \tag{2.10}$$

where $\vec{H}$ is the magnetic field and $\vec{P}$ is the atomic polarization of the medium induced by the electric field $\vec{E}$. Taking the curl of equation (2.9) and using equation (2.10) results in

$$\nabla \times (\nabla \times \vec{E}) + \mu_0 \epsilon_0 \frac{\partial^2 \vec{E}}{\partial t^2} = -\mu_0 \frac{\partial^2 \vec{P}}{\partial t^2} \tag{2.11}$$

where the additional term in the wave equation for $\vec{E}$ is due to the polarization $\vec{P}$. This term is responsible for various optical effects such as double refraction, absorption, dispersion as well as non-linear effects such as three and four wave mixing. Equation (2.11) will be used later in Chapters 5 and 6 where we examine the propagation of laser beams through a gaseous atomic ensemble.

2.5 Summary

In this chapter we have provided the basic mathematical ideas that will be used in the remainder of the thesis.

Chapter 3

Two-level atom interacting with a uniform laser beam

3.1 Introduction

When an atom interacts with the electric field of a laser beam one of two things can occur; absorption or emission. The simplest model to investigate is that of a two-level atom interacting with a laser beam. The beam, whose frequency is kept close to atomic resonance, is treated classically and the atom, quantum mechanically. Despite the degree of simplicity, the derivation to this problem (given in this chapter) is valid for more complex problems that will be discussed later in the thesis.

This chapter briefly discusses the concepts needed to understand light-atom interactions and is organised as follows: Section 3.2 provides some background theory to the problem and derives the optical Bloch equations. The optical Bloch equations are solved numerically using the Runge-Kutta technique. The results obtained are given in Section 3.3.

3.2 Solving the optical Bloch equations

We consider an atom having two states[1], ϕ_1 and ϕ_2, with energies, E_1 and E_2 respectively. These can be represented by Figure 3.1 where ϕ_1 is blue representing the ground state and ϕ_2 is red representing the excited state.

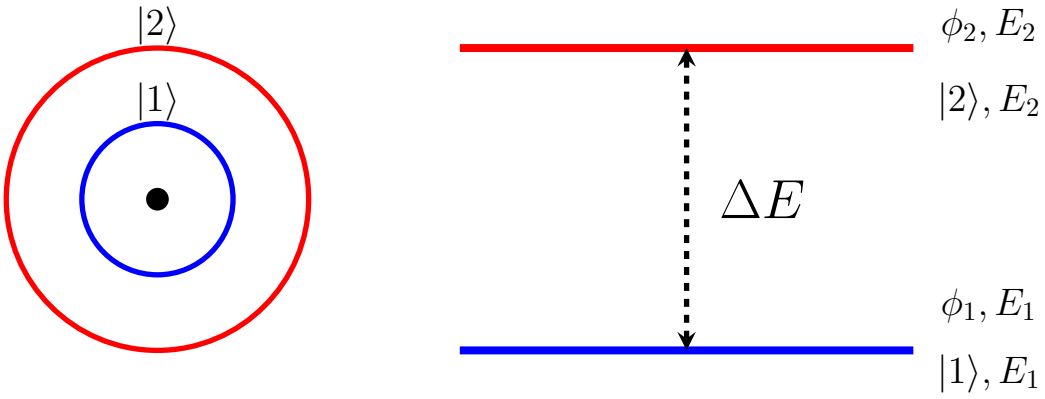

Figure 3.1: *A two-level system. On the left is the* ***classical atomic model*** *while on the right is the* ***energy level diagram****. Two notations are used to label the states, ϕ_1 and ϕ_2 or $|1\rangle$ and $|2\rangle$. Red represents the excited state and blue the ground state. ΔE here represents the difference in the energy between the two states.*

States ϕ_1 and ϕ_2 can also be represented using the Dirac notation, $|1\rangle$ and $|2\rangle$ respectively, this is used to compact the notation.

[1]A state is a complete description of a system. This takes into account parameters such as the position and momentum at a particular moment in time and space.

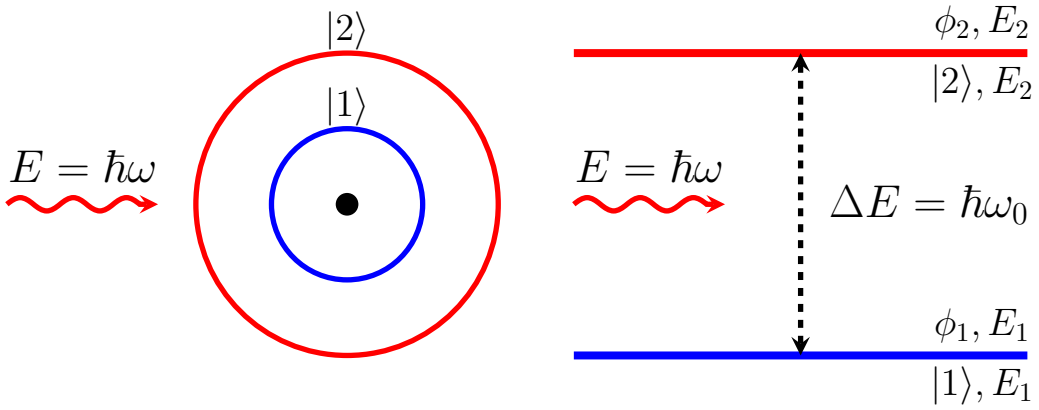

Figure 3.2: *A schematic diagram representing the interaction of a laser beam with a two level atom. The energy of the photon is $E = \hbar\omega$. The electric dipole moment of the atom causes it to interact with the electric field of the laser.*

The difference in energy between the two states corresponds to a frequency of

$$\omega_0 = \frac{E_2 - E_1}{\hbar} \tag{3.1}$$

also referred to as the atomic resonant frequency, where $\hbar$ is the Dirac constant[2].

Figure 3.2 depicts the case when the atom interacts with a photon. The resonant frequency, ω_0, should not be confused with ω in Figure 3.2, this is the frequency corresponding to the photon from the laser beam. This interaction occurs when $\omega \approx \omega_0$, i.e. the atom, usually in ϕ_1, transitions to ϕ_2 when the photon frequency matches the resonant frequency.

The interaction results in the wave function[3] to become a time dependent

[2]The Dirac constant is equal to the Plank constant divided by 2π. i.e. $\hbar = \frac{h}{2\pi}$

[3]The wave function, ψ contains all the information there is to know about the atomic system and is also a function of the position of the electron.

superposition state. We write the new state as

$$\Psi = C_1\psi_1 + C_2\psi_2 \tag{3.2}$$

where

$$\psi_1 = \phi_1 e^{\frac{-\imath E_1 t}{\hbar}}$$

and

$$\psi_2 = \phi_2 e^{\frac{-\imath E_2 t}{\hbar}}$$

In other words, the new state, equation (3.2), is a linear combination of ψ_1 and ψ_2 where C_1 and C_2 will be time dependent due to the time dependent perturbation/interaction with the photon. Equation (3.2) is known as a *superposition*[4] state. It contains the time dependent component and a space dependent part. We now need to find C_1 and C_2. This is done as follows.

We want to examine how Ψ behaves with respect to time. For this, Ψ must satisfy Schrödinger's time dependent equation

$$\imath\hbar\frac{\partial\Psi}{\partial t} = \hat{H}\Psi \tag{3.3}$$

where $\hat{H} = \hat{H}_0 + \hat{H}_I$, this is the new total energy operator. $\hat{H}_0$ is the Hamiltonian[5] belonging to the atom. $\hat{H}_I$ is an additional term in the Hamiltonian to cater for the interaction and is given by

$$\hat{H}_I = -e\vec{E}\cdot\hat{\vec{D}}\cos\omega t \tag{3.4}$$

where $-e\hat{\vec{D}}$ represents the dipole moment[6] (Meystre and Sargent, 2007) op-

[4]Superposition means that a system can be in multiple states simultaneously.

[5]Hamiltonian refers to the total operator for the energy of the atom, i.e. $\hat{H} = \frac{1}{2}\frac{\hat{p}^2}{m} + V$

[6]The electric dipole moment for a pair of opposite charges is defined as the magnitude of the charge multiplied by the distance between them and the defined direction is toward the positive charge

erator of the atom, $\vec{E}$ is the electric field or amplitude of the laser beam and $\cos\omega t$ represents the time variation of the electric field of the laser beam. Substituting for ψ in equation (3.3) gives:

$$\begin{aligned} i\hbar\tfrac{\partial}{\partial t}(C_1\psi_1 + C_2\psi_2) &= (H_0 + H_I)(C_1\psi_1 + C_2\psi_2) \\ i\hbar\Big[\tfrac{\partial C_1}{\partial t}\psi_1 + C_1\tfrac{\partial \psi_1}{\partial t} + \tfrac{\partial C_2}{\partial t}\psi_2 + C_2\tfrac{\partial \psi_2}{\partial t}\Big] &= C_1H_0\psi_1 + C_2H_0\psi_2 + C_1H_I\psi_1 + C_2H_I\psi_2 \end{aligned}$$

Since

$$\imath\hbar\frac{\partial \psi_1}{\partial t} = H_0\psi_1$$

and

$$\imath\hbar\frac{\partial \psi_2}{\partial t} = H_0\psi_2$$

these terms will cancel and the resulting equation (Loudon, 2000) is

$$\imath\hbar\Big[\frac{\partial C_1}{\partial t}\psi_1 + \frac{\partial C_2}{\partial t}\psi_2\Big] = C_1H_I\psi_1 + C_2H_I\psi_2 \tag{3.5}$$

Thus we see that H_0 does not appear in the above equation.

Multiplying equation (3.5) by ψ_1^* from the left, integrating over all the space and using orthogonality results in

$$\begin{aligned} \int \psi_1^*\Big[i\hbar\Big(\frac{\partial C_1}{\partial t}\psi_1 + \frac{\partial C_2}{\partial t}\psi_2\Big)\Big]dv &= \int \psi_1^*\Big[C_1H_I\psi_1 + C_2H_I\psi_2\Big]dv \\ \int i\hbar\Big[\frac{\partial C_1}{\partial t}\psi_1\psi_1^* + \frac{\partial C_2}{\partial t}\psi_2\psi_1^*\Big]dv &= C_1\int \psi_1^*H_I\psi_1 dv + C_2\int \psi_1^*H_I\psi_2 dv \\ i\hbar\frac{\partial C_1}{\partial t}\int \psi_1\psi_1^* dv + i\hbar\frac{\partial C_2}{\partial t}\int \psi_2\psi_1^* dv &= C_1\int \Big(\phi_1^* e^{\frac{iE_1t}{\hbar}} H_I\phi_1 e^{\frac{-iE_1t}{\hbar}}\Big)dv \\ &+ C_2\int \Big(\phi_1^* e^{\frac{iE_1t}{\hbar}} H_I\phi_2 e^{\frac{-iE_2t}{\hbar}}\Big)dv \\ i\hbar\frac{\partial C_1}{\partial t}\Big[1\Big] + i\hbar\frac{\partial C_2}{\partial t}\Big[0\Big] &= C_1\langle\phi_1|H_I\phi_1\rangle + C_2e^{\frac{-i(E_2-E_1)t}{\hbar}}\langle\phi_1|H_I|\phi_2\rangle \\ i\hbar\frac{\partial C_1}{\partial t} &= C_1\langle 1|H_I|1\rangle + C_2e^{-i\omega_0 t}\langle 1|H_I|2\rangle \end{aligned} \tag{3.6}$$

Similarly, multiplying equation (3.5) by ψ_2^* from the left, integrating over all the space and using orthogonality results in

$$\begin{aligned}
\int \psi_2^*\Big[i\hbar\Big(\frac{\partial C_1}{\partial t}\psi_1+\frac{\partial C_2}{\partial t}\psi_2\Big)\Big]dv &= \int \psi_2^*\Big[C_1H_I\psi_1+C_2H_I\psi_2\Big]dv \\
\int i\hbar\Big[\frac{\partial C_1}{\partial t}\psi_1\psi_2^*+\frac{\partial C_2}{\partial t}\psi_2\psi_2^*\Big]dv &= C_1\int \psi_2^*H_I\psi_1dv+C_2\int \psi_2^*H_I\psi_2dv \\
i\hbar\frac{\partial C_1}{\partial t}\int \psi_1\psi_2^*dv+i\hbar\frac{\partial C_2}{\partial t}\int \psi_2\psi_2^*dv &= C_1\int \Big(\phi_2^*e^{\frac{iE_2t}{\hbar}}H_I\phi_1e^{\frac{-iE_1t}{\hbar}}\Big)dv \\
&+ C_2\int \Big(\phi_2^*e^{\frac{iE_2t}{\hbar}}H_I\phi_2e^{\frac{-iE_2t}{\hbar}}\Big)dv \\
i\hbar\frac{\partial C_1}{\partial t}\Big[0\Big]+i\hbar\frac{\partial C_2}{\partial t}\Big[1\Big] &= C_1e^{\frac{i(E_2-E_1)t}{\hbar}}\langle\phi_2|H_I\phi_1\rangle+C_2\langle\phi_2|H_I|\phi_2\rangle \\
i\hbar\frac{\partial C_2}{\partial t} &= C_1e^{i\omega_0t}\langle 2|H_I|1\rangle+C_2\langle 2|H_I|2\rangle \qquad (3.7)
\end{aligned}$$

Equation (3.6) is simplified using equation (3.4) to give

$$\begin{aligned}
i\hbar\frac{\partial C_1}{\partial t} &= C_1\langle 1|H_I|1\rangle+C_2e^{-i\omega_0t}\langle 1|H_I|2\rangle \\
i\hbar\frac{\partial C_1}{\partial t} &= 0+C_2e^{-i\omega_0t}\langle 1|-e\vec{E}\cdot\hat{\vec{D}}\cos\omega t|2\rangle
\end{aligned}$$

where $\vec{D}=X_{12}=\int dV\psi_1^*X\psi_2$ and X is the x-component of the atomic dipole moment $\vec{D}$. Therefore

$$i\hbar\frac{\partial C_1}{\partial t}=C_2e^{-i\omega_0t}eEX_{12}\cos\omega t$$

We set $\hbar\nu=eEX_{12}$ where ν is the *Rabi* frequency, thus

$$\nu\cos(\omega t)e^{-\imath\omega_0t}C_2=\imath\frac{\partial C_1}{\partial t} \qquad (3.8)$$

and similarly (3.7) is simplified to give

$$\nu\cos(\omega t)e^{\imath\omega_0t}C_1=\imath\frac{\partial C_2}{\partial t} \qquad (3.9)$$

Rewriting equation (3.2) in Dirac notation[7]

$$|\psi\rangle = C_1|\psi_1\rangle + C_2|\psi_2\rangle = C_1|1\rangle + C_2|2\rangle \tag{3.10}$$

allows for the density operator to be applied where the density operator is given by

$$\hat{\rho} = \sum_i P_i|i\rangle\langle i| \tag{3.11}$$

and P_i is the probability of being in state $|i\rangle$. For a pure state, the density matrix can be obtained using

$$\begin{aligned} \hat{\rho} &= |\psi\rangle\langle\psi| \\ &= (C_1|1\rangle + C_2|2\rangle)(C_1^*\langle 1| + C_2^*\langle 2|) \\ &= C_1C_1^*|1\rangle\langle 1| + C_2C_2^*|2\rangle\langle 2| + C_1C_2^*|1\rangle\langle 2| + C_2C_1^*|2\rangle\langle 1| \end{aligned} \tag{3.12}$$

where the matrix elements of ρ are:

$$\rho_{11} = C_1C_1^* = |C_1|^2 \tag{3.13}$$

$$\rho_{22} = C_2C_2^* = |C_2|^2 \tag{3.14}$$

$$\rho_{12} = C_1C_2^* \tag{3.15}$$

$$\rho_{21} = C_2C_1^* \tag{3.16}$$

It should be noted that $\rho_{11} + \rho_{22} = 1$ which comes from interpreting the modulus squared of the superposition state as a probability density. Taking the time derivative of the above equation gives

$$\frac{\partial \rho_{ij}}{\partial t} = C_i\frac{\partial C_j^*}{\partial t} + \frac{\partial C_i}{\partial t}C_j^*$$

[7]Dirac notation is also known as bra-ket notation. It is a standard notation used to describe quantum states.

Substituting equations (3.8) and (3.9) into the above equation gives the equations for the elements of the density matrix.

When the terms of rapid oscillations[8] are removed, the optical Bloch equations are formed. We make use of the following substitutions for convenience

$$\tilde{\rho}_{12} = e^{\imath(\omega_0-\omega)t}\rho_{12} \qquad and \qquad \tilde{\rho}_{21} = e^{-\imath(\omega_0-\omega)t}\rho_{21}$$

Below is the set of Bloch equations: (the tilde has been dropped for convenience)

$$\frac{\partial\rho_{11}}{\partial t} = \frac{1}{2}\imath\nu(\rho_{12} - \rho_{21}) \tag{3.17}$$

$$\frac{\partial\rho_{12}}{\partial t} = \frac{1}{2}\imath\nu(\rho_{11} - \rho_{22}) + \imath(\omega_0 - \omega)\rho_{12} \tag{3.18}$$

$$\frac{\partial\rho_{21}}{\partial t} = -\frac{1}{2}\imath\nu(\rho_{11} - \rho_{22}) - \imath(\omega_0 - \omega)\rho_{12} \tag{3.19}$$

$$\frac{\partial\rho_{22}}{\partial t} = -\frac{1}{2}\imath\nu(\rho_{12} - \rho_{21}) \tag{3.20}$$

Equations (3.17) to (3.20) can be solved using any of the numerical methods for solving differential equations. It can be seen that $\partial\rho_{11}/\partial t = -\partial\rho_{22}/\partial t$ and $\partial\rho_{12}/\partial t = \partial\rho^*_{21}/\partial t$.

These equations now need to be generalised by means of adding the effects of spontaneous emission[9]. Spontaneous emission introduces damping[10] terms into the optical Bloch equations with a term containing the damping

[8]Terms oscillating at a frequency $(\omega_0 + \omega)$ have a negligible effect compared to terms oscillating at a frequency $(\omega_0 - \omega)$. The $(\omega_0 + \omega)$ terms can be omitted, as they never occur in real experiments. This is known as the rotating wave approximation (Loudon, 2000).

[9]If an atom is in the excited state, it can decay to the ground state by the process of spontaneous emission. The difference in energies between the two states is released by the atom as a photon.

[10]Damping refers to an influence within or acting on an oscillatory system. It has the effect of reducing, restricting or even preventing oscillations.

constant γ_{sp}. The solutions will no longer be purely oscillatory, the system will begin to settle down into a steady state after some time.

The new equations (Loudon, 2000) are

$$\frac{\partial \rho_{11}}{\partial t} = \frac{1}{2}\imath\nu(\rho_{12} - \rho_{21}) + 2\gamma_{sp}\rho_{22} \tag{3.21}$$

$$\frac{\partial \rho_{12}}{\partial t} = \frac{1}{2}\imath\nu(\rho_{11} - \rho_{22}) + \Big[\imath(\omega_0 - \omega) - \gamma_{sp}\Big]\rho_{12} \tag{3.22}$$

$$\frac{\partial \rho_{21}}{\partial t} = -\frac{1}{2}\imath\nu(\rho_{11} - \rho_{22}) + \Big[-\imath(\omega_0 - \omega) - \gamma_{sp}\Big]\rho_{12} \tag{3.23}$$

$$\frac{\partial \rho_{22}}{\partial t} = -\frac{1}{2}\imath\nu(\rho_{12} - \rho_{21}) - 2\gamma_{sp}\rho_{22} \tag{3.24}$$

This is a phenomenological approach to cater for dissipation. Equations (3.17) to (3.20) can alternatively be derived from the Liouville-von Neumann equation (see for example Kölle (2014))

$$\dot{\rho} \;=\; -\frac{\imath}{\hbar}\left[\hat{H}, \hat{\rho}\right] \tag{3.25}$$

for the case of no dissipation where

$$\hat{H} \;=\; \begin{pmatrix} 0 & \frac{1}{2}\hbar\nu e^{-\imath t\Delta} \\ \frac{1}{2}\hbar\nu e^{\imath t\Delta} & 0 \end{pmatrix} \tag{3.26}$$

in the interaction picture[11] and where Δ is the detuning between the laser frequency and the atomic resonant frequency. Now going back to equation (3.25) we get

$$\imath\hbar \begin{pmatrix} \dot{\rho}_{11} & \dot{\rho}_{12} \\ \dot{\rho}_{21} & \dot{\rho}_{22} \end{pmatrix} \;=\; \left[\begin{pmatrix} 0 & \frac{1}{2}\hbar\nu e^{-\imath t\Delta} \\ \frac{1}{2}\hbar\nu e^{\imath t\Delta} & 0 \end{pmatrix}, \begin{pmatrix} \rho_{11} & \rho_{12} \\ \rho_{21} & \rho_{22} \end{pmatrix} \right]$$

[11]The interaction picture is similar to the Schrödinger picture but only involves the interaction Hamiltonian.

Using another unitary operator[12] we remove the time dependence of $\hat{H}$ and get

$$H = \hbar \begin{pmatrix} \Delta & \frac{1}{2}\nu \\ \frac{1}{2}\nu & 0 \end{pmatrix} \tag{3.27}$$

The first unitary operator was used to obtain the interaction Hamiltonian in equation (3.26). Equation (3.27) is now used in equation (3.25) to derive the optical Bloch equations, equations (3.17) to (3.20).

3.3 Results

We have solved the optical Bloch equations numerically, using the Runge-Kutta technique, to obtain the state of a two-level atom that interacts with a uniform laser beam. Equations (3.17) and (3.20) indicate the rate of change of probability of the atom being in the ground state and in the excited state, respectively. ρ_{11} indicates the probability of the atom being in the ψ_1 state and ρ_{22} indicates the probability of the atom being in the ψ_2 state where ψ is the time dependent part together with a time dependent phase factor. ρ_{12} and ρ_{21} are the coherence terms of the wave functions. These equations form the density matrix, $\left(\begin{smallmatrix} \rho_{11} & \rho_{12} \\ \rho_{21} & \rho_{22} \end{smallmatrix}\right)$ where the diagonal elements, ρ_{11} and ρ_{22}, are known as populations and hold real values. The off-diagonal elements, ρ_{12} and ρ_{21}, are the coherences and are made up of complex values.

In Appendix A, Figure A.1 shows a simple flowchart of the numerical calculation. The following sections depict the numerical results for varying parameters.

[12] A unitary operator, $\hat{U}$ is an operator whose Hermitian adjoint equals its inverse.

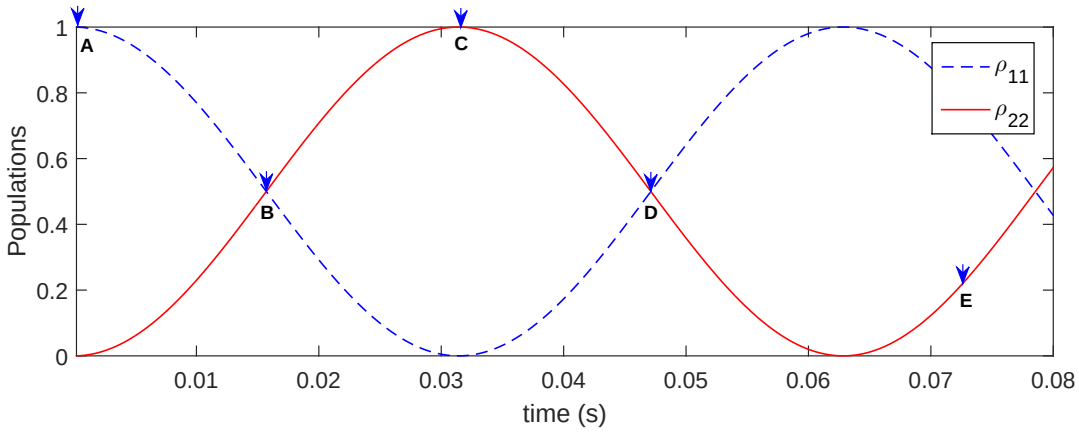

Figure 3.3: *Probability of the state of the atom with respect to time. The blue curve(- - -) represents* ρ_{11} *which is the probability of the atom being in the ground state,* ψ_1*. The red curve(—) represents* ρ_{22} *which is the probability of the atom being in the excited state,* ψ_2*. At* $t = 0\ s$*, Label A, the ground state population,* ρ_{11}*, is* 100% *the excited state population,* ρ_{22}*, is* 0%*. Labels B and D, the ground and excited state populations are* 50%*, the atom is in superposition. Label C,* $\rho_{11} = 0\%$ *and* $\rho_{22} = 100\%$*. Label E,* 80% *of the population is in the ground state and* 20% *in the excited state, still superposition state however more likely to be in* ρ_{11}*.*

3.3.1 General Features

We look at the most basic of laser-atom interactions where the beam frequency matches the atomic resonant frequency resulting in Figure 3.3 and Figure 3.4. In these figures the atom is initialised to be in the ground state, ψ_1 and the laser is switched on at time $t = 0\ s$ and kept on. The variation of the density matrix elements ρ_{11}, ρ_{12}, ρ_{21} and ρ_{22} are presented below.

In Figure 3.3 $\rho_{11} = 1$ (blue - - -) and $\rho_{22} = 0$ (red ——) means the atom has a probability of 100% of being in the ground state, ψ_1, at $t = 0\ s$ (Label A). As time goes on, ρ_{11} decreases and ρ_{22} increases to a point where the state of the atom consists of 50% of ψ_1 and 50% of ψ_2 (Label B). This indicates that

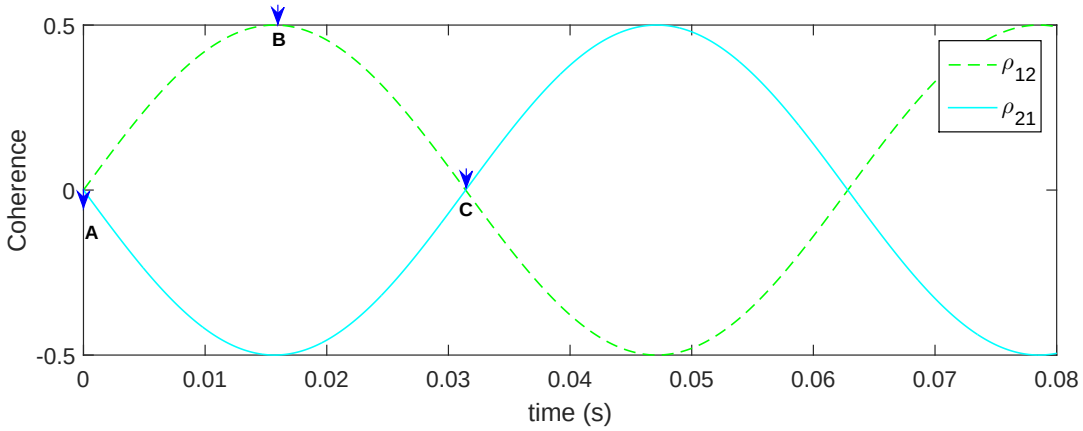

Figure 3.4: *Graph of coherence of the atom with respect to time. The green curve(- - -) represents* ρ_{12} *and the cyan curve(—) represents* ρ_{21}*. These terms indicate superposition of the atom. Labels A and C show the coherence between* ρ_{11} *and* ρ_{22} *as having a value of zero, i.e. there is no superposition. Label B shows a value of* 0.5 *indicating maximum superposition. As long as the system continues to oscillate, superposition exists.*

the atom is now definitely in both states at the same time, a superposition with equal probability of being in state ψ_1 and ψ_2. As time goes on further, ρ_{11} continues to decrease while ρ_{22} continues to increase. This means the atom is now in the excited state, ψ_2 (Label C), as the probability of the atom being in the ground state is 0%. Oscillations continue over time and the atom is once again in a definite state of superposition (Label D). The atom is still in superposition when the atom consists of 80% of ψ_1 and 20% of ψ_2 (Label E), this just means the atom is more likely to be in the ground state than in the excited state, when a measurement of the state is made.

Recall, the atom is initialised to be in the ground state, ψ_1. In Figure 3.4 ρ_{12} (green - - -) and ρ_{21} (cyan ——) represent the coherence terms of of the wave functions of ψ_1 and ψ_2. In other words, Figure 3.4 shows us when the atom is in superposition. At time $t = 0\,s$ (Label A), the coherence between

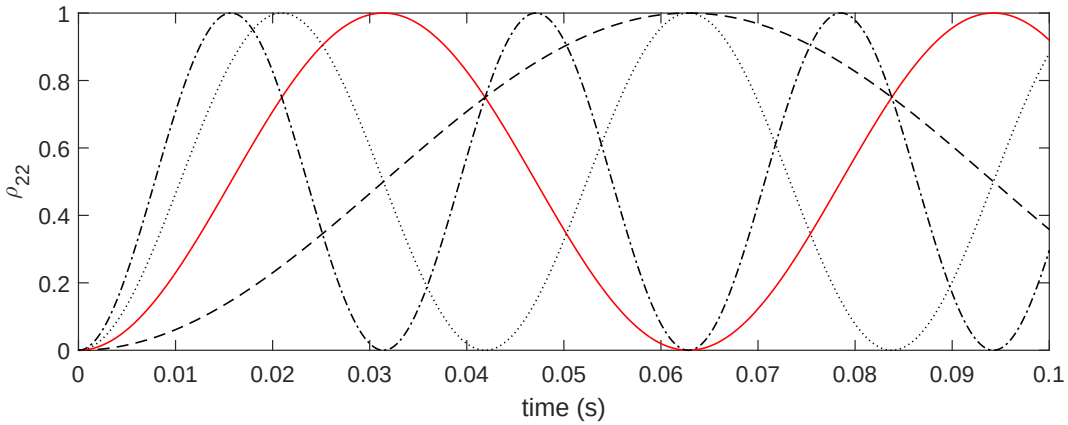

Figure 3.5: *ρ_{22} is plotted for various Rabi frequencies. The graph shows a frequency of* 50 s^{-1} *(black - - -),* 100 s^{-1} *(red —),* 150 s^{-1} *(black ...) and* 200 s^{-1} *(black _._.). The detuning in each case was set to* 0 s^{-1}.

the two states ψ_1 and ψ_2 is *zero*. Here the atom is in the ground state, refer to Figure 3.3 at time $t = 0\ s$. The atom is definitely in superposition when ρ_{12} and ρ_{21} have a value of 0.5 (Label B), this can also be seen in Figure 3.3 (Label B). After some time the coherence between the two states becomes *zero* (Label C), once again the atom is now in the excited state.

3.3.2 Varying Rabi Frequency, ν

In this section we look at how varying ν, the Rabi frequency, affects the probability density of the atom. The atom is initialised to be in the ground state, ψ_1, at time $t = 0s$. The laser is also switched on at this time. Figure 3.5 shows a plot of ρ_{22} versus time for various Rabi frequencies. Here the various frequency values tested are:

- 50 s^{-1} (black - - -)
- 100 s^{-1} (red ——)

- 150 s^{-1} (black ...)
- 200 s^{-1} (black _._.)

From Figure 3.5, it can be seen that the atom oscillates symmetrically between the ground state, ψ_1, and the excited state, ψ_2 continuously. The solid red curve (100 s^{-1}) in Figure 3.5 shows the Rabi frequency that has been chosen as a standard value for all other simulations.

3.3.3 Varying Detuning, $\Delta = \omega_0 - \omega$

Detuning refers to the tuning of a laser to a frequency that is slightly different to the resonant frequency of a quantum system.

Recall, the energy between two states of an atom is

$$\Delta E = \hbar\omega_0$$

and the energy of a photon is

$$E = \hbar\omega$$

Equating these terms results in

$$\omega_0 - \omega = 0 \tag{3.28}$$

where the laser frequency equals the resonant frequency of the atom. Varying the frequency of the laser, ω, results in Figure 3.6. At $t = 0\ s$ the atom is initialised to be in the ground state, ψ_1, and the laser is switched on. Plotting ρ_{22} shows the excitation time[13] of the atom. Changing the detuning results in the frequency of oscillations to change. As detuning increases, the frequency of oscillations of ρ_{22} increases and the probability of transitioning

[13]Excitation time refers to the time taken for the atom to make a full transition the upper level from $t = 0\ s$.

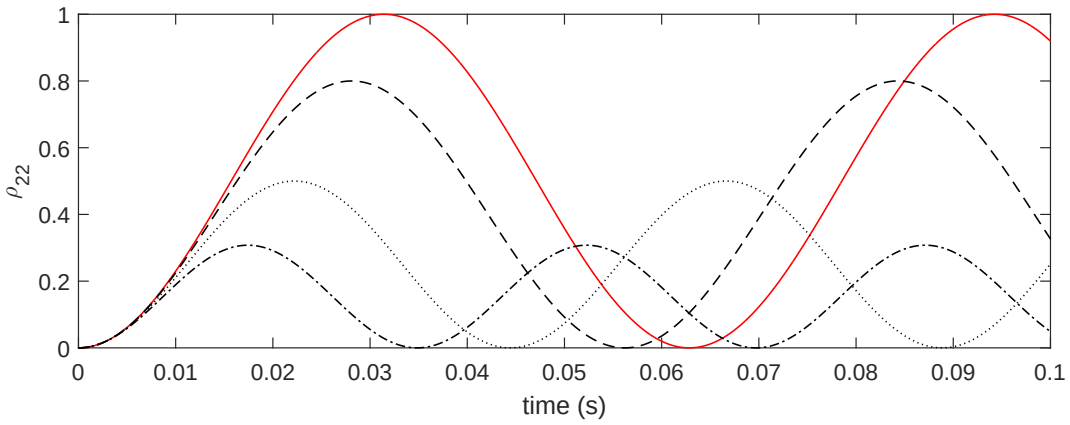

Figure 3.6: *ρ_{22} is plotted against time for various values of detuning. The graph shows a detuning frequency of 0 s^{-1} (red —), 50 s^{-1} (black - - -), 100 s^{-1} (black ...) and 150 s^{-1} (black _._.). As the detuning value increases the probability of the atom transitioning between states decreases.*

between states decreases.

Figure 3.6 shows the effect various laser frequencies have on excitation times compared to the case of having no detuning, solid red curve ($\Delta = 0s^{-1}$). The values tested are:

- 0 s^{-1} (red ——) : This is the case for when $\omega_0 = \omega$. The frequency of oscillation is equal to the Rabi frequency in this case.
- 50 s^{-1} (black - - -) : An increase in the detuning frequency to 50 s^{-1} results in the atom having only a $\pm 80\%$ probability of being in the excited state, ψ_2, at the maximum point.
- 100 s^{-1} (black ...) : An increase in the detuning frequency to 100 s^{-1} results in the atom having only a $\pm 50\%$ probability of being in the excited state, ψ_2, at the maximum point.

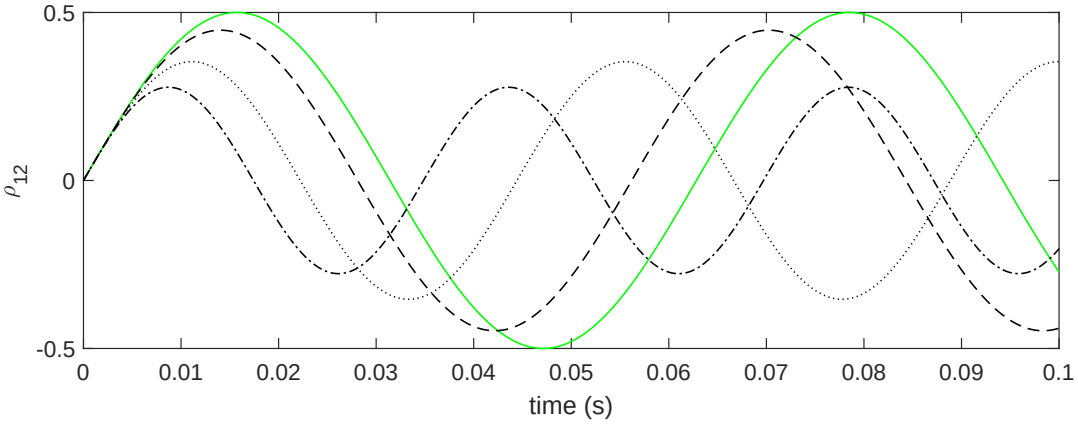

Figure 3.7: *ρ_{12} is plotted against time for various vales of detuning. The graph shows a detuning frequency of 0 s^{-1} (green —), 50 s^{-1} (black - - -), 100 s^{-1} (black ...) and 150 s^{-1} (black _.._.). As the detuning value increases the coherence between ρ_{11} and ρ_{22} decreases.*

- 150 s^{-1} (black _.._.) : An increase in the detuning frequency to 150 s^{-1} results in the atom having only a $\pm 30\%$ probability of being in the excited state, ψ_2, at the maximum point.

Increasing the detuning frequency results in a decrease of the probability of the atom being in the excited state, ψ_2. The frequency of the oscillations also increase as the detuning frequency is increased. The coherence terms, ρ_{12} and ρ_{21}, are also affected by these changes in detuning frequency. Figure 3.7 shows the effects on ρ_{12} where the solid green curve (0 s^{-1}) depicts no detuning. Plotting ρ_{12} shows us how the coherence between the wave function, ψ_1 and ψ_2, varies. The various values used are:

- $0 s^{-1}$ (green ——) : This is the case for when $\omega_0 = \omega$, the Rabi frequency, i.e. no detuning and therefore 100% superposition can occur.

- 50 s^{-1} (black - - -) : An increase in the detuning frequency to 50 s^{-1} results in the coherence between states to decrease to a value of ± 0.45.

- $100\ s^{-1}$ (black ...) : An increase in the detuning frequency to $100\ s^{-1}$ results in the coherence between states to decrease to a value of ± 0.38.
- $150\ s^{-1}$ (black _._.) : An increase in the detuning frequency to $150\ s^{-1}$ results in the coherence between states to decrease to a value of ± 0.25.

Increasing the detuning frequency results in a decrease of the coherence between the ground state, ψ_1, and the excited state, ψ_2. The frequency of oscillations increase as the detuning frequency is increased, similar to Figure 3.6.

3.3.4 Dissipation, γ_{sp}

Dissipation refers to the process by which an energy gradually decays to an equilibrium, i.e. the amplitude of the oscillations are decreased. Equations (3.21) to (3.24) are solved numerically where γ_{sp} is the term used to cater for the dissipation. At $t = 0\,s$ the atom is initialised to be in the ground state, ψ_1 and the laser is switched on. Figure 3.8 shows plots of ρ_{22} (**A**) and ρ_{12} (**B**) for the case where there is both dissipation and no dissipation. From these figures we see how the oscillation amplitude gets affected when the dissipation coefficient is non-zero. Figure 3.8 corresponds to a case of zero detuning where the following values were used for dissipation:

- **A**: ρ_{22} is plotted against time where $\gamma_{sp} = 0$ (red ——) and $\gamma_{sp} = 8$ (black - - -).
- **B**: ρ_{12} is plotted against time where $\gamma_{sp} = 0$ (green ——) and $\gamma_{sp} = 8$ (black - - -).

Increasing the dissipation coefficient results in a decrease of the amplitude of the oscillations between the ground state, ψ_1, and the excited state, ψ_2. The frequency of the oscillations remain constant. Figure 3.8(**A**) show that an increase in the dissipation coefficient, γ_{sp}, results in the amplitude of the

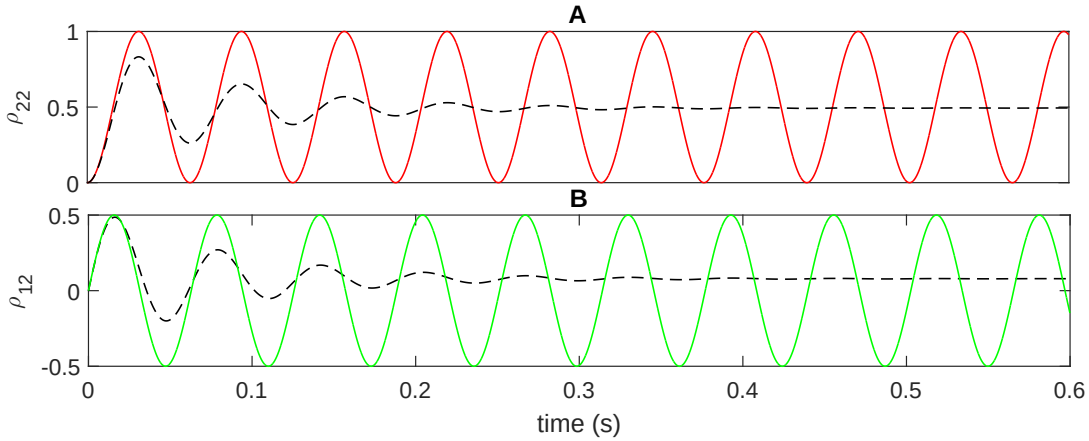

Figure 3.8: *A comparison of results for different dissipation coefficient values. In* ***A*** ρ_{22} *is plotted and in* ***B*** ρ_{12} *is plotted. The graphs show dissipation coefficients of* 0 *for solid curves and dissipation coefficients of* 8 *for dashed curves. As the dissipation coefficient increases, the amplitude of the oscillations decrease until the system reaches an equilibrium.*

oscillations to decrease in time to an equilibrium of $\sim 50\%$. The diminished oscillation means that superposition ceases to exist, the atom is now in either ψ_1 or ψ_2, but not both. Similarly, the coherence terms, Figure 3.8(**B**), also show that an increase in the dissipation coefficient results in the oscillation amplitude to decrease. In this instance the equilibrium reached has a value of zero[14], this means that superposition no longer exists. In the limit of large t, oscillations completely die out and superposition is completely destroyed when there is dissipation.

As long as the graphs are oscillating, superposition exists. This means that the areas on the graphs where there are no oscillations, the atom is in either the ground state or in the excited state but not in both simultaneously.

[14]In principle it should go to zero, however in Figure 3.8(**B**) it does not. This is probably due to a computational issue.

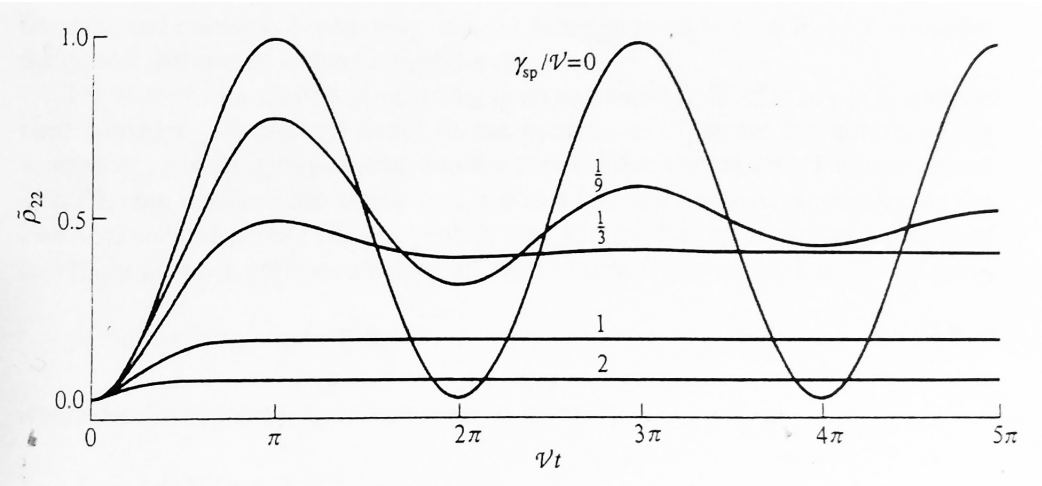

Figure 3.9: *Degree of atomic excitation for zero detuning and ratios of varying dissipation γ_{sp} to Rabi frequency ν (Loudon, 2000).*

As a comparison with standard textbook results, Figure 3.9 shows a plot of ρ_{22} as a function of time for various ratios of dissipation/Rabi frequency values. Our results shown in Figure 3.8, corresponding to $\gamma_{sp}/\nu = 0$ compare very well with Figure 3.9. Our case of $\gamma_{sp}/\nu = 8/15.91$ compares qualitatively reasonably well with the graph of $\gamma_{sp}/\nu = 1/9$ in Figure 3.9, although the values are not the same.

3.4 Summary

In this chapter we have examined an atom interacting with a uniform laser beam. We have solved the optical Bloch equations numerically for various values of Rabi frequency and dissipation. These results compare very well with standard analytical solutions and provide a sense of confidence in the numerical analysis of laser-atom interactions.

Chapter 4

Two-level atom interacting with a modulated laser beam

4.1 Introduction and background

In this chapter we look at the interaction between a two-level atom, that is at rest having a resonant frequency ω_0, and a modulated laser beam. We use the same approach as in the previous chapter i.e., a semi-classical approach where the atom is quantized but the laser is treated classically. However the laser frequency is modulated. The frequency as well as the level of modulation is varied in our approach. This approach was also used by Pisipati, Almakrami, Joshi, and Serna (2012), however they used a full quantum mechanical model.

The optical Bloch equations (4.1) to (4.4) (Loudon, 2000), quoted here,

are still used to simulate this process.

$$\frac{\partial \rho_{11}}{\partial t} = \frac{1}{2}\imath\nu(\rho_{12} - \rho_{21}) + 2\gamma_{sp}\rho_{22} \tag{4.1}$$

$$\frac{\partial \rho_{12}}{\partial t} = \frac{1}{2}\imath\nu(\rho_{11} - \rho_{22}) + \Big[\imath(\omega_0 - \omega) - \gamma_{sp}\Big]\rho_{12} \tag{4.2}$$

$$\frac{\partial \rho_{21}}{\partial t} = -\frac{1}{2}\imath\nu(\rho_{11} - \rho_{22}) + \Big[-\imath(\omega_0 - \omega) - \gamma_{sp}\Big]\rho_{12} \tag{4.3}$$

$$\frac{\partial \rho_{22}}{\partial t} = -\frac{1}{2}\imath\nu(\rho_{12} - \rho_{21}) - 2\gamma_{sp}\rho_{22} \tag{4.4}$$

Recall from Chapter 3, equations (4.1) and (4.4) tell us the time variation of the probability of the atom being in the ground state, ψ_1, or in the excited state, ψ_2, respectively and equations (4.2) and (4.3) are the time variation of the coherence terms. The laser frequency, ω in the above equations is altered by including terms of modulation by means of a sinusoidal variation to the laser frequency. The modulated detuning is then

$$(\omega_0 - \omega) = \delta + D\sin(\omega_m t) \tag{4.5}$$

where δ has a fixed value, ω_m is the modulation frequency and D represents the level of modulation, that is it gives the change in detuning relative to the steady value δ. Making use of various parameters in equation (4.5) gives rise to interesting behaviour of the atomic dynamics. These are discussed next.

In Appendix A, Figure A.2 shows a simple flowchart of the numerical calculation.

4.2 Results

We have used Matlab® to solve the optical Bloch equations numerically for a two-level system that interacts with a modulated beam. The level of modulation and frequency were both varied. We have investigated the following cases:

1. $\omega_m = 20\ s^{-1} >$ Rabi frequency, modulation level small, $D \approx \delta$
2. $\omega_m = 20\ s^{-1} >$ Rabi frequency, modulation level large, $D \approx 2.5\delta$
3. $\omega_m = 7\ s^{-1} <$ Rabi frequency, modulation level small, $D \approx \delta$
4. $\omega_m = 7\ s^{-1} <$ Rabi frequency, modulation level large, $D \approx 2.5\delta$
5. $\omega_m =$ Rabi frequency, modulation level small, $D \approx \delta$
6. $\omega_m =$ Rabi frequency, modulation level large, $D \approx 2.5\delta$

The above values have been chosen in a way that allowed us to obtain results similar to those obtained by Pisipati et al. (2012). Results for the above are shown respectively in Figures 4.1 to 4.6. In these figures a Rabi value of 12.73 s^{-1} was used (obtained from values chosen for simulations). In each of these figures (**A**) shows the time series of ρ_{11} (blue curve) and ρ_{22} (red curve), (**B**) shows the phase space plot ($\partial\rho_{11}/\partial t$ vs ρ_{11}) and (**C**) shows the Fourier transform of ρ_{11}. In (**A**) only a few cycles have been plotted for the time series while more were required for the phase space and power spectral density plots.

We now describe some basic features of all these graphs. Figures 4.1 and 4.2 show plots for the modulated frequency being greater than the Rabi frequency. In Figure 4.1(**A**) the time series shows almost uniform amplitude, which is expected since we used a small modulation level. In the phase space plot (**B**) we see an almost regular pattern, where the atom begins in

the ground state $\rho_{11} = 1$, follows an elliptical path and returns almost back to the ground state. In the Fourier spectra (**C**) there is predominantly one component at the Rabi frequency (ignoring the DC component at 0 s^{-1}).

In Figure 4.2(**A**) the time series shows a slight variation in the amplitude, which is expected since we used a large modulation level. The phase space plot (**B**) shows an almost regular pattern, where the atom begins in the ground state $\rho_{11} = 1$ and follows various elliptical paths due to the variation in amplitude. Compared to Figure 4.1(**A**) there is a greater variability in the phase space plot and greater deviation from a purely elliptical pattern. In the Fourier spectra (**C**) there is predominantly one component at the Rabi frequency (ignoring the DC component at 0 s^{-1}). We also begin to see the formation of additional components on either side of the Rabi frequency.

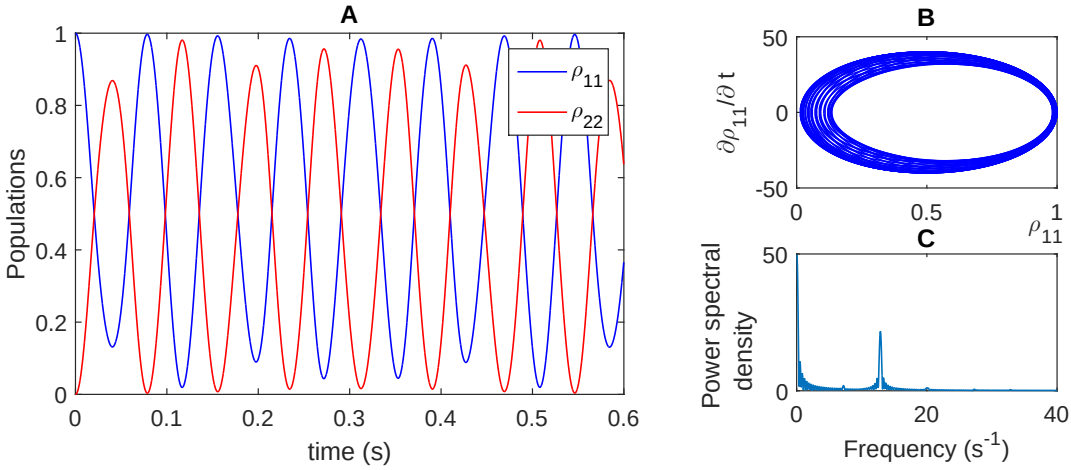

Figure 4.1: *Two-level atom interacting with a laser beam where the modulated frequency is greater than the Rabi frequency and the amplitude of modulation is small. The plots are:* ***A****-time series;* ***B****-phase space plot and* ***C****-fast Fourier transform*

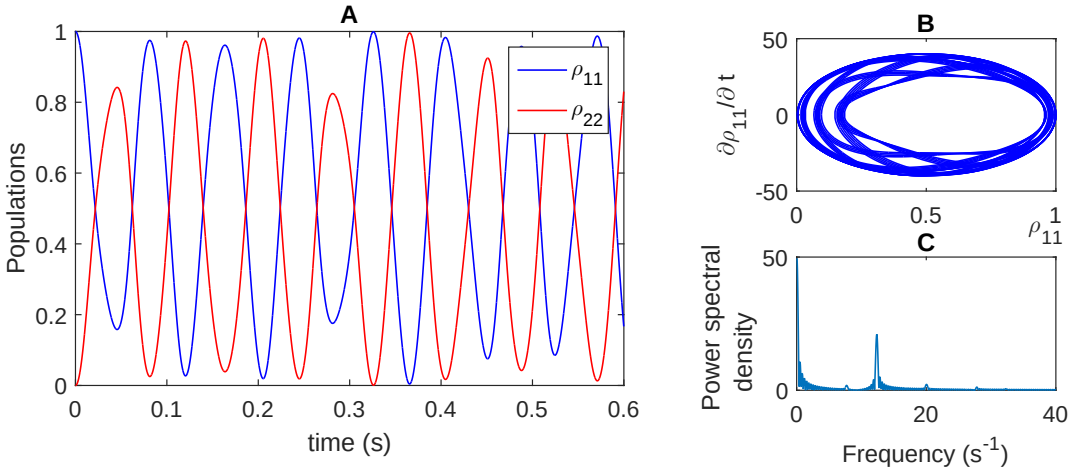

Figure 4.2: *Two-level atom interacting with a laser beam where the modulated frequency is greater than the Rabi frequency and the amplitude of modulation is large. The plots are:* ***A****-time series;* ***B****-phase space plot and* ***C****-fast Fourier transform*

Figures 4.3 and 4.4 show plots for the modulated frequency being less than the Rabi frequency. In Figure 4.3(**A**) the time series shows almost uniform amplitude, which is expected since a small modulation level was used. However, in the phase space plot (**B**) a regular pattern is not seen. The atom begins in the ground state $\rho_{11} = 1$, follows numerous elliptical paths and a deviation from the ground state can be seen. From cycle to cycle, the path does not repeat itself in phase-space, although it shows up in previous plots it becomes more evident for these plots. In the Fourier spectra (**C**) there is predominantly one component at $13.66\,s^{-1}$ and we see the formation of an additional component at $6.71\,s^{-1}$ (ignoring the DC component at $0\,s^{-1}$).

The time series in Figure 4.4(**A**) distinctly shows modulation in the curves. In the phase space plot (**B**) we see an irregular pattern. The atom oscillates between the ground state and excited states in phase-space but also has tendencies to deviate from the elliptical path. The atom is beginning to

display chaotic behaviour. In the Fourier spectra (**C**) the components that arise have the similar amplitudes and the Rabi frequency lies between them - 7.13 s^{-1} and 14.80 s^{-1} (ignoring the DC component at 0 s^{-1}).

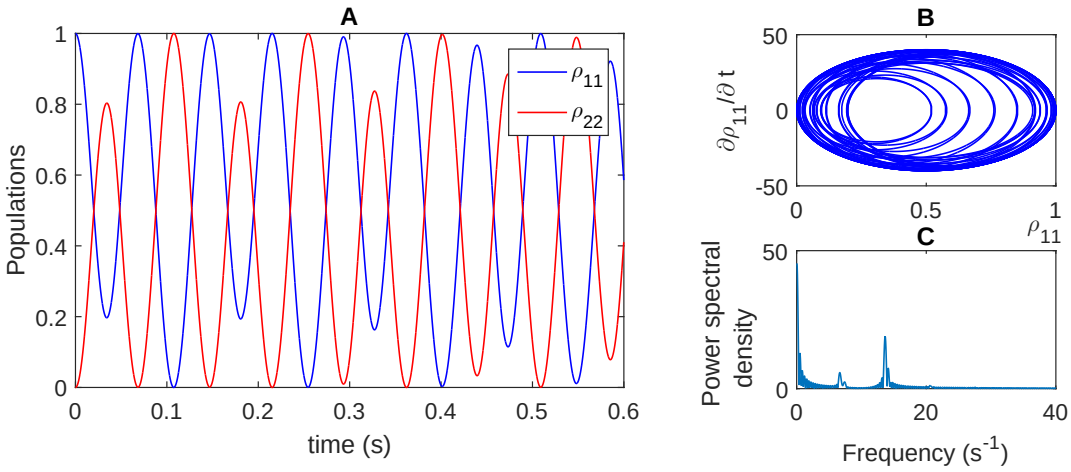

Figure 4.3: *Two-level atom interacting with a laser beam where the modulated frequency is less than the Rabi frequency and the amplitude of modulation is small. The plots are:* ***A****-time series;* ***B****-phase space plot and* ***C****-fast Fourier transform*

Figures 4.5 and 4.6 show plots for the modulated frequency being equal to the Rabi frequency. In Figure 4.5(**A**) the time series shows an irregular curve. The phase space plot (**B**) shows that atom deviates from the ground state from cycle to cycle - the path does not repeat itself in phase-space. The atom seems to behave in a chaotic manner. In the Fourier spectra (**C**) there are three components that arise at 2.36 s^{-1}, 10.72 s^{-1} and 15.37 s^{-1}, none of which appear at the Rabi frequency (ignoring the DC component at 0 s^{-1}).

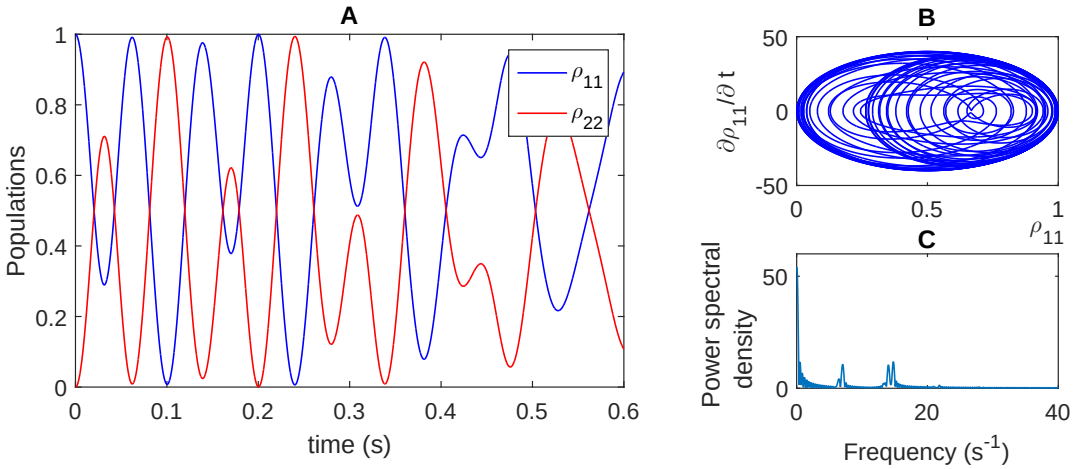

Figure 4.4: *Two-level atom interacting with a laser beam where the modulated frequency is less than the Rabi frequency and the modulation amplitude is large. The plots are:* ***A****-time series;* ***B****-phase space plot and* ***C****-fast Fourier transform*

In the time series shown in Figure 4.6(**A**) an irregular curve can once again be seen. The phase space plot (**B**) is similar to the the plot in Figure 4.5, it just covers a greater area in the space. In the Fourier spectra (**C**) there are three components that arise at 3.89 s^{-1}, 9.19 s^{-1} and 16.94 s^{-1}, none of which appear at the Rabi frequency (ignoring the DC component at 0 s^{-1}). The component beginning to form at 13.01 s^{-1} is close to the Rabi frequency.

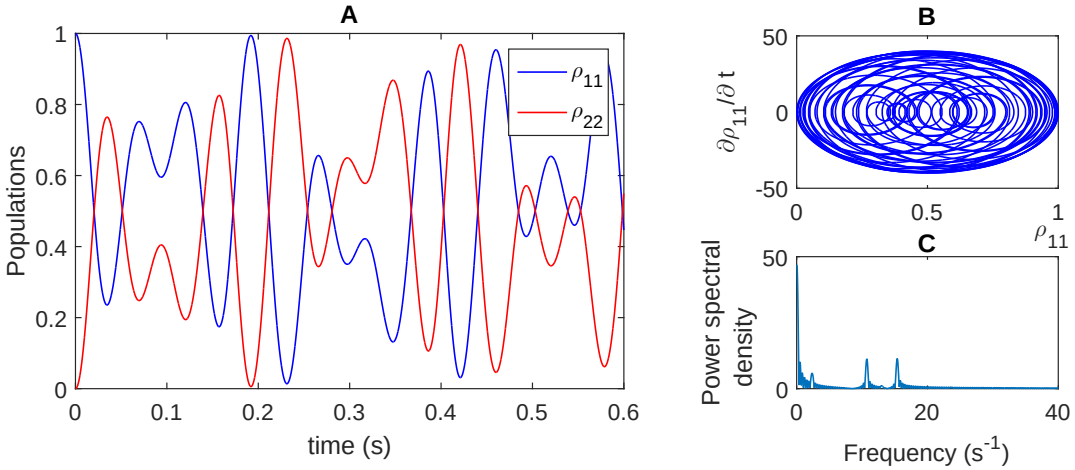

Figure 4.5: *Two-level atom interacting with a laser beam where the modulated frequency is approximately equal to the Rabi frequency and the amplitude of modulation is small. The plots are:* ***A****-time series;* ***B****-phase space plot and* ***C****-fast Fourier transform*

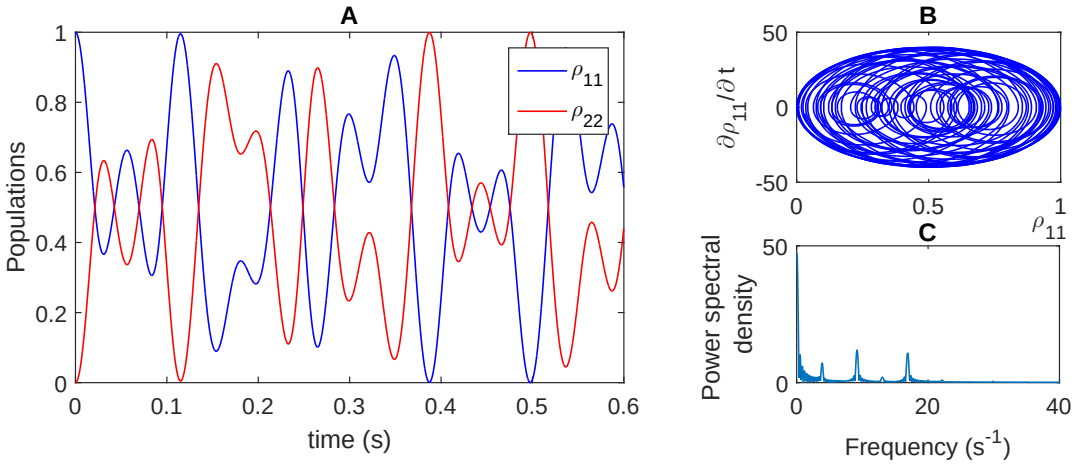

Figure 4.6: *Two-level atom interacting with a laser beam where the modulated frequency is approximately equal to the Rabi frequency and the amplitude of modulation is large. The plots are:* ***A****-time series;* ***B****-phase space plot and* ***C****-fast Fourier transform*

As mentioned previously, Pisipati et al. (2012) conducted similar investigations. They made use of no modulation, as well as monochromatic and bi-chromatic modulation where the frequencies used had integer, rational and irrational values as well as overtones of the Rabi frequency. The values we used were chosen to be above or below our Rabi frequency and when simulated gave results that are similar to theirs in the time series as well as is phase space.

4.3 Summary

Using the optical Bloch equations, we have shown that atoms behave in a chaotic manner when they are exposed to laser modulation. Three different scenarios were tested, modulation frequency being greater than, less than and approximately equal to the Rabi frequency, each producing different results.

When the modulated frequency was greater than the Rabi frequency a small deviation from the normal oscillatory pattern was seen. This deviation increased when the modulated frequency was less than the Rabi frequency. The deviation was most noticeable when the modulation frequency had a value closely equal to the Rabi frequency. In each case the atom does not repeat its path in phase space - chaotic behaviour was present.

Chapter 5

Saturated Absorption Spectroscopy

5.1 Introduction

Previously we looked at the effects of light on atoms, in this chapter we investigate the change in laser beam intensity as the beam interacts with a sample of two-level atoms. The equations derived in Chapter 3 along with Maxwell's equations have been used to generate the results.

This chapter discusses saturated absorption spectroscopy by giving some background theory in Section 5.2 followed by results of absorption spectroscopy as well as saturated absorption spectroscopy simulations in Sec-

tion 5.3. We have also included some experimental results. The material presented in this chapter follows those of Grynberg, Aspect, and Fabre (2010) and Levenson (1982).

5.2 Background Theory

We investigate the interaction between laser beams of frequency ω and a sample of atoms having two levels separated in frequency by ω_0. Figure 5.1 shows a simple setup to determine the absorption spectra of a gaseous sample. A laser beam (called the probe beam), E_1, whose frequency can be varied propagates in the positive z-direction through the gaseous sample, after which the intensity of the beam is measured by a photodiode. The change in intensity as the frequency is varied is known as the absorption spectrum.

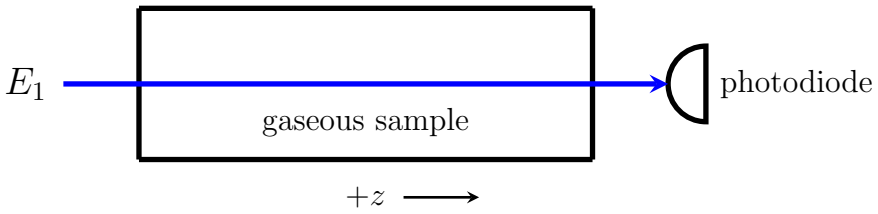

Figure 5.1: Basic arrangement for absorption spectroscopy.

The atoms have thermal velocities, and therefore have different speeds, which cause a broadening of the absorption spectra. To counteract this, a second beam (called a pump beam), E_2, is introduced in the opposite direction (negative z-direction), as in Figure 5.2.

The effect of the pump beam is to pump most of the atoms into the upper energy levels resulting in a saturation of the sample. However, because the beams propagate in opposite directions they interact with atoms having

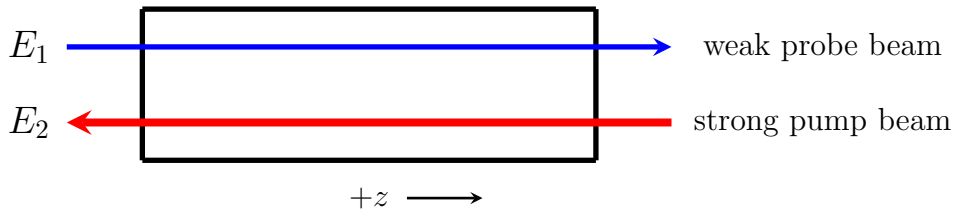

Figure 5.2: Basic arrangement for saturated absorption spectroscopy.

different velocities. This can be seen in Figure 5.3 (Grynberg et al., 2010). Note that Figure 5.3 shows the propagation in the x-direction, our discussion is based in the z-direction. When the laser frequency is far away from the atomic resonant frequency, as in Figure 5.3(**a**), the probe and pump beams interact with different groups of atoms and excite them respectively. The stronger pump beam causes a greater reduction in the ground state atoms than the less intense probe beam. At $\omega_0 = \omega$, Figure 5.3(**b**), both the beams interact with the same group of zero velocity atoms. Because the pump beam saturates these atoms having zero velocity, it leaves fewer atoms for absorption by the probe beam. This then shows up as a reduction in the absorption spectrum, Figure 5.4, and results in peaks superimposed on the Doppler broadened signal.

We want to solve for the absorption spectrum numerically making use of the following method (see for example (Grynberg et al., 2010)): The probe beam having a weak electric field is given by

$$\vec{E}_1 = \mathcal{E}_1 e^{\imath kz} e^{-\imath\omega t} + c.c. \tag{5.1}$$

as it propagates through a gaseous sample in the positive z-direction. The pump beam E_2, which has the same frequency as E_1 but a much stronger electric field is given by

$$\vec{E}_2 = \mathcal{E}_2 e^{-\imath kz} e^{-\imath\omega t} + c.c. \tag{5.2}$$

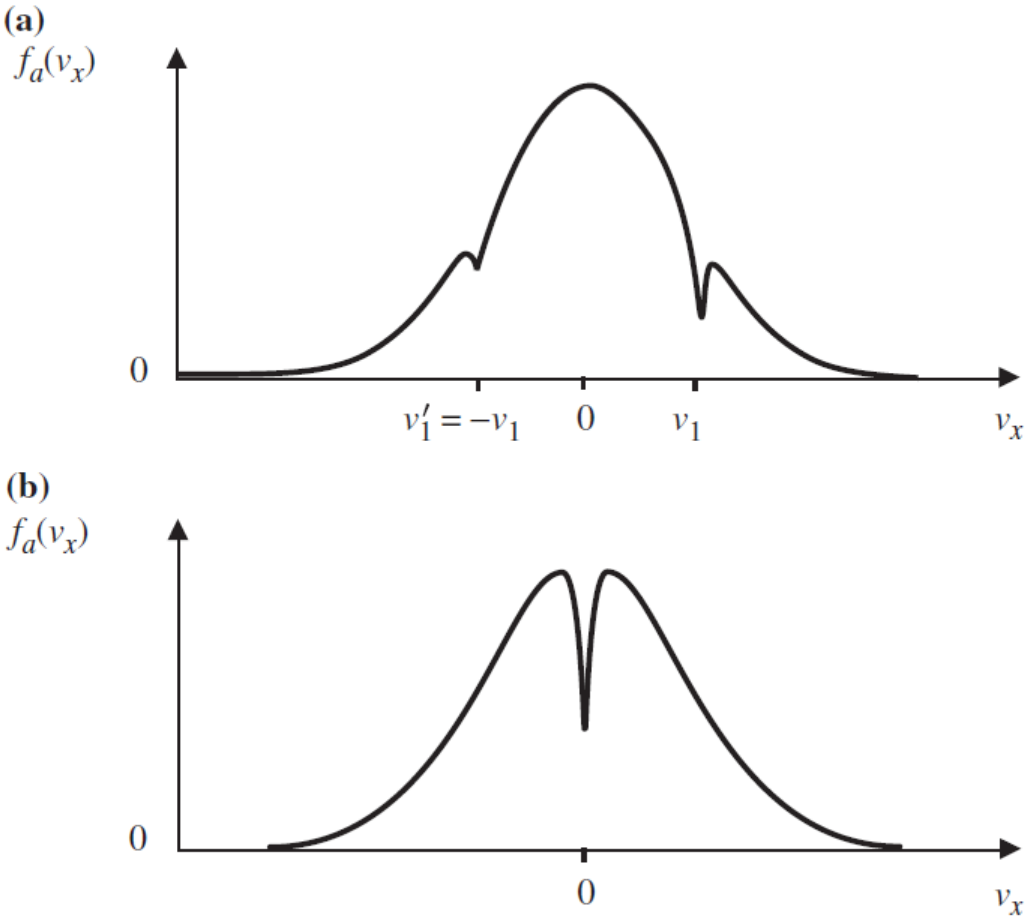

Figure 5.3: *Velocity distribution of the ground state atoms.* ***(a)*** *when* $\omega_0 \neq \omega$ *the probe and pump beams each interact with different groups of atoms and excite them respectively.* ***(b)*** *at* $\omega_0 = \omega$ *both beams interact with the same group of atoms resulting in a greater absorption (Grynberg et al., 2010).*

as it propagates through the gaseous sample in the negative z-direction. In the above equations $\mathcal{E}_1$ and $\mathcal{E}_2$ are the amplitudes of the electric fields and k

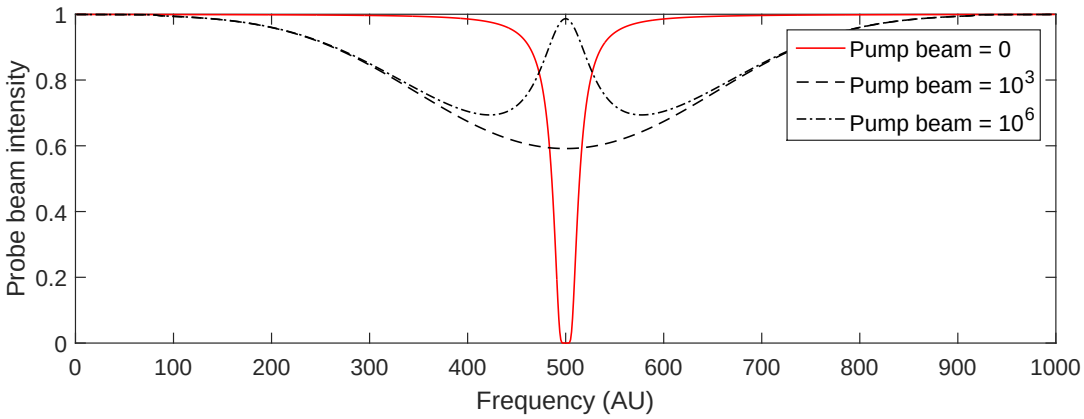

Figure 5.4: *The intensity of the probe beam, E_1, as the field of the pump beam, E_2 is increased. The graph shows the absorption of E_1 when E_2 is* 0 *(red —),* 10^3 *(black - - -) and* 10^6 *(black _._).*

is the wave number. The total electric field is given by[1]

$$\begin{aligned} E^+ &= E_1^+ + E_2^+ \\ &= (\mathcal{E}_1 e^{\imath kz} + \mathcal{E}_2 e^{-\imath kz}) e^{-\imath\omega t} \end{aligned} \tag{5.3}$$

The behaviour of the electric field of the laser beam, as it propagates, is described by the wave equation

$$\nabla^2 \vec{E} - \frac{1}{c^2}\frac{\partial^2}{\partial t^2}\left(\vec{E} + \frac{\vec{P}}{\varepsilon_0}\right) = 0 \tag{5.4}$$

where $\vec{P}$ represents the polarization due to the applied electric field and is given by $\vec{P} = \chi\varepsilon_0\vec{E}$ where $\vec{P}$ is defined in terms of the linear susceptibility (Lambropoulos and Petrosyan, 2006).

We will assume that the pump beam is strong enough so that it does

[1] E^+ - '+' represents the positive frequency component of the electric field.

not vary much. We will also assume that the medium is homogeneous and isotropic. The slowly varying approximation is then used to obtain the following equation for a wave in the positive z-direction for the amplitude $\mathcal{E}_1$

$$\frac{\partial \mathcal{E}_1}{\partial z} = \imath \frac{\omega}{2\epsilon_0 nc} P \tag{5.5}$$

and is used to predict the behaviour of the electric field as it propagates through the isotropic sample. In equation (5.5), P represents the magnitude of the polarization in the z-direction and n represents the refractive index of the medium.

Analytical solution for E:

$$\frac{\partial E}{\partial z} = \imath \frac{\omega}{2\epsilon_0 nc} P \tag{5.6}$$

$$\frac{\partial E}{\partial z} = \imath \frac{\omega}{2\epsilon_0 nc} (\chi \epsilon_0 E) \tag{5.7}$$

$$\int \frac{\partial E}{E} = \int \imath \frac{\omega}{2nc} \chi \partial z \tag{5.8}$$

$$\ln(E) = \imath \frac{\omega}{2nc} \chi z + constant \tag{5.9}$$

$$E = A e^{\imath \frac{\omega}{2nc} \chi z} \tag{5.10}$$

Since we are looking at how laser beams are affected when propagating through a sample of two-level atoms, we once again make use of the optical Bloch equations with added dissipation terms (Grynberg et al., 2010) to

determine the polarization of the atoms as follows:

$$\dot{\rho}_{11} = -\imath\frac{\Omega_1}{2}(\rho_{21} - \rho_{12}) + \Gamma_{sp}\rho_{22} \tag{5.11}$$

$$\dot{\rho}_{22} = \imath\frac{\Omega_1}{2}(\rho_{21} - \rho_{12}) - \Gamma_{sp}\rho_{22} \tag{5.12}$$

$$\dot{\rho}_{12} = \imath(\omega_0 - \omega)\rho_{12} - \imath\frac{\Omega_1}{2}(\rho_{22} - \rho_{11}) - \gamma\rho_{12} \tag{5.13}$$

At steady state the time derivatives on the left are zero. Setting the LHS to 0, we can solve for ρ_{11}, ρ_{22} and ρ_{12} (Grynberg et al., 2010).

$$\rho_{11} = 1 - \rho_{22} \tag{5.14}$$

$$\rho_{22} = \frac{1}{2}\frac{\Omega_1^2\frac{\gamma}{\Gamma_{sp}}}{(\omega_0 - \omega)^2 + \gamma^2 + \Omega_1^2\frac{\gamma}{\Gamma_{sp}}} \tag{5.15}$$

$$\rho_{12} = \imath\frac{\Omega_1}{2}\frac{\gamma + \imath(\omega_0 - \omega)}{(\omega_0 - \omega)^2 + \gamma^2 + \Omega_1^2\frac{\gamma}{\Gamma_{sp}}} \tag{5.16}$$

$$\rho_{21} = \rho_{12}^* \tag{5.17}$$

In the above, Ω_1^2 represents the intensity and $\gamma = \Gamma_{sp}/2$. The derivation of equations (5.14) to (5.17) can be found in Appendix B. The expectation value of the electric dipole moment due to the probe beam is $\langle D\rangle = Tr(\rho\hat{D})$ where $\hat{D} = -e\vec{r}$ is the dipole moment operator which is represented by $\left(\begin{smallmatrix} 0 & D_{12} \\ D_{21} & 0 \end{smallmatrix}\right)$. Where D_{ij} is the matrix element $\langle i|\hat{D}|j\rangle$ and $|i\rangle$ and $|j\rangle$ are the ground and excited states of the two-level atom. The diagonal matrix elements are zero since $\langle i|\hat{D}|i\rangle$ results in an integrand that is odd, thus the integral gives zero, bearing in mind that $\hat{D}$ is an odd function. (Grynberg et al., 2010). The

expectation value $\langle D \rangle$ in matrix form is

$$\begin{aligned}
\langle D \rangle &= Tr\left[\begin{pmatrix} \rho_{11} & \rho_{12} \\ \rho_{21} & \rho_{22} \end{pmatrix}\begin{pmatrix} 0 & D_{12} \\ D_{21} & 0 \end{pmatrix}\right] && (5.18)\\
&= Tr\left[\begin{pmatrix} \rho_{12}D_{21} & \rho_{11}D_{12} \\ \rho_{22}D_{21} & \rho_{21}D_{12} \end{pmatrix}\right] && (5.19)\\
&= \rho_{12}D_{21} + \rho_{21}D_{12} && (5.20)\\
&= \rho_{12}D_{21} + \ c.c. && (5.21)
\end{aligned}$$

This gives

$$\langle D \rangle = \imath\frac{\Omega_1}{2}\frac{\gamma + \imath(\omega_0 - \omega)}{(\omega_0 - \omega)^2 + \gamma^2 + \Omega_1^2\frac{\gamma}{\Gamma_{sp}}}D_{21} \qquad (5.22)$$

where $\Omega_1 = -D_{12} \cdot \frac{\vec{E}}{\hbar}$ resulting in

$$\langle D \rangle = \imath\frac{|D_{12}|^2}{2\hbar}\frac{\gamma + \imath(\omega_0 - \omega)}{(\omega_0 - \omega)^2 + \gamma^2 + \Omega_1^2\frac{\gamma}{\Gamma_{sp}}}E_0 e^{-\imath\omega t} + c.c. \qquad (5.23)$$

The total polarization due to the probe beam is

$$\begin{aligned}
\langle P \rangle &= \frac{N}{V}\langle D \rangle \\
&= \frac{N}{V}\imath\frac{|D_{12}|^2}{2\hbar}\frac{\gamma + \imath(\omega_0 - \omega)}{(\omega_0 - \omega)^2 + \gamma^2 + \Omega_1^2\frac{\gamma}{\Gamma_{sp}}}E_0 e^{-\imath\omega t} + c.c. && (5.24)
\end{aligned}$$

In equation (5.24), $\frac{N}{V}$ represents the number of atoms per unit volume. We use this in Maxwell's equation. But the number of atoms in the ground state is altered by the pump beam. Using equation (5.14), the fraction of atoms that are available and in the ground state is given by

$$\begin{aligned}
\rho_{11} - \rho_{22} &= 1 - 2\rho_{22} && (5.25)\\
&= 1 - \frac{\Omega_2^2}{\Gamma_{sp}}\frac{\gamma}{(\omega_0 - \omega_2)^2 + \gamma^2 + \Omega_2^2\frac{\gamma}{\Gamma_{sp}}} && (5.26)
\end{aligned}$$

and is unity for all ω except close to $\omega_2 = \omega_0$ where ω_2 is the frequency of the pump beam as seen by the atoms moving with velocity v. These are the atoms that partake in polarization.

The above assumes all atoms are stationary, but the atoms however will have thermal motion. The velocities of the atoms will be distributed according to the Maxwell Boltzmann distribution, Figure 5.5, which was generated from

$$g_{MB}(v) = \frac{1}{\sqrt{\pi} v_0} e^{-\frac{v^2}{v_0^2}} \tag{5.27}$$

where $v_0 = \sqrt{2k\frac{Temp}{mass}}$ is the distribution parameter, or deviation, and $g_{MB}(v)dv$ is the number of atoms in the interval from v to $v + dv$.

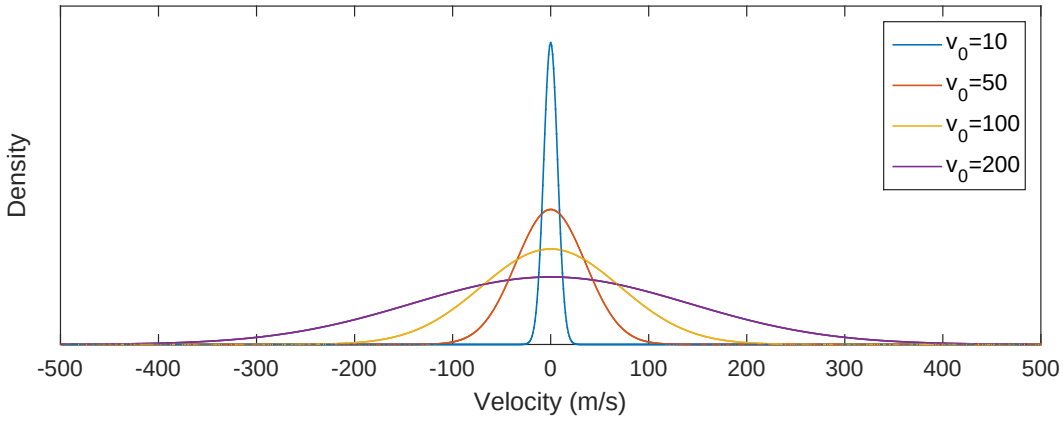

Figure 5.5: *Maxwell Boltzmann distribution showing the density of atoms across a particular range of velocities. As velocity increases, the density of atoms having zero velocity decreases.*

The thermal motion of the atoms creates a Doppler shift in the absorption and emission of laser light. If an atom is moving toward the laser beam, the atom *sees* the laser beam as blue shifted. If an atom is moving away from

the laser beam, the atom *sees* the laser beam as red shifted. We therefore need to sum up the polarization due to all the atoms. The final polarization (see for example Levenson (1982)) is then

$$\begin{aligned}\langle P\rangle_{total} &= \int g_{MB} \times (\rho_{11}-\rho_{22}) \times \langle P\rangle \\ &= \int dv \left[\frac{1}{\sqrt{\pi}v_0}e^{-\frac{v^2}{v_0^2}}\right]\left[1-\frac{\Omega_2^2}{\Gamma_{sp}}\frac{\gamma}{(\omega_0-\omega_2)^2+\gamma^2+\Omega_2^2\frac{\gamma}{\Gamma_{sp}}}\right]\ldots \\ &\quad \ldots\left[\frac{N}{V}\frac{|D_{12}|^2}{2\hbar}\frac{\imath\gamma+(\omega_0-\omega_1)}{(\omega_0-\omega_1)^2+\gamma^2+\Omega_1^2\frac{\gamma}{\Gamma_{sp}}}E_0e^{-\imath\omega t}\right] \qquad (5.28)\end{aligned}$$

where $\omega_1 = \omega(1+\frac{\nu}{c})$ (frequency of the probe beam seen by the atoms) and $\omega_2 = \omega(1-\frac{\nu}{c})$ (frequency of the pump beam seen by the atoms) cater for the Doppler shift of the atoms with velocity ν (Levenson, 1982).

5.3 Results

5.3.1 Absorption Spectroscopy

First we analyse the system with all the atoms having zero velocity and interacting with the probe beam alone. Recall, $\vec{P} = \varepsilon_0\chi\frac{\vec{E}}{2}e^{-\imath\omega t}$ where χ is the complex dielectric susceptibility. Polarization due to the probe beam is given by equation (5.24). Equating these two equations, neglecting the Ω_1 term in the denominator at low intensity and making χ the subject gives

$$\chi = \frac{N}{V}\frac{|D_{12}|^2}{\varepsilon_0\hbar}\frac{(\omega_0-\omega)+\imath\gamma}{(\omega_0-\omega)^2+\gamma^2} \qquad (5.29)$$

We only consider the imaginary part of equation (5.29) as this represents the absorption of the atomic vapour. This is then used in equation (5.10) which

results in the analytical solution (Beer's law)

$$|I| = I_0 e^{-2\alpha z} \tag{5.30}$$

where I is the electric field intensity and

$$\alpha = \frac{\omega}{2\varepsilon_0 nc} \frac{N}{V} \frac{|D_{12}|^2}{2\hbar} \frac{\gamma}{(\omega_0 - \omega)^2 + \gamma^2} \tag{5.31}$$

is the attenuation coefficient (Grynberg et al., 2010; Meystre and Sargent, 2007; Lambropoulos and Petrosyan, 2006).

This demonstrates absorption and is depicted by Figure 5.6. Figure 5.6 also shows a comparison between the analytical solution (red dashed star curve), where I is calculated using equation (5.30), and the numerical solution (blue dashed square curve), where I is obtained by solving equation (5.28) together with equation (5.5). In these ω_2 and v_0 are set to zero. In Appendix A, Figure A.3 shows a simple flowchart of the numerical calculation. Figure 5.6 shows satisfactory agreement between the two solutions where the probe beam intensity is measured at and close to atomic resonance.

Another way in which absorption can be observed is by simulating the intensity of the beam across the length of the tube as shown in Figure 5.7.

When the laser frequency is much less than the atomic resonant frequency, $\omega_0 \gg \omega$, the probe beam intensity does not significantly change throughout the length of the tube as depicted by the black (- - -) curve in Figure 5.7. This is similar for the case when the laser frequency is much greater than the atomic resonant frequency, $\omega_0 \ll \omega$, depicted by the black (. . .) curve in Figure 5.7. When the laser frequency is set to the atomic resonant frequency, $\omega_0 = \omega$, the red (—) curve in Figure 5.7 arises. This curve indicates that

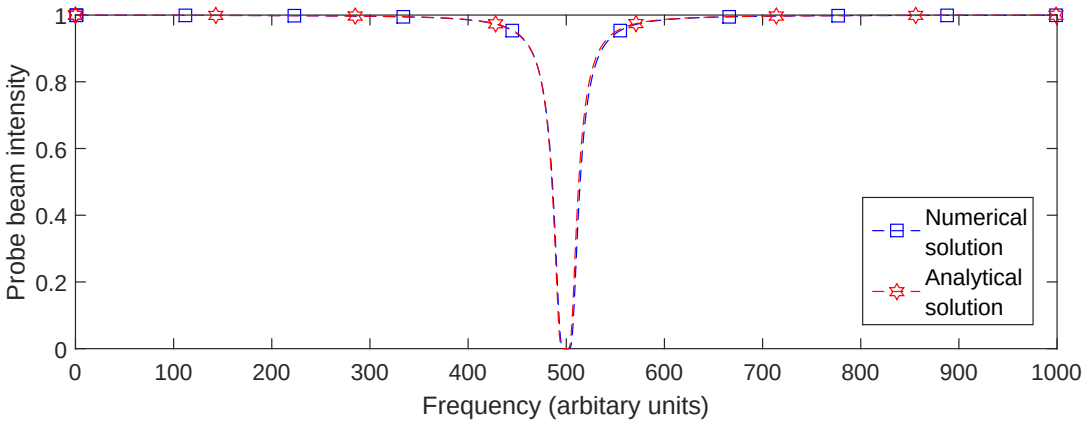

Figure 5.6: *A comparison between the analytical (red) and numerical (blue) solution where the probe beam intensity is measured at and close to atomic resonance.*

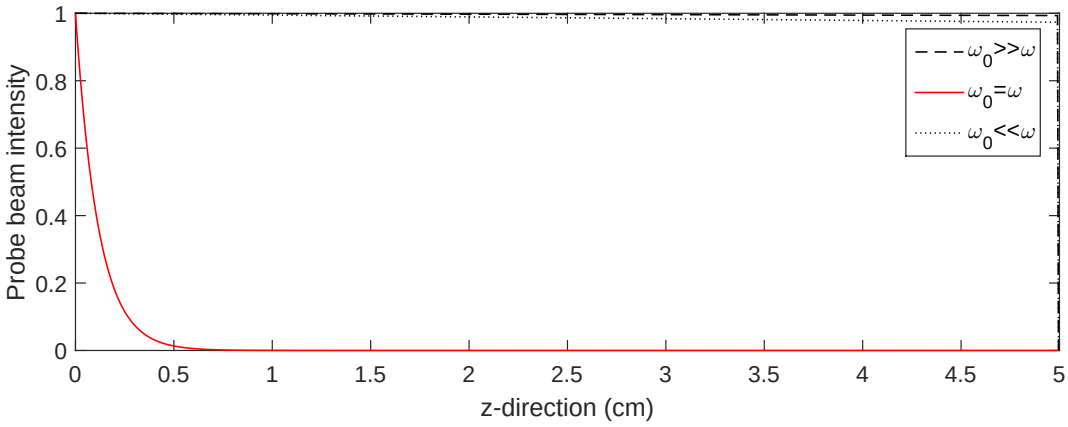

Figure 5.7: *Laser beam intensity measured across the length of a gaseous sample. In the above, ω_0 corresponds to the atomic resonant frequency and ω is the laser frequency. Absorption can be seen when $\omega_0 = \omega$, the red curve.*

the laser beam intensity drops exponentially across the tube - the beam is absorbed by the atoms in the sample.

5.3.2 Saturated Absorption Spectroscopy

An introduction of the second laser beam E_2 (pump beam), having a stronger electric field than the probe beam E_1, results in the ground and excited state populations of the atoms to be altered.

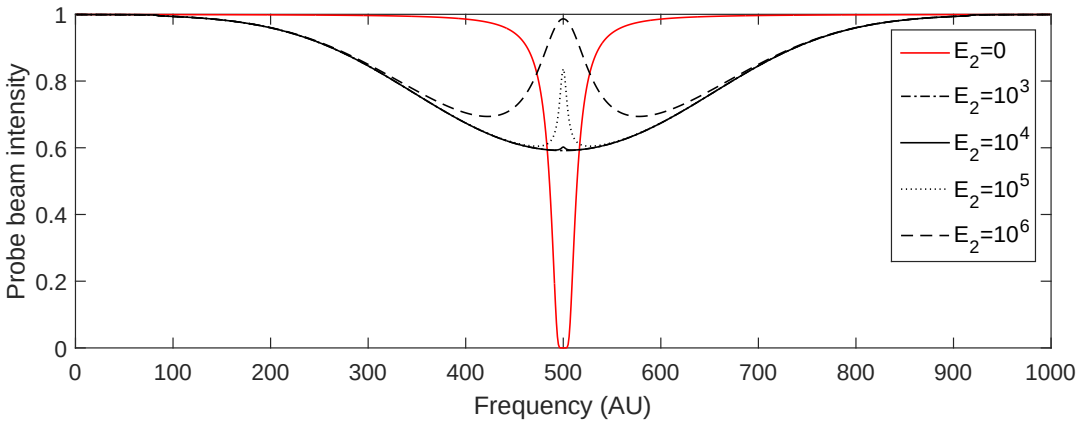

Figure 5.8: *The probe beam intensity E_1, with increasing values of the pump beam field, E_2. The red curve depicts the probe beam intensity for all atoms having zero velocity and with the pump beam electric field being zero. The black curves were generated taking into account the thermal velocities of the atoms and increasing the pump beam electric field.*

The electric field of the pump beam is made strong enough to saturate the sample, therefore changing the measured absorption. Figure 5.8 demonstrates this change where the red (—) curve depicts the probe beam intensity for all atoms having zero velocity and the pump beam electric field being zero. The thermal velocities of the atoms are then taken into account and the pump beam electric field is gradually increased. From Figure 5.8 the

various black curves depict the effect of the pump beam on the sample. It can be seen that when the thermal velocities are taken into account the absorption profile is broadened whilst the absorption at and close to resonance is decreased (showing the true Lorentzian profile) resulting in the intensity to increase. We assume in the above that the pump beam is strong enough so that it remains unchanged as it propagates through the sample.

A saturated absorption experiment was done in our laboratory using rubidium (^{87}Rb) with an external cavity diode laser (ECDL) (Wyngaard, 2017). The result of the $F = 1 \rightarrow F' = 0, 1, 2$ transitions can be seen in Figure 5.9. These levels are discussed in Chapter 2.

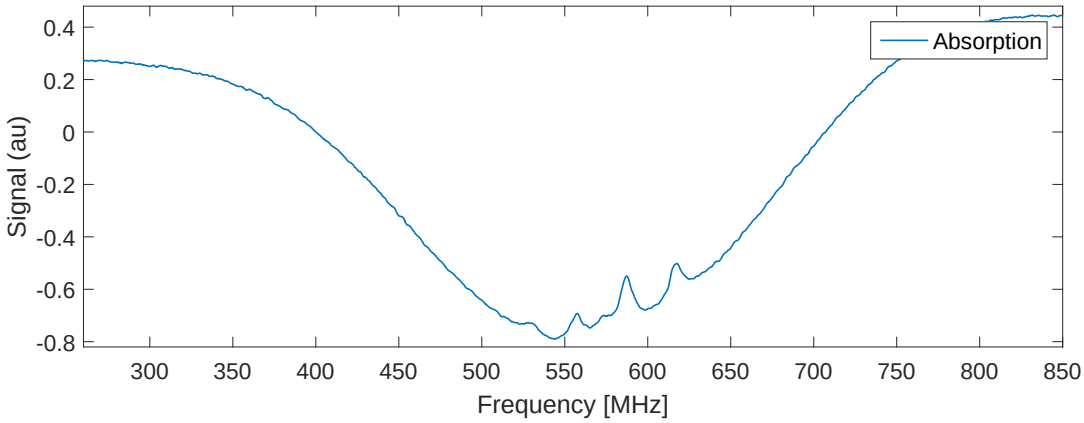

Figure 5.9: *Experimental result of saturated absorption spectroscopy for rubidium (^{87}Rb) for $F = 1 \rightarrow F' = 0, 1, 2$ transition (Wyngaard, 2017).*

Here we should see six peaks because there are three excited states and three crossover resonances[2]. However, only five peaks appear as two of the peaks are too close to resolve and appear as one. These are the most prominent peaks that arise from the laser beams interacting with two velocity

[2]A cross over resonance occurs when the laser is detuned halfway between two excited states that share a common ground state.

groups. Note the absorption peaks are shifted to the right. The reason for this is not clear at this stage.

5.4 Summary

We have investigated the interactions between two-level atoms and laser beam intensity. Matlab® has been used to simulate the processes of absorption spectroscopy and saturated absorption spectroscopy. Maxwell's equations for the electric field is solved numerically. In using Maxwell's equations the polarization of the atoms was required. This was determined from the optical Bloch equations.

In saturated absorption spectroscopy a pump beam and a probe laser beam are used. The effects of saturation by the pump beam on the probe beam has been demonstrated. This shows up as Lorentzian peaks superimposed on the Doppler broadened spectra. While the atoms have thermal velocities, these Lorentzian peaks are due solely to atoms with zero velocity.

Chapter 6

Four-wave mixing

6.1 Introduction

We now look at the non-linear process called four-wave mixing that occurs when two or more pump beams, having different frequencies, interact with four different levels of a non-linear medium. We make use of general energy levels in a diamond configuration to familiarise ourselves with possible experimental outcomes when using rubidium, for example, in a four-wave mixing experiment.

For our theoretical and computational analysis we use a semi-classical approach where the atom is treated quantum mechanically and the photons are treated classically. We make use of perturbation theory to find the third and

fourth order density matrix elements from which the atomic polarization is determined (see for example Boyd, Malcuit, Gauthier, and Rzaewski (1987); Levenson (1982)). Maxwell's equations are then used to find the intensities of the generated photons.

This chapter discusses some of the theory pertaining to four-wave mixing and briefly gives a derivation of the density matrix elements in Section 6.2. This is followed by the results obtained from simulations in Section 6.3. The full theoretical analysis of all the required equations is quite elaborate and complicated. Therefore, in this chapter we present the key ideas and equations needed to understand four-wave mixing in a diamond configuration. The full details of all the derivations are given in Appendix C. Some of our findings have been published in Patel, De Jager, Nkosi, Wyngaard, and Govender (2017).

6.2 Theoretical Analysis

We study the non-linear parametric process of four-wave mixing by having two pump beams, of different frequencies, interact with a non-linear medium. Figure 6.1 shows a possible scenario involving a diamond energy level structure where $|1\rangle$, $|2\rangle$, $|3\rangle$ and $|4\rangle$ are four relevant energy levels of the atom with $|1\rangle$ being the ground state and $|2\rangle$, $|3\rangle$ and $|4\rangle$ being excited states. In our analysis co-propagating beams, E_1 and E_2, having different wavelengths are used as pumps beams. These pump beams interact with the atom resulting in polarization. The non-linear properties of the atom causes the polarization to contain terms at new frequencies that lead to the radiation of light at these new frequencies. We therefore investigate the production/variation of E_3 and E_4 across the longitudinal section of the sample.

Four-wave mixing is the parametric process of annihilating two pump

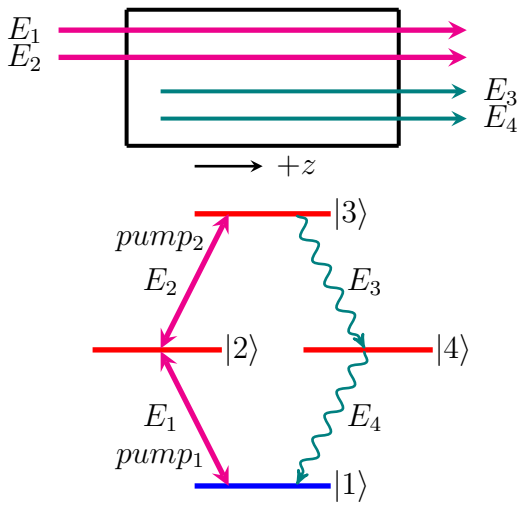

Figure 6.1: *Four-wave mixing geometry. E_1 and E_2 represent the electric fields of the pump beams and E_3 and E_4 represent the internally generated photons.*

photons, and generating two emitted photons without transferring atomic population to excited levels. In our simulation we chose four levels in a diamond configuration that could represent those of rubidium as shown in Figure 6.2. We are interested in this process since it is one scheme for generating entangled photons.

The above is different from a non-parametric process where atoms are transferred (pumped) into $|2\rangle$, $|3\rangle$ and $|4\rangle$ stepwise. So states $|2\rangle$, $|3\rangle$ and $|4\rangle$ will be populated. If atoms are transferred into states $|2\rangle$, $|3\rangle$ and $|4\rangle$ then, strictly speaking, one does not have four-wave mixing happening. There is one-photon absorption twice and spontaneous or stimulated one-photon emission twice. (*"Decay" usually means spontaneous emission.*) In the case of spontaneous decay, the generated photons are not coherent with one another.

These two processes described above are in competition with each other.

Therefore if four-wave mixing is the desired process, then one should avoid having the pump photons exactly on resonance with the dipole allowed transitions (e.g. pump_1 on resonance with the $|1\rangle \rightarrow |2\rangle$ transition frequency) so that one-photon absorption does not dominate.

Figure 6.2 shows the energy level structure we have used to examine four-wave mixing. These levels, in principle, could represent the levels in rubidium as shown. The states shown in brackets represent those of ^{87}Rb. E_1 to E_4 are the corresponding energies of each level (these should not be confused with the electric fields), ω_1 and ω_2 are the frequencies of two pump laser beams and ω_3 and ω_4 are the frequencies of two internally generated photons.

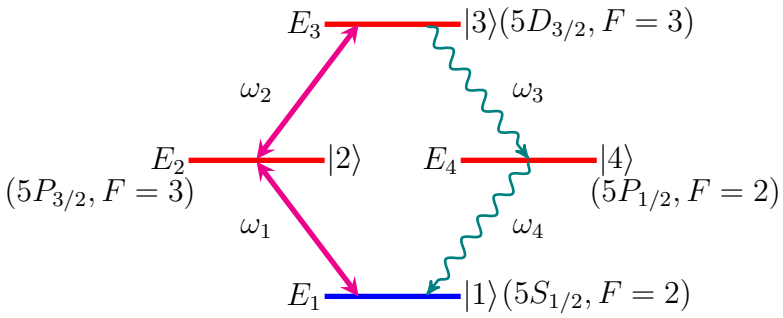

Figure 6.2: *Four-wave mixing geometry showing the relevant states of rubidium 87. See text for description of variables.*

We will assume that the pump laser beams are strong enough so that they do not get depleted as they propagate through the atomic ensemble. We will also assume that all photons propagate in the positive z-direction. The atomic levels are assumed to be such that the photons of frequency ω_1, ω_2, ω_3 and ω_4 couple only transitions between $|1\rangle \leftrightarrow |2\rangle$, $|2\rangle \leftrightarrow |3\rangle$, $|3\rangle \leftrightarrow |4\rangle$ and $|4\rangle \leftrightarrow |1\rangle$, respectively, that is they are very much detuned compared to the other transitions.

We now explain the derivation of the equation needed for predicting the electric fields, E_3 and E_4. As mentioned previously, the full details of these derivations are provided in Appendix C. The total electric field is then

$$E = \sum_{i=1}^{4} \left(\tilde{E}_i e^{-\imath\omega_i t} + c.c. \right) \tag{6.1}$$

where

$$\tilde{E}_i = \mathcal{E}_i(z) e^{\imath k_i z} \tag{6.2}$$

The behaviour of the electric fields E_3 and E_4 corresponding to frequencies ω_3 and ω_4 respectively are described by Maxwell's equations:

$$\frac{\partial}{\partial z} E_3(z) = \imath \frac{\omega_3}{2\epsilon c} \frac{N}{V} \mu_{34} \rho_{34}^{(3)} \tag{6.3}$$

$$\frac{\partial}{\partial z} E_4(z) = \imath \frac{\omega_4}{2\epsilon c} \frac{N}{V} \mu_{41} \rho_{41}^{(3)} \tag{6.4}$$

where $\rho_{ij}^{(3)}$ are the third order density matrix elements and are obtained from the master equation as described below. These equations, equations (6.3) and (6.4), are derived from Maxwell's wave equation (given in Chapter 5, equation (5.5)) where we have written the polarization in terms of $\rho_{34}^{(3)}$ and $\rho_{41}^{(3)}$.

The total Hamiltonian is

$$H = H_0 + H_I \tag{6.5}$$

where H_0 is the unperturbed Hamiltonian, $H_I = -\hat{\vec{\mu}} \cdot \vec{E}$ and $-\hat{\mu}$ is the dipole

moment of the atom. We will use the following as a basis:

$$|\Psi_1\rangle = e^{-\imath E_1 t/\hbar}|1\rangle \tag{6.6}$$
$$|\Psi_2\rangle = e^{-\imath E_2 t/\hbar}|2\rangle \tag{6.7}$$
$$|\Psi_3\rangle = e^{-\imath E_3 t/\hbar}|3\rangle \tag{6.8}$$
$$|\Psi_4\rangle = e^{-\imath E_4 t/\hbar}|4\rangle \tag{6.9}$$

In the above basis

$$H_0 = \begin{pmatrix} E_1 & 0 & 0 & 0 \\ 0 & E_2 & 0 & 0 \\ 0 & 0 & E_3 & 0 \\ 0 & 0 & 0 & E_4 \end{pmatrix} \tag{6.10}$$

and $H'_I = e^{-\imath H_0 t/\hbar}\, H_I\, e^{\imath H_0 t/\hbar}$ becomes

$$E \begin{pmatrix} 0 & -\mu_{12}e^{\imath\omega_{12}t} & -\mu_{13}e^{\imath\omega_{13}t} & -\mu_{14}e^{\imath\omega_{14}t} \\ -\mu_{21}e^{\imath\omega_{21}t} & 0 & -\mu_{23}e^{\imath\omega_{23}t} & 0 \\ -\mu_{31}e^{\imath\omega_{31}t} & -\mu_{32}e^{\imath\omega_{32}t} & 0 & -\mu_{34}e^{\imath\omega_{34}t} \\ -\mu_{41}e^{\imath\omega_{41}t} & 0 & -\mu_{43}e^{\imath\omega_{43}t} & 0 \end{pmatrix} \tag{6.11}$$

where $\omega_{ij} = (E_i - E_j)/\hbar$ and $\mu_{ij} = \langle i|\hat{\mu}|j\rangle$. Then the Liouville-von Neumann equation (also known as the master equation) that we solve is

$$\dot{\rho} = -\frac{\imath}{\hbar}\,[H'_I, \rho] + relaxation\, terms \tag{6.12}$$

Using perturbation theory we let

$$\rho = \rho^{(0)} + \lambda\rho^{(1)} + \lambda^2\rho^{(2)} + ... \tag{6.13}$$

We also expand each $\rho^{(i)}$ in frequency as well and we also replace H'_I by $\lambda H'_I$.

$$\begin{aligned}[\dot{\rho}^{(0)} + \lambda\dot{\rho}^{(1)} + \lambda^2\dot{\rho}^{(2)} + \lambda^3\dot{\rho}^{(3)} + ...] &= -\frac{\imath}{\hbar}[\lambda H'_I, (\rho^{(0)} + \lambda\rho^{(1)} + \lambda^2\rho^{(2)} + \lambda^3\rho^{(3)} + ...)] \\ &\quad + relaxation\, terms \end{aligned} \tag{6.14}$$

After expanding and grouping the terms by order we get the following set of equations:

$$\lambda^0 : \qquad \lambda^0\dot{\rho}^{(0)} = 0 + relaxation\, terms \tag{6.15}$$

$$\lambda^1 : \qquad \lambda^1\dot{\rho}^{(1)} = [\lambda H'_I, \rho^{(0)}] + relaxation\, terms \tag{6.16}$$

$$\lambda^2 : \qquad \lambda^2\dot{\rho}^{(2)} = [\lambda H'_I, \lambda\rho^{(1)}] + relaxation\, terms \tag{6.17}$$

$$\lambda^3 : \qquad \lambda^3\dot{\rho}^{(3)} = [\lambda H'_I, \lambda^2\rho^{(2)}] + relaxation\, terms \tag{6.18}$$

$$\lambda^4 : \qquad \lambda^4\dot{\rho}^{(4)} = [\lambda H'_I, \lambda^3\rho^{(3)}] + relaxation\, terms \tag{6.19}$$

and so on.

For equation (6.15), the zero order, we assume $\rho^{(0)}_{11} = 1$ with all other terms being zero, i.e.

$$\rho^{(0)} = \begin{pmatrix} 1 & 0 & 0 & 0 \\ 0 & 0 & 0 & 0 \\ 0 & 0 & 0 & 0 \\ 0 & 0 & 0 & 0 \end{pmatrix} \tag{6.20}$$

We then solve equation (6.16) for the first order which results in the following density matrix

$$\rho^{(1)} = \begin{pmatrix} 0 & \tilde{\rho}^{(1)}_{12}e^{\imath\omega_{12}t} & 0 & \tilde{\rho}^{(1)}_{14}e^{\imath\omega_{14}t} \\ \tilde{\rho}^{(1)}_{21}e^{\imath\omega_{21}t} & 0 & 0 & 0 \\ 0 & 0 & 0 & 0 \\ \tilde{\rho}^{(1)}_{41}e^{\imath\omega_{41}t} & 0 & 0 & 0 \end{pmatrix} \tag{6.21}$$

where $\tilde{\rho}_{ij}$ are algebraic terms as a function of detuning, frequency separation and decay rates. Similarly equation (6.17) and equation (6.18) give

$$\rho^{(2)} = \begin{pmatrix} \tilde{\rho}_{11}^{(2)} & 0 & \tilde{\rho}_{13}^{(2)} e^{\imath\omega_{13}t} & 0 \\ 0 & \tilde{\rho}_{22}^{(2)} & 0 & \tilde{\rho}_{24}^{(2)} e^{\imath\omega_{24}t} \\ \tilde{\rho}_{31}^{(2)} e^{\imath\omega_{31}t} & 0 & 0 & 0 \\ 0 & \tilde{\rho}_{42}^{(2)} e^{\imath\omega_{42}t} & 0 & \tilde{\rho}_{44}^{(2)} \end{pmatrix} \tag{6.22}$$

and

$$\rho^{(3)} = \begin{pmatrix} 0 & \tilde{\rho}_{12}^{(3)} e^{\imath\omega_{12}t} & 0 & \tilde{\rho}_{14}^{(3)} e^{\imath\omega_{14}t} \\ \tilde{\rho}_{21}^{(3)} e^{\imath\omega_{21}t} & 0 & \tilde{\rho}_{23}^{(3)} e^{\imath\omega_{23}t} & 0 \\ 0 & \tilde{\rho}_{32}^{(3)} e^{\imath\omega_{32}t} & 0 & \tilde{\rho}_{34}^{(3)} e^{\imath\omega_{34}t} \\ \tilde{\rho}_{41}^{(3)} e^{\imath\omega_{41}t} & 0 & \tilde{\rho}_{43}^{(3)} e^{\imath\omega_{43}t} & 0 \end{pmatrix} \tag{6.23}$$

and equation (6.19) can be solved to give the fourth order population terms. The terms $\tilde{\rho}_{ij}^{(1)}$, $\tilde{\rho}_{ij}^{(2)}$ and $\tilde{\rho}_{ij}^{(3)}$ in the above density matrices are too cumbersome to include here. These can be viewed in Appendix C. The third order terms that are important for solving Maxwell's equation for the ω_3 and ω_4 terms are

$$\begin{aligned} \tilde{\rho}_{34}^{(3)} = \frac{1}{(\Delta_{34} - \imath\Gamma_{34})} \Bigg[& \frac{1}{\hbar^3} \frac{\mu_{21}\mu_{32}\mu_{14}\tilde{E}_1\tilde{E}_2\tilde{E}_4^*}{(\Delta_{42} + \imath\Gamma_{42})} \left(\frac{1}{(\Delta_{21} - \imath\Gamma_{21})} - \frac{1}{(\Delta_{41} + \imath\Gamma_{41})} \right) \\ & + \frac{1}{\hbar^3} \frac{\mu_{34}|\mu_{14}|^2\tilde{E}_3|\tilde{E}_4|^2}{\gamma_{41}} \left(\frac{2\Gamma_{41}}{\Delta_{41}^2 + \Gamma_{41}^2} \right) \\ & - \frac{1}{\hbar^3} \frac{\mu_{21}\mu_{32}\mu_{14}\tilde{E}_1\tilde{E}_2\tilde{E}_4}{(\Delta_{21} - \imath\Gamma_{21})(\Delta_{31} - \imath\Gamma_{31})} \\ & - \frac{1}{\hbar^3} \frac{\mu_{34}|\mu_{14}|^2\tilde{E}_3|\tilde{E}_4|^2}{(\Delta_{41} - \imath\Gamma_{41})(\Delta_{31'} - \imath\Gamma_{31})} \Bigg] e^{-\imath\omega_3 t} \end{aligned} \tag{6.24}$$

and

$$\tilde{\rho}_{41}^{(3)} = \frac{1}{(\Delta_{41} - \imath\Gamma_{41})}\Bigg[-\frac{1}{\hbar^3}\frac{|\mu_{12}|^2\mu_{41}|\tilde{E}_1|^2\tilde{E}_4}{\gamma_{21}}\left(\frac{2\Gamma_{21}}{\Delta_{21}^2+\Gamma_{21}^2}\right) - \frac{1}{\hbar^3}\frac{\mu_{41}|\mu_{14}|^2\tilde{E}_4|\tilde{E}_4|^2}{\gamma_{41}}\left(\frac{4\Gamma_{41}}{\Delta_{41}^2+\Gamma_{41}^2}\right) + \frac{1}{\hbar^3}\frac{\mu_{21}\mu_{32}\mu_{43}\tilde{E}_1\tilde{E}_2\tilde{E}_3}{(\Delta_{21}-\imath\Gamma_{21})(\Delta_{31}-\imath\Gamma_{31})} + \frac{1}{\hbar^3}\frac{|\mu_{34}|^2\mu_{41}|\tilde{E}_3|^2\tilde{E}_4}{(\Delta_{41}-\imath\Gamma_{41})(\Delta_{31'}-\imath\Gamma_{31})} - \frac{1}{\hbar^3}\frac{|\mu_{21}|^2\mu_{41}|\tilde{E}_1|^2\tilde{E}_4}{(\Delta_{42}-\imath\Gamma_{42})}\left(\frac{1}{(\Delta_{21}+\imath\Gamma_{21})}-\frac{1}{(\Delta_{41}-\imath\Gamma_{41})}\right)\Bigg]e^{-\imath\omega_4 t} \tag{6.25}$$

where Δ_{ij} represents the detuning between levels $|i\rangle$ and $|j\rangle$, Γ_{ij} represents the decay rate of the corresponding coherence ρ_{ij} and γ_{ij} represents the decay of the population ρ_{ii}. Equations (C.141), (C.140), (C.142) and (C.144) in Appendix C.6 for $\rho_{44}^{(4)}$, $\rho_{33}^{(4)}$, $\rho_{22}^{(4)}$ and $\rho_{11}^{(4)}$ are the fourth order terms giving us the populations of each state as the pump lasers' frequencies are varied, i.e. varying the detuning.

Using the following definition of Rabi frequencies

$$\begin{aligned}\Omega_1 &= \mu_{12}E_1/\hbar \\ \Omega_2 &= \mu_{23}E_2/\hbar \\ \Omega_3 &= \mu_{34}E_3/\hbar \\ \Omega_4 &= \mu_{41}E_4/\hbar\end{aligned} \tag{6.26}$$

we rewrite all the equations in terms of these Rabi frequencies and solve numerically self consistently together with Maxwell's equations for various values of z along the atomic ensemble and various values of detuning. Thus the Rabi frequencies are directly proportional to the electric fields of the various photon beams. The above approach is used for a different geometry of four-wave mixing by Boyd et al. (1987).

6.3 Results and discussion

We perform a numerical solution for the intensities of the ω_3 and ω_4 photons across the longitudinal section of the atomic ensemble in the direction z (see Figure 6.1). The z direction is discretized, and at each discretized point we compute $\tilde{\rho}_{34}^{(3)}$ and $\tilde{\rho}_{41}^{3}$ using equations (6.24) and (6.25) respectively. At $z = 0$ E_3 and E_4 are initialized with a very small value to get the process going. The $\tilde{\rho}_{34}^{(3)}$ and $\tilde{\rho}_{41}^{(3)}$ values are then used in Maxwell's equations (6.3) and (6.4) to determine the new values of E_3 and E_4. These values are then used in the next discretized z value. The process is repeated.

We provide plots of E_3 and E_4 (more correctly $|\Omega_3|^2$ and $|\Omega_4|^2$) versus z for various settings of detuning. In the present analysis we used the following parameters in the computations:

- $\frac{N}{V} \approx 10^8$
- $\mu_{ij} \approx 10^{-30}$
- $\gamma_{ij} \approx 10^9$
- $\Gamma_{ij} \approx 10^9$

These values were chosen based on typical values for rubidium (Steck, 2013, 2015). Also provided are the composite plots of intensities at the point where the lasers exit the sample. Discussions of each plot are provided immediately after each plot is presented. Note that we quote detuning in non-dimensional form relative to the decay rate Γ_{ij} of the corresponding density matrix elements coherence term.

To understand the plots presented we refer to the notation in Figure 6.3 which shows the four-wave mixing geometry with the pump$_1$ (Δ_{21}) and pump$_2$ (Δ_{32}) detunings. When neither of the beams have been detuned the process can occur with a maximum transfer of atomic populations. If pump$_1$ has a negative detuning, pump$_2$ needs to be positively detuned for maximum population transfer. Similarly, if pump$_1$ has a positive detuning, pump$_2$ needs to be negatively detuned. This should be noted when looking at Figures 6.12 to 6.17 where in each case one detuning value is kept constant while the other is varied and the intensities are then measured.

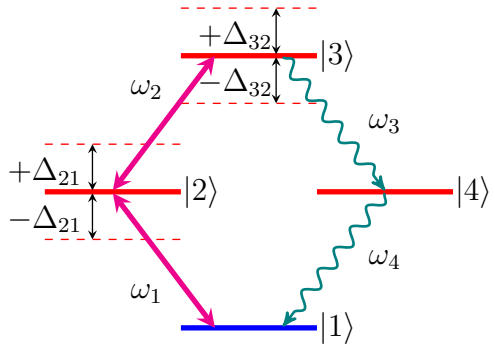

Figure 6.3: *Four-wave mixing geometry of a general atom showing positive and negative detuning.* ω_1 *and* ω_2 *are the frequencies of the pump beams and* ω_3 *and* ω_4 *are the frequencies of the generated photons.*

The variation in the intensities of the ω_3 and ω_4 photons can be seen as a function of distance along the sample length in Figures 6.4 and 6.5 as both pump beam detunings are varied. In both figures, plot **A** shows the variation of $|\Omega_3|^2$ and plot **B** shows the variation of $|\Omega_4|^2$. Figure 6.4 shows the intensities as the detuning of pump$_1$ (Δ_{21}/Γ_{21}) is varied while pump$_2$ (Δ_{32}/Γ_{32}) is kept at zero. Figure 6.5 shows the same thing but for pump$_1$ at zero and pump$_2$ being varied. We can see that the intensities of the internally generated photons grow exponentially. These intensities depend heavily on the detuning of the laser beams. At zero detuning (maroon

curve in all plots) the intensity is always greatest throughout the length of the tube. As the detuning is increased the intensity of the photon beams decrease. As detuning is increased there is still a growth in photon intensities, but of lower values compared to when there is zero detuning. While zero detuning results in maximum photon intensities, zero detuning will also result in population transfer between levels. This will increase spontaneous emission which is undesirable. This will be illustrated and discussed later on.

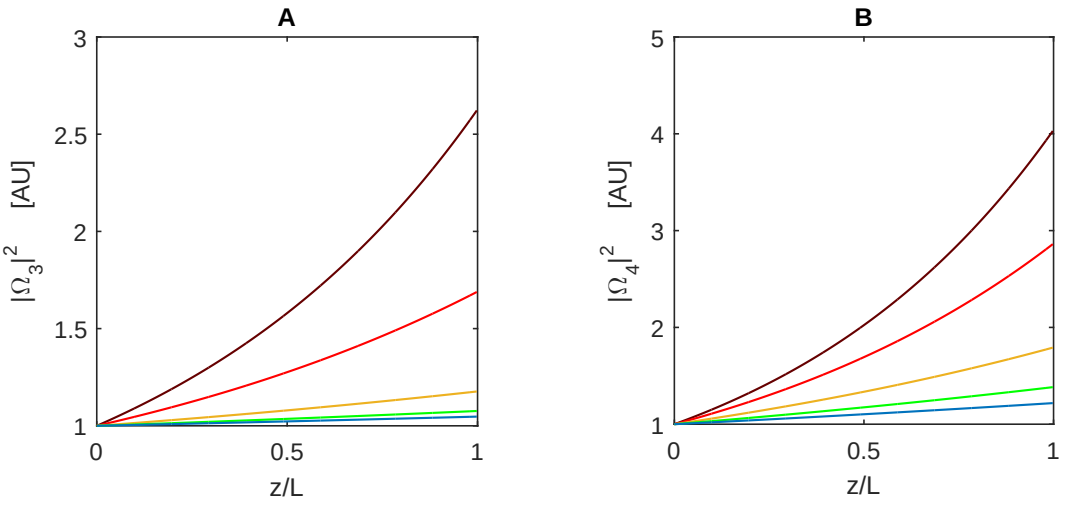

Figure 6.4: *Variation of Rabi frequencies* $|\mathbf{\Omega_3}|^\mathbf{2}$ *(**A**) and* $|\mathbf{\Omega_4}|^\mathbf{2}$ *(**B**) across the tube length as the detuning of pump*$_1$ *(*Δ_{21}/Γ_{21}*) is increased. Detuning values used: 0 (maroon), 0.5 (red), 1 (yellow), 1.5 (green) and 2 (blue).*

Figures 6.6 and 6.7 show colour maps for the Rabi frequencies Ω_3 and Ω_4 respectively as functions of detuning, Δ_{21}/Γ_{21} and Δ_{32}/Γ_{32}, and of z corresponding to the exit point of the laser beams. In both cases the pump$_1$ and pump$_2$ beams are both being detuned while the Rabi frequencies are being measured. Similarly, Figures 6.8 to 6.11 show colour maps of the population terms for the same detuning values. In all of the plots the values range from blue having a low intensity to maroon having a high intensity. Note, the

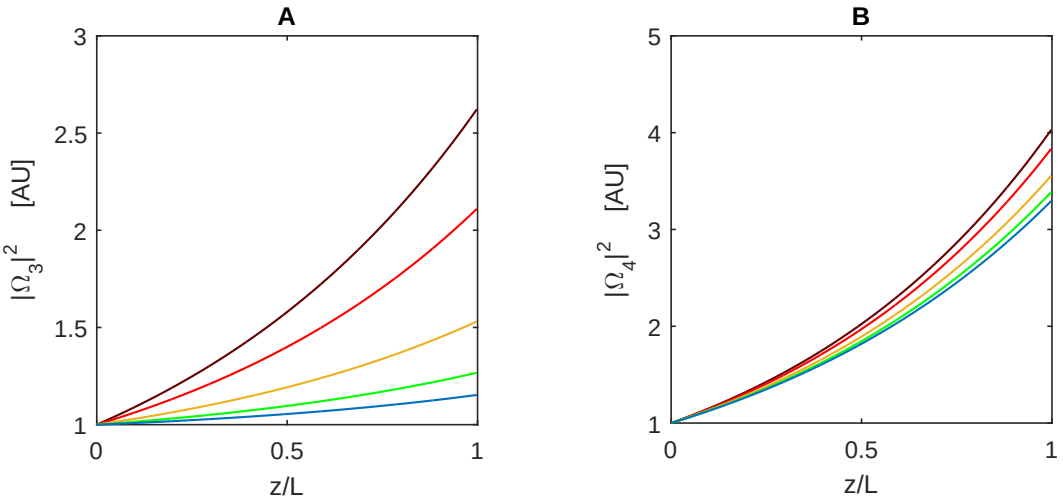

Figure 6.5: *Variation of Rabi frequencies* $|\mathbf{\Omega_3}|^\mathbf{2}$ ***(A)*** *and* $|\mathbf{\Omega_4}|^\mathbf{2}$ ***(B)*** *across the tube length as the detuning of pump*$_2$ (Δ_{32}/Γ_{32}) *is increased. Detuning values used: 0 (maroon), 0.5 (red), 1 (yellow), 1.5 (green) and 2 (blue).*

populations are for the atoms near the end of the tube where the beam exits.

From Figure 6.6, we see that the plot is elongated i.e. it is more sensitive to Δ_{21}. This is evident from the elliptical shape of the 2D intensity profile. For a fixed Δ_{32}, the intensity reduces much faster as Δ_{21} varies, compared to when Δ_{21} is fixed and Δ_{32} varies. This has also been demonstrated in the intensity versus tube length plots, Figures 6.4 and 6.5, for Ω_3 and Ω_4. As Δ_{21} approaches zero more atoms are transferred to $|2\rangle$. We also see this in Figure 6.8 and see very little variation with respect to Δ_{32} because the pump$_2$ beam only affects transfer between $|2\rangle$ and $|3\rangle$. Figure 6.9 shows that as Δ_{21} approaches zero ρ_{22} increases rapidly and as Δ_{32} approaches zero ρ_{22} decreases slightly. This is indicative of population transfer from $|1\rangle \rightarrow |2\rangle$ and $|2\rangle \rightarrow |3\rangle$ respectively. Figures 6.10 and 6.11 show an increase in the populations as the detunings approach zero. We also see that the plots are more sensitive to Δ_{21}.

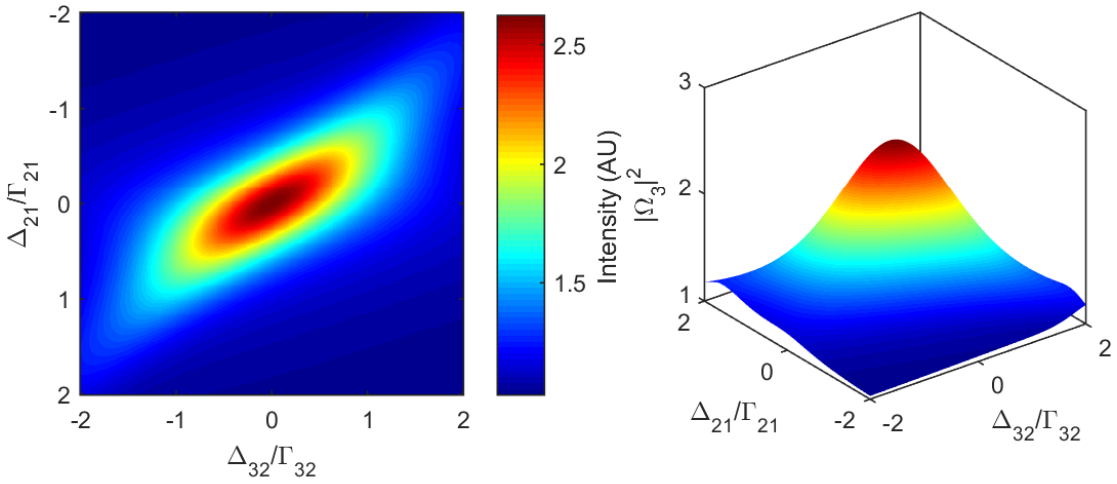

Figure 6.6: *Colour plot of* $|\mathbf{\Omega_3}|^\mathbf{2}$ *as a function of detuning of pump*$_1$ (Δ_{21}/Γ_{21}) *and pump*$_2$ (Δ_{32}/Γ_{32}).

In all the figures we see that the Rabi frequencies, Ω_3 and Ω_4, increase as the detuning decreases. As the detuning approaches zero the intensity profile begins to flatten. This is due to the fact that levels/states $|2\rangle$, $|3\rangle$ and $|4\rangle$ are also being populated as detuning is reduced and this does not give rise to coherent photons. The peak values of the populations also show a shift away from zero detuning, when one detuning is fixed the other detuning has to compensate for the shift. These can be seen in Figures 6.12, 6.14, 6.15 and 6.17.

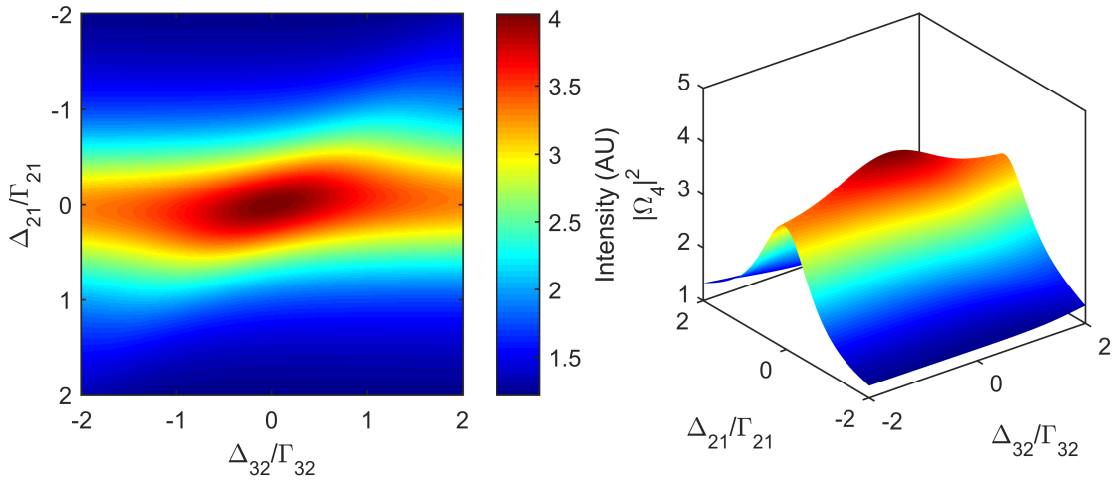

Figure 6.7: *Colour plot of* $|\mathbf{\Omega_4}|^\mathbf{2}$ *as a function of detuning of pump*$_1$ (Δ_{21}/Γ_{21}) *and pump*$_2$ (Δ_{32}/Γ_{32}).

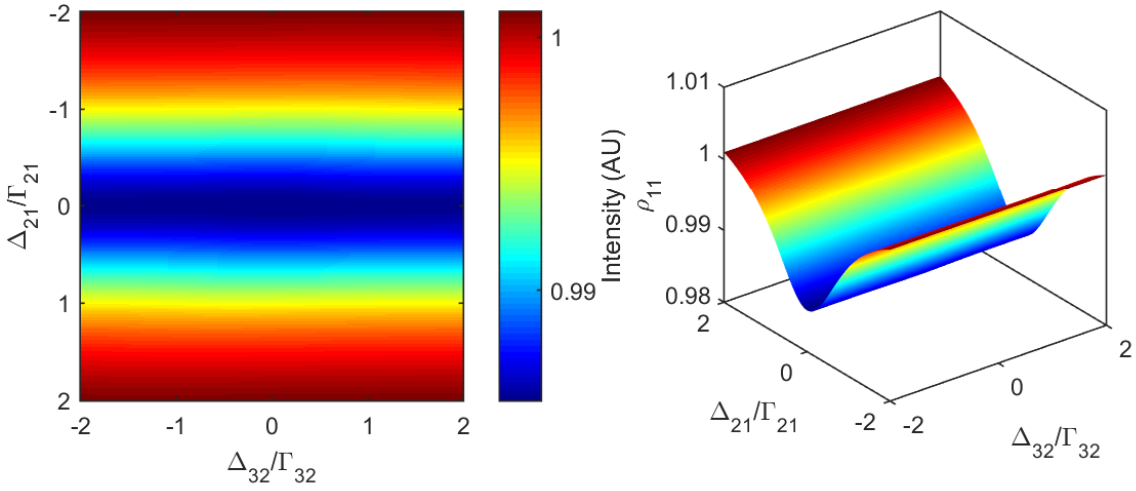

Figure 6.8: *Colour plot of the population of* $\rho_{\mathbf{11}}$ *as a function of detuning of pump*$_1$ (Δ_{21}/Γ_{21}) *and pump*$_2$ (Δ_{32}/Γ_{32}). *Note that this is the population of the ground state,* $|1\rangle$, *of the atoms near the end of the tube.*

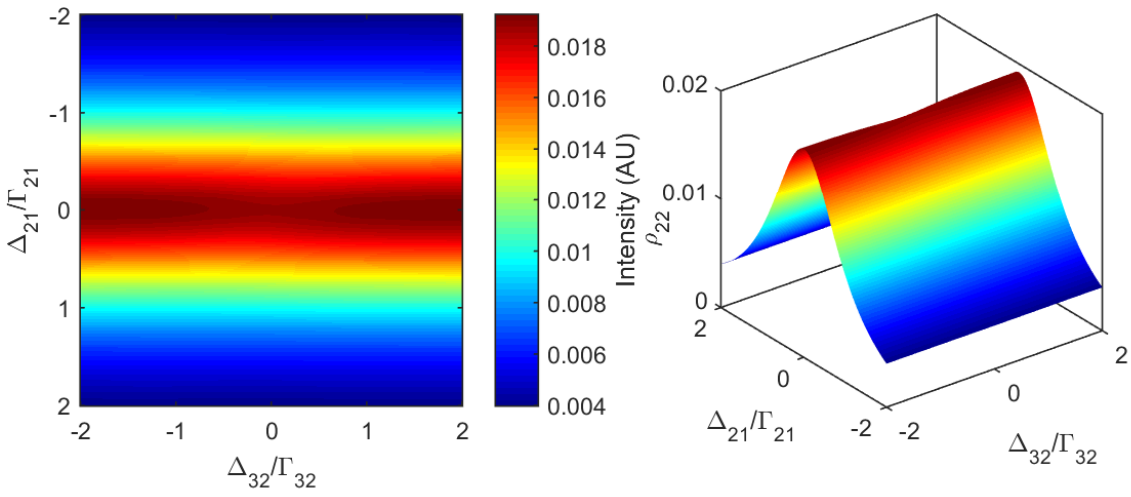

Figure 6.9: *Colour plot of the population of* $\rho_{\mathbf{22}}$ *as a function of detuning of pump*$_1$ (Δ_{21}/Γ_{21}) *and pump*$_2$ (Δ_{32}/Γ_{32}). *Note that this is the population of the excited state* $|2\rangle$ *of the atoms near the end of the tube.*

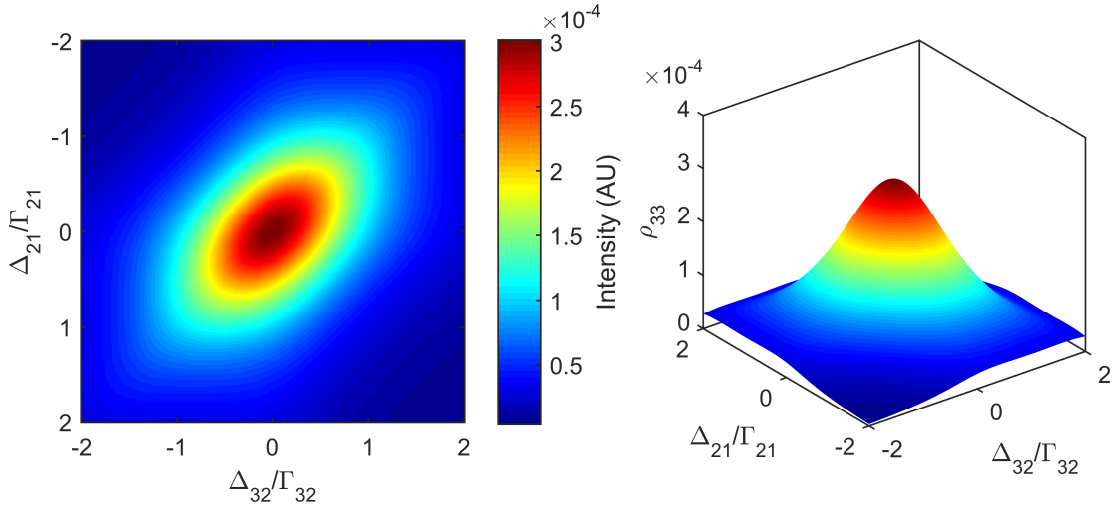

Figure 6.10: *Colour plot of the population of* $\rho_{\mathbf{33}}$ *as a function of detuning of pump*$_1$ (Δ_{21}/Γ_{21}) *and pump*$_2$ (Δ_{32}/Γ_{32}). *Note that this is the population of the excited state* $|3\rangle$ *of the atoms near the end of the tube.*

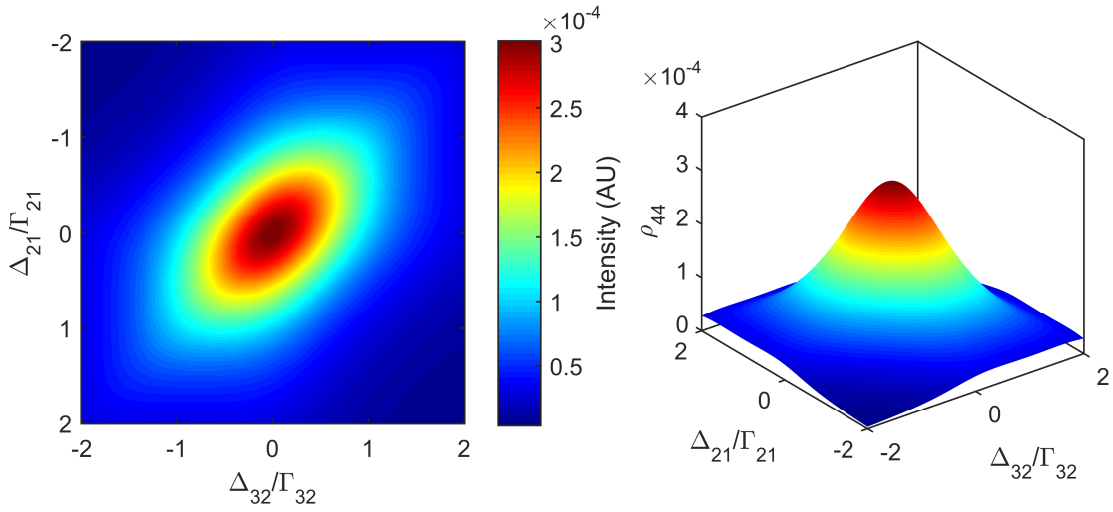

Figure 6.11: *Colour plot of the population of* $\rho_{\mathbf{44}}$ *as a function of detuning of pump*$_1$ (Δ_{21}/Γ_{21}) *and pump*$_2$ (Δ_{32}/Γ_{32}). *Note that this is the population of the excited state* $|4\rangle$ *of the atoms near the end of the tube.*

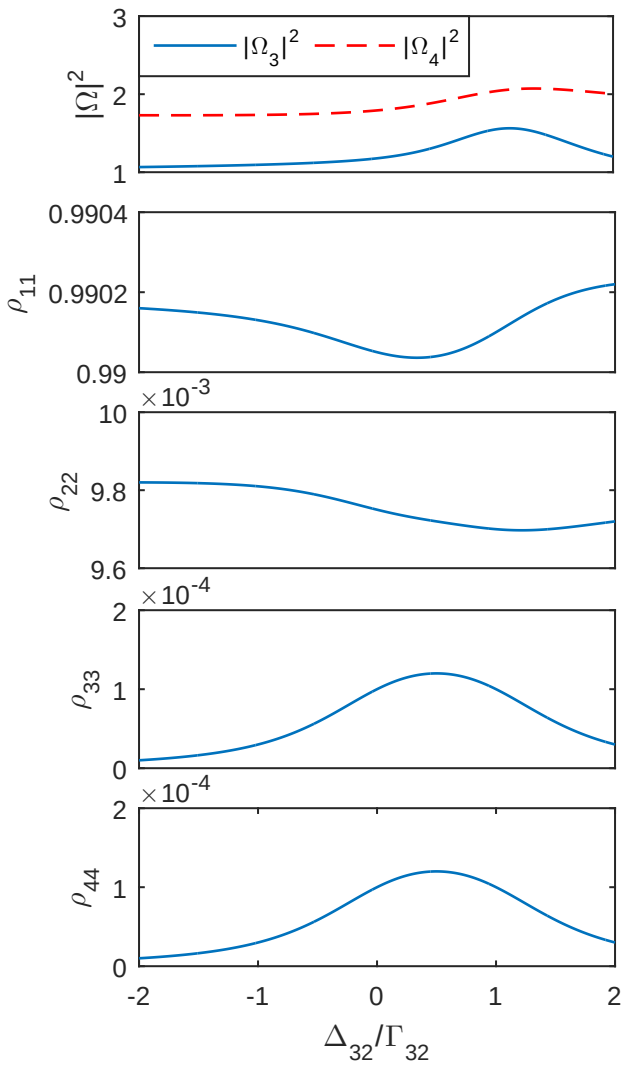

Figure 6.12: *Plots from top to bottom are of Rabi frequency ($|\Omega|^2$) and populations (ρ_{11}, ρ_{22}, ρ_{33} and ρ_{44}) as the pump$_2$ beam is varied (Δ_{32}/Γ_{32}). Pump$_1$ beam is kept constant at a negative detuning ($\Delta_{21} = -1000 \times 10^6$).*

Figure 6.12 shows results for $\Delta_{21} = -1000 \times 10^6$ as Δ_{32} is varied. Since Δ_{21} is large compared to ω_0 (large detuning), the atoms will not get excited from $|1\rangle \rightarrow |2\rangle$. From the slight decrease in ρ_{11} we can assume that most of the atoms have remained in the ground state. As Δ_{32} decreases, corresponding to a smaller detuning, we see ρ_{22} decreasing slightly. This is because atoms have been excited from $|2\rangle \rightarrow |3\rangle$. At the same time ρ_{33} and ρ_{44} have increased by approximately the same amount. Note that ρ_{33} and ρ_{44} are shifted to the right relative to zero detuning. This is due to the fact that pump$_2$ beam needs to be positively detuned to counteract the negative detuning of pump$_1$ beam in order to get maximum transfer of population to levels $|3\rangle$ and $|4\rangle$.

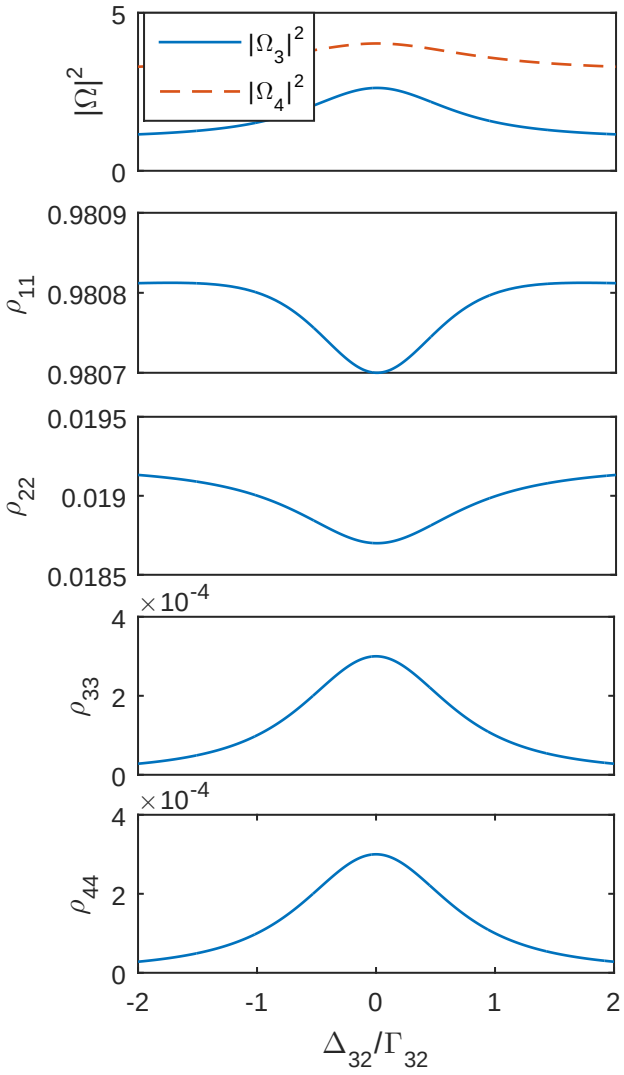

Figure 6.13: *Plots from top to bottom are of Rabi frequency ($|\Omega|^2$) and populations (ρ_{11}, ρ_{22}, ρ_{33} and ρ_{44}) as the pump$_2$ beam is varied (Δ_{32}/Γ_{32}). Pump$_1$ beam is kept constant at zero detuning ($\Delta_{21} = 0$).*

Figure 6.13 shows results for $\Delta_{21} = 0$ as Δ_{32} is varied. Since there is no detuning between $|1\rangle$ and $|2\rangle$, the atoms will get excited from $|1\rangle \rightarrow |2\rangle$. A significant decrease in ρ_{11} can be seen (comparing values away from $\Delta_{32}/\Gamma_{32} = 0$) when compared to ρ_{11} from Figure 6.12 indicating that the atoms have transitioned to $|2\rangle$. As a result the range of ρ_{22} has also increased. As Δ_{32} approaches zero (small detuning), ρ_{22} decreases, atoms are being transferred from $|2\rangle \rightarrow |3\rangle$. The population of ρ_{33} has therefore increased. An increase in the population of ρ_{44} can also be seen. All the plots show peaks and troughs at $\Delta_{32}/\Gamma_{32} = 0$.

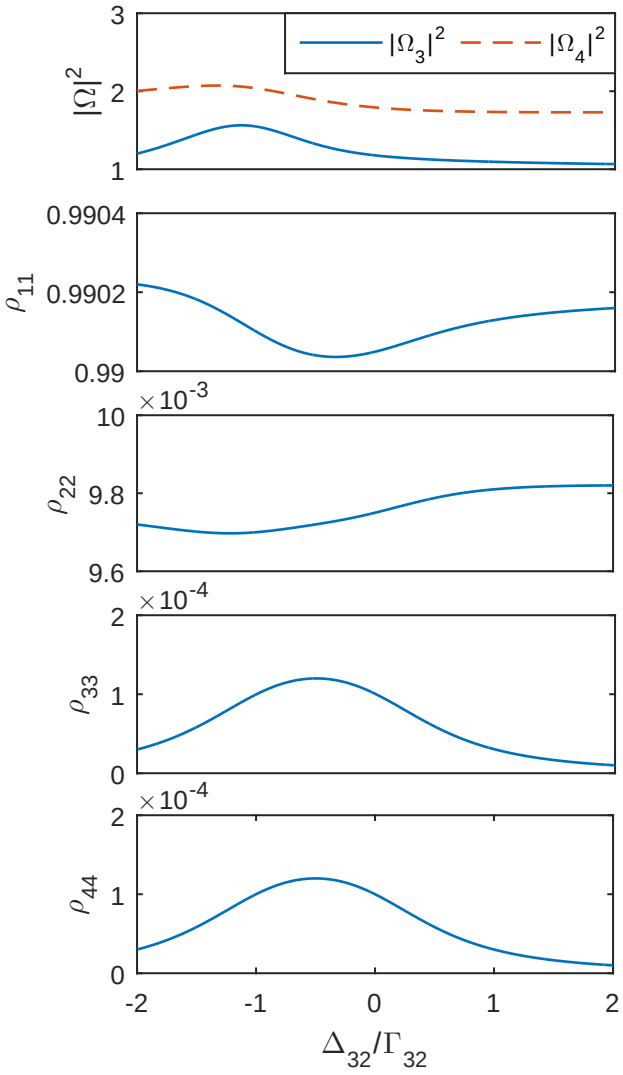

Figure 6.14: *Plots from top to bottom are of Rabi frequency ($|\Omega|^2$) and populations (ρ_{11}, ρ_{22}, ρ_{33} and ρ_{44}) as the pump$_2$ beam is varied (Δ_{32}/Γ_{32}). Pump$_1$ beam is kept constant at a positive detuning ($\Delta_{21} = 1000 \times 10^6$).*

Figure 6.14 shows results for $\Delta_{21} = 1000 \times 10^6$ as Δ_{32} is varied. Results here are similar to those of Figure 6.12 since Δ_{21} is large compared to ω_0 (large detuning). The difference here is that a positive detuning has been used for the pump$_1$ beam. We see that the plots have been shifted in the negative direction as opposed to being shifted in the positive direction previously for when there is a negative detuning. This is due to the fact that pump$_2$ beam needs to now be negatively detuned to counteract the positive detuning of pump$_1$ beam in order to get maximum transfer of population to levels $|3\rangle$ and $|4\rangle$.

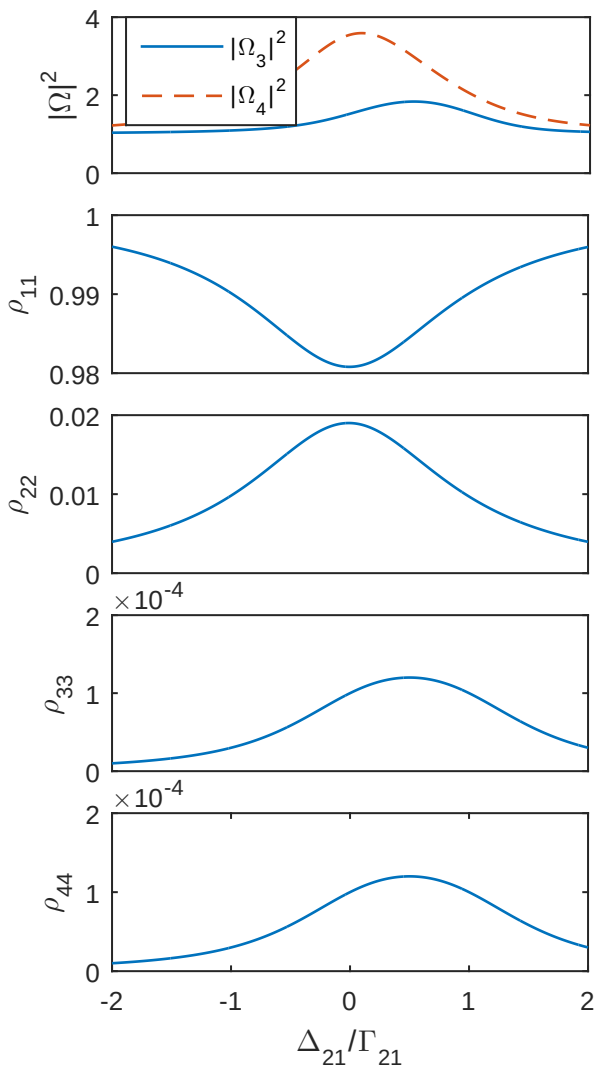

Figure 6.15: *Plots from top to bottom are of Rabi frequency ($|\Omega|^2$) and populations (ρ_{11}, ρ_{22}, ρ_{33} and ρ_{44}) as the pump$_1$ beam is varied (Δ_{21}/Γ_{21}). Pump$_2$ beam is kept constant at a negative detuning ($\Delta_{32} = -1000 \times 10^6$).*

Figure 6.15 shows results for $\Delta_{32} = -1000 \times 10^6$ as Δ_{21} is varied. Although Δ_{32} is large compared to ω_0 (large detuning), there are still atoms that will get excited from $|2\rangle \rightarrow |3\rangle$. As Δ_{21} decreases more atoms transfer to level $|2\rangle$ reaching a peak at $\Delta_{21} = 0$. The plots of ρ_{33} and ρ_{44} show shifted peaks due to the negative detuning of Δ_{32}.

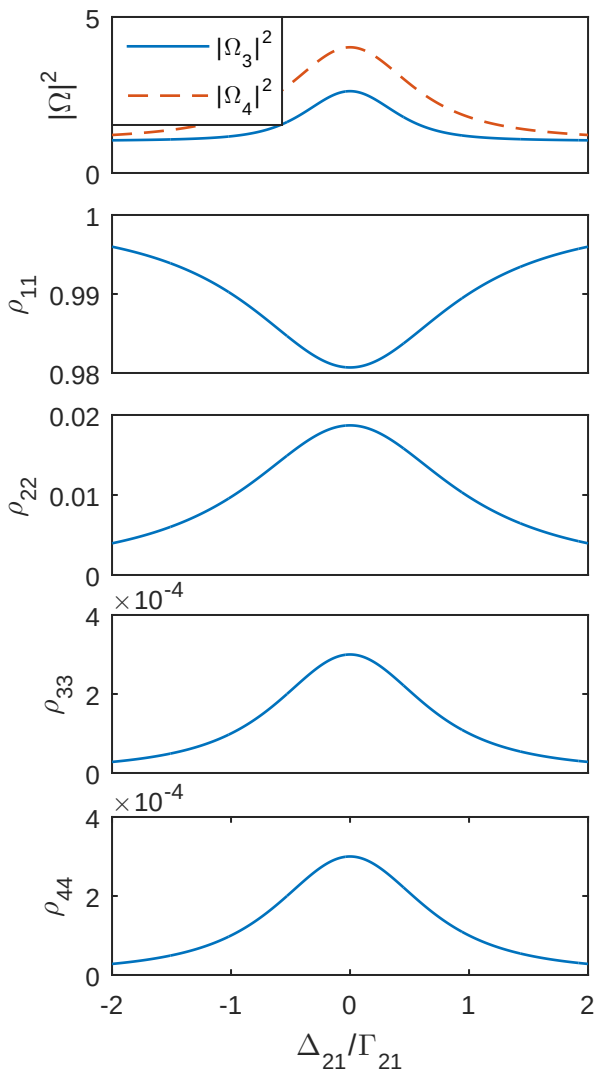

Figure 6.16: *Plots from top to bottom are of Rabi frequency ($|\Omega|^2$) and populations (ρ_{11}, ρ_{22}, ρ_{33} and ρ_{44}) as the pump$_1$ beam is varied (Δ_{21}/Γ_{21}). Pump$_2$ beam is kept constant at zero detuning ($\Delta_{32} = 0$).*

Figure 6.16 shows results for $\Delta_{32} = 0$ as Δ_{21} is varied. Since there is no detuning atoms will get excited from $|2\rangle \rightarrow |3\rangle$. Since $\Delta_{32} = 0$, as Δ_{21} is decreased there will be population transfer from $|1\rangle \rightarrow |2\rangle \rightarrow |3\rangle \rightarrow |4\rangle$. Thus all plots show peaks or troughs at $\Delta_{21} = 0$.

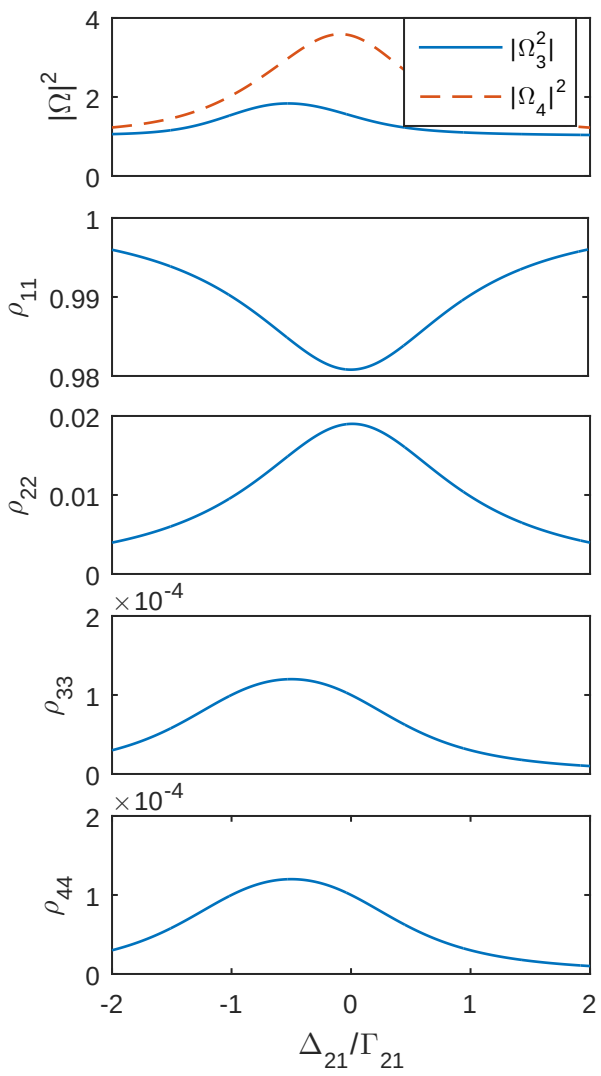

Figure 6.17: *Plots from top to bottom are of Rabi frequency ($|\Omega|^2$) and populations (ρ_{11}, ρ_{22}, ρ_{33} and ρ_{44}) as the pump$_1$ beam is varied (Δ_{21}/Γ_{21}). Pump$_2$ beam is kept constant at a positive detuning ($\Delta_{32} = 1000 \times 10^6$).*

Figure 6.17 shows results for $\Delta_{32} = 1000 \times 10^6$ as Δ_{21} is varied. Results here are similar to those of Figure 6.15 since Δ_{32} is large compared to ω_0 (large detuning). The difference here is that a positive detuning has been used for the pump$_2$ beam. Plots for ρ_{11} and ρ_{22} have not been affected by the change in detuning. We see that the plots for ρ_{33} and ρ_{44} have been shifted in the negative direction as opposed to being shifted in the positive direction previously for when there is a negative detuning. This is due to the fact that the pump$_1$ beam needs to now be negatively detuned to counteract the positive detuning of the pump$_2$ beam in order to get maximum transfer of population to levels $|3\rangle$ and $|4\rangle$.

Finally, to put everything into context, it should be noted that we want to use four-wave mixing to generate coherent photon beams, while at the same time trying to minimise the emission of spontaneously generated photons. The spontaneous photons are directly proportional to the populations ρ_{22}, ρ_{33} and ρ_{44}. The figures presented here show that to ensure high coherent beams we need to choose the detuning Δ_{21} and Δ_{32} such that the Rabi frequencies Ω_3 and Ω_4 are maximum while ρ_{22}, ρ_{33} and ρ_{44} are away from the peak values. See for example Figures 6.12 and 6.14.

6.4 Summary

In this chapter we have investigated the non-linear process called four-wave mixing. Our approach makes use of co-propagating pump beams, having different frequencies, interacting with four energy levels having a diamond configuration of a generalised atom. The atom was treated quantum mechanically while the lasers were treated classically. Atomic polarization was determined from the density matrix elements obtained from perturbation theory and the photon intensities from Maxwell's equations. In our simulation the dependence of the dipole matrix element on laser polarization was not taken into account.

Various scenarios have been tested. While the detuning of the pump$_2$ (Δ_{32}) beam was kept constant, the detuning of the pump$_1$ (Δ_{21}) beam was varied and vice versa. Maximum intensities of the coherent beams were shown to be dependent on the detuning of pump$_1$ and pump$_2$. The populations were also shown to be dependent on the detuning of the pump beams. There are certain values of detuning for which there is maximum coherent beam intensity while the populations are away from their peak values.

Chapter 7

Summary and conclusion

The aim of this thesis was to obtain a deeper understanding of laser-atom interactions and non-linear processes. We did this by performing a theoretical and numerical study in order to simulate four-wave mixing (FWM) in an ensemble of cold atoms and to study the characteristics of the entangled photons that are generated by the FWM process. In order to achieve the aim a number of objectives had to be met. Some of these include the development of computational skills by solving well known physics problems using various numerical methods as well as getting familiar with the important concepts and notations of quantum physics in order to comprehend atomic behaviour.

As an aid to the development of some of the skills required, a study of the interaction between a uniform laser beam and a two-level atom was performed. A semi-classical approach was used where the atom was treated quantum mechanically and the laser beam classically. The optical Bloch equations were used to determine the populations and coherences of the atoms. We have found that when a laser beam, having a frequency equal to the atomic resonant frequency, interacts with an atom, the atom oscillates between the ground and excited states (Rabi oscillations). The oscillations show that the probability of the atom being in either sate has equal likelihood

and that it is also possible for the atom to be in both states simultaneously - superposition. An increase in the detuning of the laser beam results in a change in the frequency of the oscillations and also decreases the probability of the atom transitioning between states. Introducing dissipation shows a decrease in the amplitude of the oscillations resulting in superposition to no longer exist.

The above approach was then modified to include a frequency modulated laser beam where the frequency as well as the level of modulation were varied. Values less than, greater than and equal to the Rabi frequency were tested. In each case the atom behaved in a chaotic manner where a high level of modulation resulted in a greater deviation from the normal regardless of the frequency value. We found that this deviation was greatest when the modulation frequency was equal to the Rabi frequency. This was seen in the phase space plots where the atom did not repeat its path from cycle to cycle.

The effects of a sample of two-level atoms on laser beam intensities were then investigated by means of the non-linear processes of absorption spectroscopy and saturated absorption spectroscopy. Maxwell's equations were solved numerically for the electric field where the atomic polarization needed was obtained analytically from the optical Bloch equations. From our results of absorption spectroscopy (probe beam interacting with zero velocity atoms), we have found that the laser beam intensity drops exponentially across the length of the tube when the laser frequency equals the atomic frequency. We then took into account all the atomic velocities and introduced a pump beam whose electric field was gradually increased (saturated absorption spectroscopy). We found that the absorption profile was broadened but a decrease in absorption occurred at and close to resonance. We have shown this as a Lorentzian peak superimposed on the Doppler broadened spectra.

The results obtained this far have showed satisfactory agreement with those found in previous works and therefore instilled confidence in the approach used.

Finally the non-linear process called four-wave mixing was studied. Two co-propagating pump beams, having different frequencies, were used to interact with four energy levels of a generalised atom having a diamond configuration. This resulted in the generation of two coherent photons. We studied the dependence of the intensities of these additional photons on pump beam detunings. In our simulation the dependence of the dipole matrix element on laser polarization was not taken into account. While the detuning of the pump_2 beam was kept constant, the detuning of the pump_1 beam was varied and vice versa. We found that maximum atomic population transfer occurred when both beams had little to no detuning. At large detuning the intensities of the generated photons were not as great as those generated when the detuning was close to zero. We also found that the intensities of the generated photons and their populations are more dependent on the detuning of the pump_1 beam than the pump_2 beam. This is because the pump_2 beam only affects the transfer of photons from $|2\rangle \rightarrow |3\rangle$. We also found that at certain values of detunings maximum intensities of coherent photons were obtained, while at the same time keeping the population of the various levels away from their maximum values. This is important in order to keep the spontaneous emission as low as possible.

In trying to keep the study simple with the main aim being to obtain an understanding of light-atom interactions, certain limitations were put into place. In our simulation of the four-wave mixing process we have not taken the dependence of the dipole moment into account and therefore treat it as a constant multiplier for the purpose of simplicity. We have also not considered

the polarization of the laser beams or the atoms. An extension to the current thesis would be to account for the dipole moments and also to consider the laser and atom polarizations. The full quantum mechanical model should be studied as opposed to the semi-classical model so that the best phase matching geometries can be found as well as the significance of quantum beats. There is no comparison between the numerical study and an experimental study in the current thesis, an addition of this to future works will ensure further accuracy to the approach used for the numerical study.

Appendices

Appendix A

Flowcharts

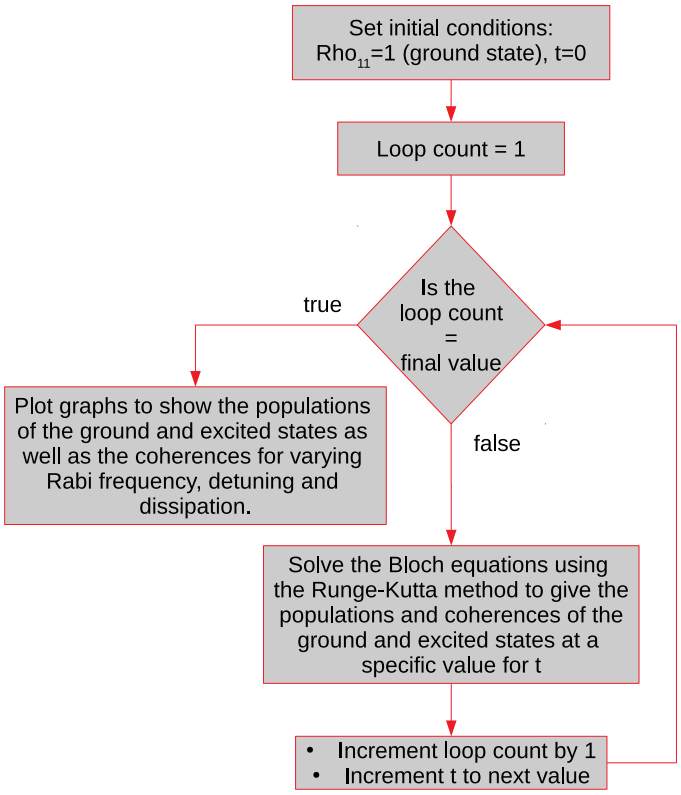

Figure A.1: *Flowchart for two-level atom interacting with a uniform beam.*

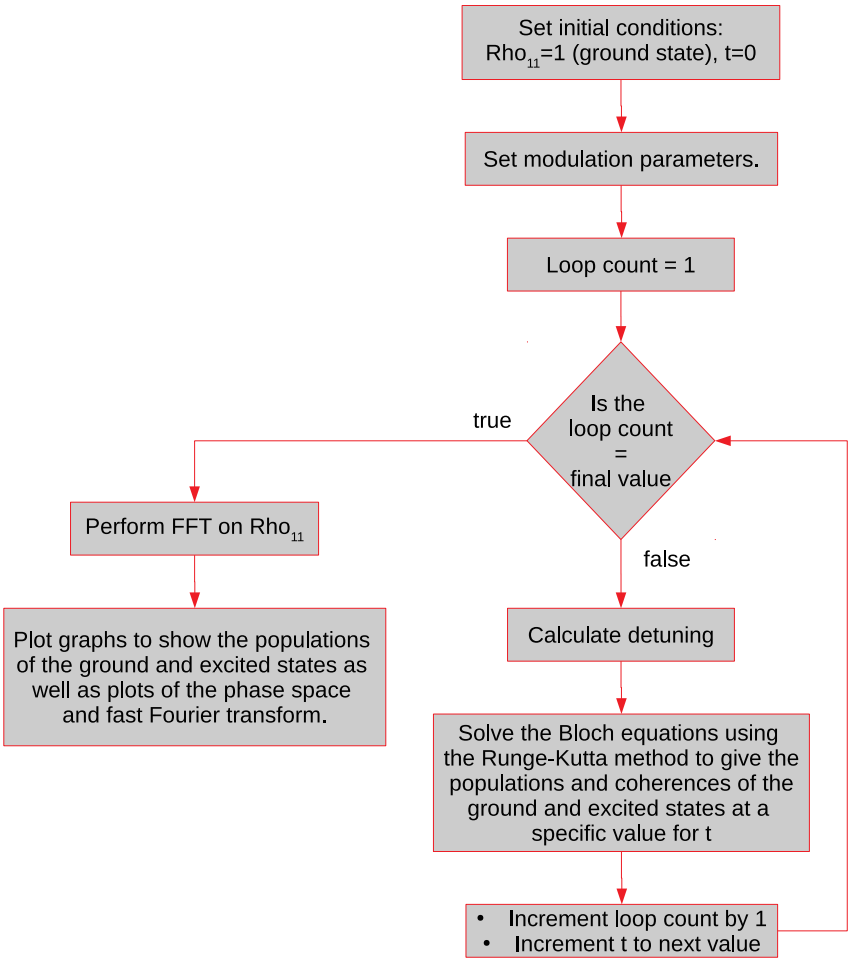

Figure A.2: *Flowchart for two-level atom interacting with a modulated beam.*

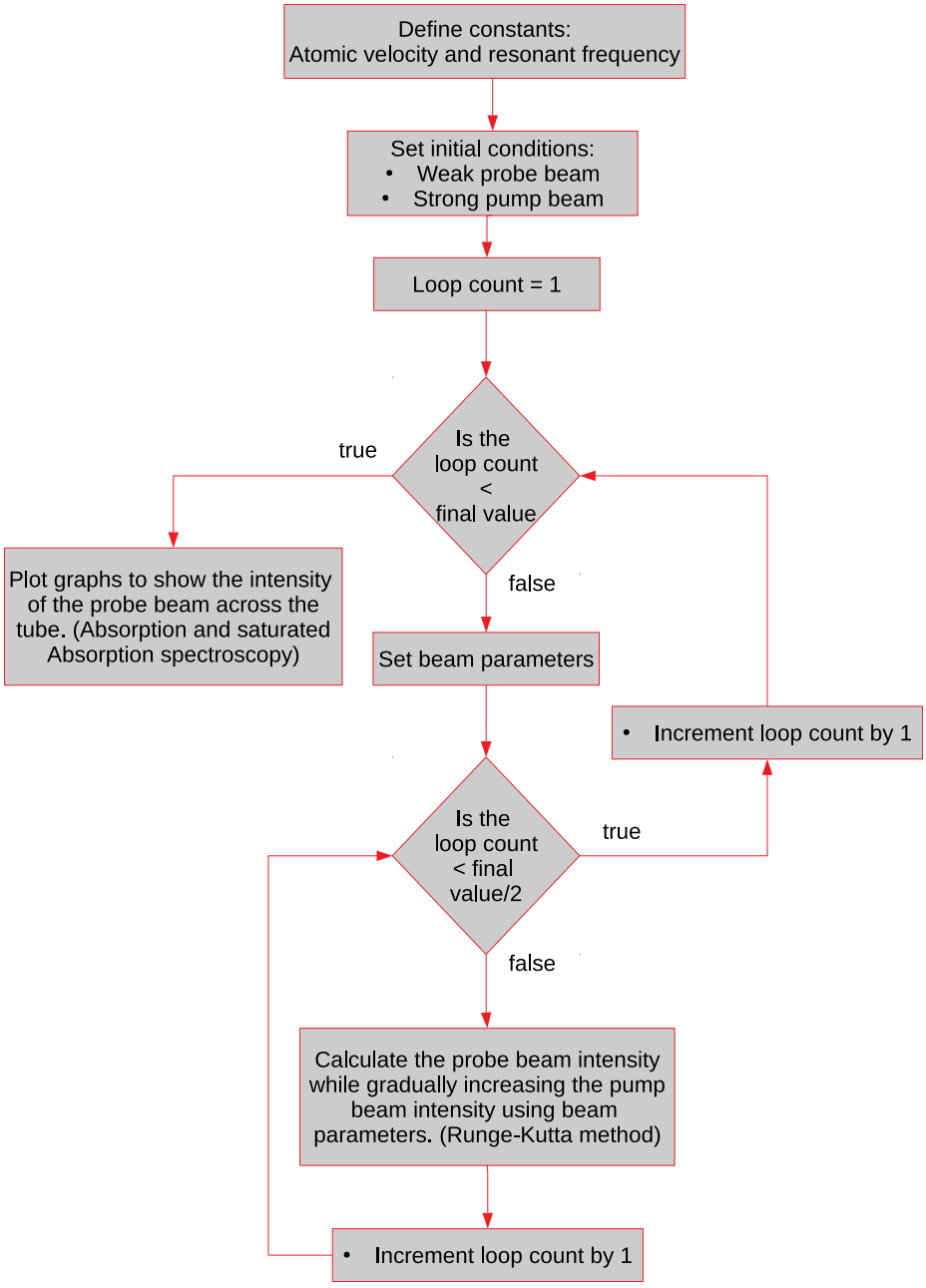

Figure A.3: *Flowchart for saturated absorption spectroscopy.*

Appendix B

Steady state solution of the optical Bloch equations

In this appendix we solve the optical Bloch equations for the steady state solution.

$$\dot{\rho}_{11} = -\imath\frac{\Omega_1}{2}(\rho_{21} - \rho_{12}) + \Gamma_{sp}\rho_{22} \tag{B.1}$$

$$\dot{\rho}_{22} = \imath\frac{\Omega_1}{2}(\rho_{21} - \rho_{12}) - \Gamma_{sp}\rho_{22} \tag{B.2}$$

$$\dot{\rho}_{12} = \imath(\omega_0 - \omega)\rho_{12} - \imath\frac{\Omega_1}{2}(\rho_{22} - \rho_{11}) - \gamma\rho_{12} \tag{B.3}$$

At steady state the time derivatives on the left are zero. Setting the LHS to 0, we can solve for ρ_{11}, ρ_{22} and ρ_{12}. We let $\Gamma_{sp} = 2\gamma$ and note that $\rho_{12}^* = \rho_{21}$. Since ρ_{11} and ρ_{22} are the population terms, their sum equals one. Therefore $\rho_{11} = 1 - \rho_{22}$.

We begin by solving equation (B.3) by setting the time derivative to zero:

$$\begin{aligned}
\dot{\rho}_{12} &= \imath(\omega_0-\omega)\rho_{12} - \imath\frac{\Omega_1}{2}(\rho_{22}-\rho_{11}) - \gamma\rho_{12} \\
0 &= \imath(\omega_0-\omega)\rho_{12} - \imath\frac{\Omega_1}{2}(\rho_{22}-\rho_{11}) - \gamma\rho_{12} \\
0 &= (\imath(\omega_0-\omega)-\gamma)\rho_{12} - \imath\frac{\Omega_1}{2}(\rho_{22}-1+\rho_{22}) \\
\rho_{12} &= \frac{\imath\frac{\Omega_1}{2}(2\rho_{22}-1)}{(\imath(\omega_0-\omega)-\gamma)} \qquad \text{(B.4)}
\end{aligned}$$

Therefore

$$\rho_{21} = \frac{-\imath\frac{\Omega_1}{2}(2\rho_{22}-1)}{(-\imath(\omega_0-\omega)-\gamma)} \qquad \text{(B.5)}$$

Next we solve equation (B.2):

$$\begin{aligned}
\dot{\rho}_{22} &= \imath\frac{\Omega_1}{2}(\rho_{21}-\rho_{12}) - \Gamma_{sp}\rho_{22} \\
0 &= \imath\frac{\Omega_1}{2}\left[\frac{-\imath\frac{\Omega_1}{2}(2\rho_{22}-1)}{(-\imath(\omega_0-\omega)-\gamma)} - \frac{\imath\frac{\Omega_1}{2}(2\rho_{22}-1)}{(\imath(\omega_0-\omega)-\gamma)}\right] - \Gamma_{sp}\rho_{22} \\
0 &= \frac{\Omega_1^2}{4}(2\rho_{22}-1)\left[\frac{-2\gamma}{(\omega_0-\omega)^2+\gamma^2}\right] - \Gamma_{sp}\rho_{22} \\
0 &= \frac{\frac{\Omega_1^2}{2}\gamma}{(\omega_0-\omega)^2+\gamma^2} - \left[\frac{\Omega_1^2\gamma}{(\omega_0-\omega)^2+\gamma^2} + \Gamma_{sp}\right]\rho_{22} \\
\rho_{22} &= \frac{\frac{\Omega_1^2}{2}\gamma}{\Omega_1^2\gamma + \Gamma_{sp}((\omega_0-\omega)^2+\gamma^2)} \qquad \text{(B.6)}
\end{aligned}$$

Since $\rho_{11} = 1 - \rho_{22}$

$$\rho_{11} = 1 - \frac{\frac{\Omega_1^2}{2}\gamma}{\Omega_1^2\gamma + \Gamma_{sp}((\omega_0 - \omega)^2 + \gamma^2)} \tag{B.7}$$

We can use equation (B.6) to solve equations (B.4) and (B.5).

$$\begin{aligned}
\rho_{12} &= \frac{\imath\frac{\Omega_1}{2}(2\rho_{22} - 1)}{(\imath(\omega_0 - \omega) - \gamma)} \\
\rho_{12} &= \frac{\imath\frac{\Omega_1}{2}}{(\imath(\omega_0 - \omega) - \gamma)}\left(2\left(\frac{\frac{\Omega_1^2}{2}\gamma}{\Omega_1^2\gamma + \Gamma_{sp}((\omega_0 - \omega)^2 + \gamma^2)}\right) - 1\right) \\
\rho_{12} &= \imath\frac{\Omega_1}{2}\left(\frac{\Gamma_{sp}(\imath(\omega_0 - \omega) + \gamma)}{\Omega_1^2\gamma + \Gamma_{sp}((\omega_0 - \omega)^2 + \gamma^2)}\right)
\end{aligned} \tag{B.8}$$

Therefore

$$\rho_{21} = -\imath\frac{\Omega_1}{2}\left(\frac{\Gamma_{sp}(-\imath(\omega_0 - \omega) + \gamma)}{\Omega_1^2\gamma + \Gamma_{sp}((\omega_0 - \omega)^2 + \gamma^2)}\right) \tag{B.9}$$

These equations for ρ_{11}, ρ_{12}, ρ_{21} and ρ_{22} are found in Chapter 5.

Appendix C

Derivation and steady state solution of density matrix elements for four-wave mixing

C.1 Introduction

In this appendix we provide the full derivation and steady state solution of the density matrix elements required for our analysis of four-wave mixing presented in Chapter 6. We make use of the energy level structure shown in Figure C.1 where the states shown in brackets could represent those of ^{87}Rb. E_1 to E_4 are the corresponding energies of each level where ω_1 and ω_2 are the frequencies of two pump laser beams and ω_3 and ω_4 are the frequencies of two internally generated photons.

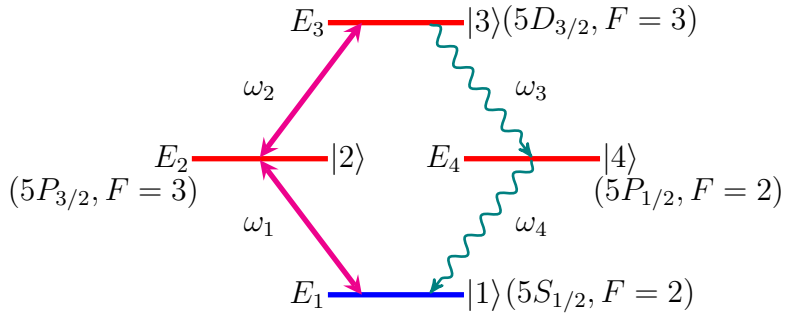

Figure C.1: *Four-wave mixing geometry showing the relevant states of rubidium 87.*

We will assume that the pump laser beams are strong enough that they do not deplete as they propagate through the atomic ensemble. We will also assume that all photons propagate in the positive z-direction. The atomic levels are assumed to be such that the photons of frequency ω_1, ω_2, ω_3 and ω_4 couple only transitions between $|1\rangle \leftrightarrow |2\rangle$, $|2\rangle \leftrightarrow |3\rangle$, $|3\rangle \leftrightarrow |4\rangle$ and $|4\rangle \leftrightarrow |1\rangle$, respectively, that is they are very much

detuned compared to the other transitions.

The total electric field is

$$E = \sum_{i=1}^{4} (\tilde{E}_i e^{-\imath\omega_i t} + c.c.) \tag{C.1}$$

where

$$\tilde{E}_i = E_i(z) e^{\imath k_i z} \tag{C.2}$$

The total Hamiltonian used is

$$H = H_0 + H_I \tag{C.3}$$

where $H_I = -\hat{\mu} \cdot E$ and $-\hat{\mu}$ is the dipole moment of the atom. We will use the following as a basis:

$$|1\rangle = e^{-\imath E_1 t/\hbar}|1\rangle \tag{C.4}$$

$$|2\rangle = e^{-\imath E_2 t/\hbar}|2\rangle \tag{C.5}$$

$$|3\rangle = e^{-\imath E_3 t/\hbar}|3\rangle \tag{C.6}$$

$$|4\rangle = e^{-\imath E_4 t/\hbar}|4\rangle \tag{C.7}$$

Therefore, in the above basis

$$H_0 = \begin{pmatrix} E_1 & 0 & 0 & 0 \\ 0 & E_2 & 0 & 0 \\ 0 & 0 & E_3 & 0 \\ 0 & 0 & 0 & E_4 \end{pmatrix} \tag{C.8}$$

and $H_I' = e^{\imath H_0 t/\hbar} H_I e^{-\imath H_0 t/\hbar}$. This becomes

$$\begin{aligned} H_I' &= e^{\imath H_0 t/\hbar} H_I e^{-\imath H_0 t/\hbar} \qquad (C.9) \\ &= \begin{pmatrix} e^{\imath E_1 t/\hbar} & 0 & 0 & 0 \\ 0 & e^{\imath E_2 t/\hbar} & 0 & 0 \\ 0 & 0 & e^{\imath E_3 t/\hbar} & 0 \\ 0 & 0 & 0 & e^{\imath E_4 t/\hbar} \end{pmatrix} \begin{pmatrix} 0 & -\mu_{12} & -\mu_{13} & -\mu_{14} \\ -\mu_{21} & 0 & -\mu_{23} & 0 \\ -\mu_{31} & -\mu_{32} & 0 & -\mu_{34} \\ -\mu_{41} & 0 & -\mu_{43} & 0 \end{pmatrix} E \begin{pmatrix} e^{-\imath E_1 t/\hbar} & 0 & 0 & 0 \\ 0 & e^{-\imath E_2 t/\hbar} & 0 & 0 \\ 0 & 0 & e^{-\imath E_3 t/\hbar} & 0 \\ 0 & 0 & 0 & e^{-\imath E_4 t/\hbar} \end{pmatrix} \\ &= E \begin{pmatrix} 0 & -\mu_{12} e^{\imath E_1 t/\hbar} & -\mu_{13} e^{\imath E_1 t/\hbar} & -\mu_{14} e^{\imath E_1 t/\hbar} \\ -\mu_{21} e^{\imath E_2 t/\hbar} & 0 & -\mu_{23} e^{\imath E_2 t/\hbar} & 0 \\ -\mu_{31} e^{\imath E_3 t/\hbar} & -\mu_{32} e^{\imath E_3 t/\hbar} & 0 & -\mu_{34} e^{\imath E_3 t/\hbar} \\ -\mu_{41} e^{\imath E_4 t/\hbar} & 0 & -\mu_{43} e^{\imath E_4 t/\hbar} & 0 \end{pmatrix} \begin{pmatrix} e^{-\imath E_1 t/\hbar} & 0 & 0 & 0 \\ 0 & e^{-\imath E_2 t/\hbar} & 0 & 0 \\ 0 & 0 & e^{-\imath E_3 t/\hbar} & 0 \\ 0 & 0 & 0 & e^{-\imath E_4 t/\hbar} \end{pmatrix} \\ &= E \begin{pmatrix} 0 & -\mu_{12} e^{\imath \omega_{12} t} & -\mu_{13} e^{\imath \omega_{13} t} & -\mu_{14} e^{\imath \omega_{14} t} \\ -\mu_{21} e^{\imath \omega_{21} t} & 0 & -\mu_{23} e^{\imath \omega_{23} t} & 0 \\ -\mu_{31} e^{\imath \omega_{31} t} & -\mu_{32} e^{\imath \omega_{32} t} & 0 & -\mu_{34} e^{\imath \omega_{34} t} \\ -\mu_{41} e^{\imath \omega_{41} t} & 0 & -\mu_{43} e^{\imath \omega_{43} t} & 0 \end{pmatrix} \qquad (C.10) \end{aligned}$$

where $\omega_{ij} = (E_i - E_j)/\hbar$ and $\mu_{ij} = \langle i|\hat{\mu}|j\rangle$. Then the Liouville-von Neumann equation (also known as the master equation) that we solve is

$$\dot{\rho} = -\frac{\imath}{\hbar}[H'_I, \rho] + relaxation\, terms \tag{C.11}$$

Making use of perturbation theory, we set

$$\rho = \rho^{(0)} + \lambda\rho^{(1)} + \lambda^2\rho^{(2)} + \lambda^3\rho^{(3)} + ... \tag{C.12}$$

and expand each $\rho^{(i)}$ in frequency as well, also replace H'_I by $\lambda H'_I$. Therefore

$$[\dot{\rho}^{(0)} + \lambda\dot{\rho}^{(1)} + \lambda^2\dot{\rho}^{(2)} + \lambda^3\dot{\rho}^{(3)} + ...] = -\frac{\imath}{\hbar}[\lambda H'_I, (\rho^{(0)} + \lambda\rho^{(1)} + \lambda^2\rho^{(2)} + \lambda^3\rho^{(3)} + ...)] + relaxation\, terms \tag{C.13}$$

$$[\dot{\rho}^{(0)} + \lambda\dot{\rho}^{(1)} + \lambda^2\dot{\rho}^{(2)} + \lambda^3\dot{\rho}^{(3)} + ...] = -\frac{\imath}{\hbar}[[\lambda H'_I, \rho^{(0)}] + [\lambda H'_I, \lambda\rho^{(1)}] + [\lambda H'_I, \lambda^2\rho^{(2)}] + ...] + relaxation\, terms \tag{C.14}$$

Then for all λ^0 terms

$$\lambda^0\dot{\rho}^{(0)} = 0 + relaxation\, terms \tag{C.15}$$

all λ^1 terms

$$\lambda^1\dot{\rho}^{(1)} = [\lambda H'_I, \rho^{(0)}] + relaxation\, terms \tag{C.16}$$

all λ^2 terms

$$\lambda^2\dot{\rho}^{(2)} = [\lambda H'_I, \lambda\rho^{(1)}] + relaxation\, terms \tag{C.17}$$

all λ^3 terms

$$\lambda^3\dot{\rho}^{(3)} = [\lambda H_I', \lambda^2\rho^{(2)}] + relaxation\, terms \tag{C.18}$$

all λ^4 terms

$$\lambda^4\dot{\rho}^{(4)} = [\lambda H_I', \lambda^3\rho^{(3)}] + relaxation\, terms \tag{C.19}$$

and so on.

C.2 Zero Order Solution

For the zero order solution we set $\rho_{11}^{(0)} = 1$ i.e all the atoms are in the ground state and all the other elements are set to zero.

$$\begin{pmatrix} 1 & 0 & 0 & 0 \\ 0 & 0 & 0 & 0 \\ 0 & 0 & 0 & 0 \\ 0 & 0 & 0 & 0 \end{pmatrix} \tag{C.20}$$

C.3 First Order Solution

Using equation (C.16) we can solve for the first order by expanding the following commutator:

$$\lambda^1 \dot{\rho}^{(1)} = -\frac{\imath}{\hbar}[\lambda H'_I, \rho^{(0)}] + relaxation\, terms \tag{C.21}$$

$$\dot{\rho}^{(1)} = -\frac{\imath}{\hbar}\left[\begin{pmatrix} 0 & H_{12} & H_{13} & H_{14} \\ H_{21} & 0 & H_{23} & 0 \\ H_{31} & H_{32} & 0 & H_{34} \\ H_{41} & 0 & H_{43} & 0 \end{pmatrix}, \begin{pmatrix} 1 & 0 & 0 & 0 \\ 0 & 0 & 0 & 0 \\ 0 & 0 & 0 & 0 \\ 0 & 0 & 0 & 0 \end{pmatrix}\right] + relaxation\, terms \tag{C.22}$$

Note that $H_{ij} = \langle i|H'|j\rangle$. When expanding the commutator we get the following equations:

$$\dot{\rho}^{(1)}_{11} = \gamma_{21}\rho^{(1)}_{22} + \gamma_{41}\rho^{(1)}_{44} \tag{C.23}$$

$$\dot{\rho}^{(1)}_{22} = \gamma_{32}\rho^{(1)}_{33} - \gamma_{21}\rho^{(1)}_{22} \tag{C.24}$$

$$\dot{\rho}^{(1)}_{33} = -\gamma_{32}\rho^{(1)}_{33} - \gamma_{34}\rho^{(1)}_{33} \tag{C.25}$$

$$\dot{\rho}^{(1)}_{44} = -\gamma_{41}\rho^{(1)}_{44} + \gamma_{34}\rho^{(1)}_{33} \tag{C.26}$$

$$\dot{\rho}^{(1)}_{12} = -\frac{\imath}{\hbar}(-H_{12}) - \Gamma_{12}\rho^{(1)}_{12} \tag{C.27}$$

$$\dot{\rho}^{(1)}_{13} = -\frac{\imath}{\hbar}(-H_{13}) - \Gamma_{13}\rho^{(1)}_{13} \tag{C.28}$$

$$\dot{\rho}_{14}^{(1)} = -\frac{\imath}{\hbar}(-H_{14}) - \Gamma_{14}\rho_{14}^{(1)} \tag{C.29}$$

$$\dot{\rho}_{21}^{(1)} = -\frac{\imath}{\hbar}(H_{21}) - \Gamma_{21}\rho_{21}^{(1)} \tag{C.30}$$

$$\dot{\rho}_{23}^{(1)} = -\Gamma_{23}\rho_{23}^{(1)} \tag{C.31}$$

$$\dot{\rho}_{24}^{(1)} = -\Gamma_{24}\rho_{24}^{(1)} \tag{C.32}$$

$$\dot{\rho}_{31}^{(1)} = -\frac{\imath}{\hbar}(H_{31}) - \Gamma_{31}\rho_{31}^{(1)} \tag{C.33}$$

$$\dot{\rho}_{32}^{(1)} = -\Gamma_{32}\rho_{32}^{(1)} \tag{C.34}$$

$$\dot{\rho}_{34}^{(1)} = -\Gamma_{34}\rho_{34}^{(1)} \tag{C.35}$$

$$\dot{\rho}_{41}^{(1)} = -\frac{\imath}{\hbar}(H_{41}) - \Gamma_{41}\rho_{41}^{(1)} \tag{C.36}$$

$$\dot{\rho}_{42}^{(1)} = -\Gamma_{42}\rho_{42}^{(1)} \tag{C.37}$$

$$\dot{\rho}_{43}^{(1)} = -\Gamma_{43}\rho_{43}^{(1)} \tag{C.38}$$

Note that Γ and γ are part of the relaxation terms. This applies to higher order solutions to be derived later.

C.3.1 Derivation of first order population terms

Solving equations (C.23) - (C.26) starting with equation (C.25) for $\dot{\rho}_{33}^{(1)}$:

$$\begin{aligned} \dot{\rho}_{33}^{(1)} &= -\gamma_{32}\rho_{33}^{(1)} - \gamma_{34}\rho_{33}^{(1)} \\ \dot{\rho}_{33}^{(1)} + \gamma_{32}\rho_{33}^{(1)} + \gamma_{34}\rho_{33}^{(1)} &= 0 \end{aligned}$$

The steady state solution is

$$\rho_{33}^{(1)} = 0 \tag{C.39}$$

In a similar fashion, we solve equation (C.26) for $\dot{\rho}_{44}^{(1)}$:

$$\dot{\rho}_{44}^{(1)} = -\gamma_{41}\rho_{44}^{(1)} + \gamma_{34}\rho_{33}^{(1)}$$

where $\rho_{33}^{(1)} = 0$, the steady state solution is

$$\rho_{44}^{(1)} = 0 \tag{C.40}$$

Then solving equation (C.24) for $\dot{\rho}_{22}^{(1)}$:

$$\dot{\rho}_{22}^{(1)} = \gamma_{32}\rho_{33}^{(1)} - \gamma_{21}\rho_{22}^{(1)}$$

since $\rho_{33}^{(1)} = 0$, therefore

$$\rho_{22}^{(1)} = 0 \tag{C.41}$$

Finally, we solve equation (C.23) for $\dot{\rho}_{11}^{(1)}$:

$$\dot{\rho}_{11}^{(1)} = \gamma_{21}\rho_{22}^{(1)} + \gamma_{41}\rho_{44}^{(1)}$$

where $\rho_{22}^{(1)} = 0$ and $\rho_{44}^{(1)} = 0$, therefore

$$\rho_{11}^{(1)} = 0 \tag{C.42}$$

C.3.2 Derivation of first order coherence terms

We then solve equations (C.27) - (C.38) where $\dot{\rho}_{21}^{(1)} = \dot{\rho}_{12}^{(1)*}$, $\dot{\rho}_{31}^{(1)} = \dot{\rho}_{13}^{(1)*}$, $\dot{\rho}_{41}^{(1)} = \dot{\rho}_{14}^{(1)*}$, $\dot{\rho}_{32}^{(1)} = \dot{\rho}_{23}^{(1)*}$, $\dot{\rho}_{42}^{(1)} = \dot{\rho}_{24}^{(1)*}$ and $\dot{\rho}_{43}^{(1)} = \dot{\rho}_{34}^{(1)*}$. It is therefore necessary to only solve for one equation in each pair. We start by solving equation (C.30) for $\dot{\rho}_{21}^{(1)}$:

$$\dot{\rho}_{21}^{(1)} = -\frac{\imath}{\hbar}(-\mu_{21}e^{\imath\omega_{21}t})E - \Gamma_{21}\rho_{21}^{(1)}$$

After re-arranging, we expand E (using equation (C.1)) and take into account only the frequencies that will resonate with the $|2\rangle - |1\rangle$ transition i.e. $e^{-\imath\omega_1 t}$.

$$\dot{\rho}_{21}^{(1)} e^{-\imath\omega_{21}t} + \Gamma_{21}\rho_{21}^{(1)} e^{-\imath\omega_{21}t} = -\frac{\imath}{\hbar}(-\mu_{21})(\tilde{E}_1 e^{-\imath\omega_1 t}) \tag{C.43}$$

We now take the steady state solution of the above equation where the right-hand side (RHS) of the equation is the driving term. Using

$$\tilde{\rho}_{ij}^{(n)} = \rho_{ij}^{(n)} e^{-\imath\omega_{ij}t} \tag{C.44}$$

we get $\tilde{\rho}_{21}^{(1)} = \rho_{21}^{(1)} e^{-\imath\omega_{21}t}$ therefore $\dot{\tilde{\rho}}_{21}^{(1)} = \dot{\rho}_{21}^{(1)} e^{-\imath\omega_{21}t} - \imath\omega_{21}\tilde{\rho}_{21}^{(1)}$, substituting this into the equation (C.43) gives

$$\dot{\tilde{\rho}}_{21}^{(1)} + \imath\omega_{21}\tilde{\rho}_{21}^{(1)} + \Gamma_{21}\tilde{\rho}_{21}^{(1)} = \frac{\imath}{\hbar}\mu_{21}\tilde{E}_1 e^{-\imath\omega_1 t}$$

Taking the steady state solution to be of the form $\tilde{\rho}_{21}^{(1)} = Ae^{-\imath\omega_1 t}$ results in

$$\tilde{\rho}_{21}^{(1)} = \frac{1}{\hbar}\frac{\mu_{21}\tilde{E}_1 e^{-\imath\omega_1 t}}{\Delta_{21} - \imath\Gamma_{21}} \tag{C.45}$$

and therefore

$$\tilde{\rho}_{12}^{(1)} = \frac{1}{\hbar}\frac{\mu_{12}\tilde{E}_1^* e^{\imath\omega_1 t}}{\Delta_{21} + \imath\Gamma_{21}} \tag{C.46}$$

where $\Delta_{21} = \omega_{21} - \omega_1$. We make use of the same approach to solve all other differential equations for

the coherence density matrix elements, keeping in mind the $\tilde{\rho}_{ij}$ contains the time independence of ρ_{ij}. We now solve equation (C.33) for $\dot{\rho}_{31}^{(1)}$:

$$\dot{\rho}_{31}^{(1)} = -\frac{\imath}{\hbar}(-\mu_{31}e^{\imath\omega_{31}}t)E - \Gamma_{31}\rho_{31}^{(1)}$$

After re-arranging, we expand E (using equation (C.1)) and take into account only the frequencies that will resonate with the $|3\rangle - |1\rangle$ transition. Since each frequency does not resonantly couple this transition, i.e. $(\omega_{31} - \omega_i)$ becomes very large, we get

$$\rho_{31}^{(1)} = 0 \tag{C.47}$$

and therefore

$$\rho_{13}^{(1)} = 0 \tag{C.48}$$

Making use of the method used to derive equations (C.45) and (C.46) we solve equation (C.36) for $\dot{\rho}_{41}^{(1)}$:

$$\dot{\rho}_{41}^{(1)} = -\frac{\imath}{\hbar}(-\mu_{41}e^{\imath\omega_{41}}t)E - \Gamma_{41}\rho_{41}^{(1)}$$

After re-arranging, we expand E (using equation (C.1)) and take into account only the frequencies that will resonate with the $|4\rangle - |1\rangle$ transition i.e. $e^{-\imath\omega_4 t}$.

$$\dot{\rho}_{41}^{(1)}e^{-\imath\omega_{41}t} + \Gamma_{41}\rho_{41}^{(1)}e^{-\imath\omega_{41}t} = -\frac{\imath}{\hbar}(-\mu_{41})(\tilde{E}_4 e^{-\imath\omega_4 t})$$

The steady state solution results in

$$\tilde{\rho}_{41}^{(1)} = \frac{1}{\hbar} \frac{\mu_{41} \tilde{E}_4 e^{-\imath\omega_4 t}}{\Delta_{41} - \imath\Gamma_{41}} \tag{C.49}$$

and therefore

$$\tilde{\rho}_{14}^{(1)} = \frac{1}{\hbar} \frac{\mu_{14} \tilde{E}_4^* e^{\imath\omega_4 t}}{\Delta_{41} + \imath\Gamma_{41}} \tag{C.50}$$

where $\Delta_{41} = \omega_{41} - \omega_4$. When solving equation (C.34) for $\dot{\rho}_{32}^{(1)}$:

$$\dot{\rho}_{32}^{(1)} = -\Gamma_{32} \rho_{32}^{(1)}$$

The steady state solution results in

$$\rho_{32}^{(1)} = 0 \tag{C.51}$$

and therefore

$$\rho_{23}^{(1)} = 0 \tag{C.52}$$

Similarly solving equation (C.37) for $\dot{\rho}_{42}^{(1)}$:

$$\dot{\rho}_{42}^{(1)} = -\Gamma_{42}\rho_{42}^{(1)}$$

The steady state solution is

$$\rho_{42}^{(1)} = 0 \tag{C.53}$$

and therefore

$$\rho_{24}^{(1)} = 0 \tag{C.54}$$

And finally, solving equation (C.38) for $\dot{\rho}_{43}^{(1)}$:

$$\dot{\rho}_{43}^{(1)} = -\Gamma_{43}\rho_{43}^{(1)}$$

The steady state solution is

$$\rho_{43}^{1} = 0 \tag{C.55}$$

and therefore

$$\rho_{34}^{1} = 0 \tag{C.56}$$

Therefore

$$\rho^{(1)} = \begin{pmatrix} 0 & \tilde{\rho}_{12}^{(1)} e^{\imath\omega_{12}t} & 0 & \tilde{\rho}_{14}^{(1)} e^{\imath\omega_{14}t} \\ \tilde{\rho}_{21}^{(1)} e^{\imath\omega_{21}t} & 0 & 0 & 0 \\ 0 & 0 & 0 & 0 \\ \tilde{\rho}_{41}^{(1)} e^{\imath\omega_{41}t} & 0 & 0 & 0 \end{pmatrix} \tag{C.57}$$

Since $\tilde{\rho}_{ij}$ will have compound $e^{-\imath\omega_{ij}}$ the terms in the above matrix will be time independent. This applies to the higher order coherence terms to be discussed below.

C.4 Second Order Solution

Using equation (C.17) we can solve for the second order by expanding the following commutator:

$$\lambda^2 \dot{\rho}^{(2)} = -\frac{\imath}{\hbar}[\lambda H_I', \lambda\rho^{(1)}] + relaxation\, terms \tag{C.58}$$

$$\dot{\rho}^{(2)} = -\frac{\imath}{\hbar}\left[\begin{pmatrix} 0 & H_{12} & H_{13} & H_{14} \\ H_{21} & 0 & H_{23} & 0 \\ H_{31} & H_{32} & 0 & H_{34} \\ H_{41} & 0 & H_{43} & 0 \end{pmatrix}, \begin{pmatrix} 0 & \rho_{12}^{(1)} & 0 & \rho_{14}^{(1)} \\ \rho_{21}^{(1)} & 0 & 0 & 0 \\ 0 & 0 & 0 & 0 \\ \rho_{41}^{(1)} & 0 & 0 & 0 \end{pmatrix}\right] + relaxation\, terms \tag{C.59}$$

Note that $H_{ij} = \langle i|H'|j\rangle$. When expanding the commutator we get the following equations:

$$\dot{\rho}_{11}^{(2)} = -\frac{\imath}{\hbar}(H_{12}\rho_{21}^{(1)} + H_{14}\rho_{41}^{(1)} - H_{21}\rho_{12}^{(1)} - H_{41}\rho_{14}^{(1)}) + \gamma_{21}\rho_{22}^{(2)} + \gamma_{41}\rho_{44}^{(2)} \tag{C.60}$$

$$\dot{\rho}_{22}^{(2)} = -\frac{\imath}{\hbar}(H_{21}\rho_{12}^{(1)} - H_{12}\rho_{21}^{(1)}) + \gamma_{32}\rho_{33}^{(2)} - \gamma_{21}\rho_{22}^{(2)} \tag{C.61}$$

$$\dot{\rho}_{33}^{(2)} = -\gamma_{32}\rho_{33}^{(2)} - \gamma_{34}\rho_{33}^{(2)} \tag{C.62}$$

$$\dot{\rho}_{44}^{(2)} = -\frac{\imath}{\hbar}(H_{41}\rho_{14}^{(1)} - H_{14}\rho_{41}^{(1)}) - \gamma_{41}\rho_{44}^{(2)} + \gamma_{34}\rho_{33}^{(2)} \tag{C.63}$$

$$\dot{\rho}_{12}^{(2)} = -\Gamma_{12}\rho_{12}^{(2)} \tag{C.64}$$

$$\dot{\rho}_{13}^{(2)} = -\frac{\imath}{\hbar}(-H_{23}\rho_{12}^{(1)} - H_{43}\rho_{14}^{(1)}) - \Gamma_{13}\rho_{13}^{(2)} \tag{C.65}$$

$$\dot{\rho}_{14}^{(2)} = -\Gamma_{14}\rho_{14}^{(2)} \tag{C.66}$$

$$\dot{\rho}_{21}^{(2)} = -\Gamma_{21}\rho_{21}^{(2)} \tag{C.67}$$

$$\dot{\rho}_{23}^{(2)} = -\frac{\imath}{\hbar}(-H_{13}\rho_{21}^{(1)}) - \Gamma_{23}\rho_{23}^{(2)} \tag{C.68}$$

$$\dot{\rho}_{24}^{(2)} = -\frac{\imath}{\hbar}(H_{21}\rho_{14}^{(1)} - H_{14}\rho_{21}^{(1)}) - \Gamma_{24}\rho_{24}^{(2)} \tag{C.69}$$

$$\dot{\rho}_{31}^{(2)} = -\frac{\imath}{\hbar}(H_{32}\rho_{21}^{(1)} + H_{34}\rho_{41}^{(1)}) - \Gamma_{31}\rho_{31}^{(2)} \tag{C.70}$$

$$\dot{\rho}_{32}^{(2)} = -\frac{\imath}{\hbar}(H_{31}\rho_{12}^{(1)}) - \Gamma_{32}\rho_{32}^{(2)} \tag{C.71}$$

$$\dot{\rho}_{34}^{(2)} = -\frac{\imath}{\hbar}(H_{31}\rho_{14}^{(1)}) - \Gamma_{34}\rho_{34}^{(2)} \tag{C.72}$$

$$\dot{\rho}_{41}^{(2)} = -\Gamma_{41}\rho_{41}^{(2)} \tag{C.73}$$

$$\dot{\rho}_{42}^{(2)} = -\frac{\imath}{\hbar}(H_{41}\rho_{12}^{(1)} - H_{12}\rho_{41}^{(1)}) - \Gamma_{42}\rho_{42}^{(2)} \tag{C.74}$$

$$\dot{\rho}_{43}^{(2)} = -\frac{\imath}{\hbar}(-H_{13}\rho_{41}^{(1)}) - \Gamma_{43}\rho_{43}^{(2)} \tag{C.75}$$

C.4.1 Derivation of second order population terms

Solving for equations (C.60) - (C.63) starting with equation (C.62) for $\dot{\rho}_{33}^{(2)}$:

$$\begin{aligned} \dot{\rho}_{33}^{(2)} &= -\gamma_{32}\rho_{33}^{(2)} - \gamma_{34}\rho_{33}^{(2)} \\ \dot{\rho}_{33}^{(2)} + \gamma_{32}\rho_{33}^{(2)} + \gamma_{34}\rho_{33}^{(2)} &= 0 \end{aligned}$$

The steady state solution is

$$\rho_{33}^{(2)} = 0 \tag{C.76}$$

We then solve equation (C.63) for $\dot{\rho}_{44}^{(2)}$:

$$\dot{\rho}_{44}^{(2)} = -\frac{\imath}{\hbar}(H_{41}\rho_{14}^{(1)} - H_{14}\rho_{41}^{(1)}) - \gamma_{41}\rho_{44}^{(2)} + \gamma_{34}\rho_{33}^{(2)}$$

where $\rho_{33}^{(2)} = 0$. We re-arrange and expand the terms:

$$\dot{\rho}_{44}^{(2)} + \gamma_{41}\rho_{44}^{(2)} = \frac{\imath}{\hbar}(-\mu_{14}E\tilde{\rho}_{41}^{(1)}e^{\imath(\omega_{14}+\omega_{41})t} + \mu_{41}E\tilde{\rho}_{14}^{(1)}e^{\imath(\omega_{41}+\omega_{14})t})$$

$$\dot{\rho}_{44}^{(2)} + \gamma_{41}\rho_{44}^{(2)} = \frac{\imath}{\hbar}\left(-\mu_{14}E\left(\frac{1}{\hbar}\frac{\mu_{41}\tilde{E}_4 e^{-\imath\omega_4 t}}{\Delta_{41} - \imath\Gamma_{41}}\right) + \mu_{41}E\left(\frac{1}{\hbar}\frac{\mu_{14}\tilde{E}_4^* e^{\imath\omega_4 t}}{\Delta_{41} + \imath\Gamma_{41}}\right)\right)$$

We now expand E (using equation (C.1)) and consider only the terms in $\pm\omega_4$ in the expansion of the above equation.

$$\dot{\rho}_{44}^{(2)} + \gamma_{41}\rho_{44}^{(2)} = \frac{\imath}{\hbar}\left(-\mu_{14}\tilde{E}_4^* e^{\imath\omega_4 t}\left(\frac{1}{\hbar}\frac{\mu_{41}\tilde{E}_4 e^{-\imath\omega_4 t}}{\Delta_{41} - \imath\Gamma_{41}}\right) + \mu_{41}\tilde{E}_4 e^{-\imath\omega_4 t}\left(\frac{1}{\hbar}\frac{\mu_{14}\tilde{E}_4^* e^{\imath\omega_4 t}}{\Delta_{41} + \imath\Gamma_{41}}\right)\right)$$

Re-arrange to get:

$$\dot{\rho}_{44}^{(2)} + \gamma_{41}\rho_{44}^{(2)} = \frac{1}{\hbar^2}|\mu_{14}|^2\tilde{E}_4^*\tilde{E}_4\left(\frac{-\imath}{\Delta_{41} - \imath\Gamma_{41}} + \frac{\imath}{\Delta_{41} + \imath\Gamma_{41}}\right)$$

$$\dot{\rho}_{44}^{(2)} + \gamma_{41}\rho_{44}^{(2)} = \frac{1}{\hbar^2}|\mu_{14}|^2\tilde{E}_4^*\tilde{E}_4\left(\frac{2\Gamma_{41}}{\Delta_{41}^2 + \Gamma_{41}^2}\right)$$

The steady solution is

$$\rho_{44}^{(2)} = \frac{1}{\hbar^2}\frac{|\mu_{14}|^2|\tilde{E}_4|^2}{\gamma_{41}}\left(\frac{2\Gamma_{41}}{\Delta_{41}^2 + \Gamma_{41}^2}\right) \tag{C.77}$$

Next we solve equation (C.61) for $\dot{\rho}_{22}^{(2)}$

$$\dot{\rho}_{22}^{(2)} = -\frac{\imath}{\hbar}(H_{21}\rho_{12}^{(1)} - H_{12}\rho_{21}^{(1)}) + \gamma_{32}\rho_{33}^{(2)} - \gamma_{21}\rho_{22}^{(2)}$$

where $\rho_{33}^{(2)} = 0$. We re-arrange and expand the terms:

$$\dot{\rho}_{22}^{(2)} + \gamma_{21}\rho_{22}^{(2)} = \frac{\imath}{\hbar}(-\mu_{12}E\tilde{\rho}_{21}^{(1)}e^{\imath(\omega_{12}+\omega_{21})t} + \mu_{21}E\tilde{\rho}_{12}^{(1)}e^{\imath(\omega_{21}+\omega_{12})t})$$

$$\dot{\rho}_{22}^{(2)} + \gamma_{21}\rho_{22}^{(2)} = \frac{\imath}{\hbar}\left(-\mu_{12}E\left(\frac{1}{\hbar}\frac{\mu_{21}\tilde{E}_1 e^{-\imath\omega_1 t}}{\Delta_{21} - \imath\Gamma_{21}}\right) + \mu_{21}E\left(\frac{1}{\hbar}\frac{\mu_{12}\tilde{E}_1^* e^{\imath\omega_1 t}}{\Delta_{21} + \imath\Gamma_{21}}\right)\right)$$

We now expand E and consider only the terms in $\pm\omega 1$ in the expansion of the above equation.

$$\dot{\rho}_{22}^{(2)} + \gamma_{21}\rho_{22}^{(2)} = \frac{\imath}{\hbar}\left(-\mu_{12}\tilde{E}_1^* e^{\imath\omega_1 t}\left(\frac{1}{\hbar}\frac{\mu_{21}\tilde{E}_1 e^{-\imath\omega_1 t}}{\Delta_{21} - \imath\Gamma_{21}}\right) + \mu_{21}\tilde{E}_1 e^{-\imath\omega_1 t}\left(\frac{1}{\hbar}\frac{\mu_{12}\tilde{E}_1^* e^{\imath\omega_1 t}}{\Delta_{21} + \imath\Gamma_{21}}\right)\right)$$

Re-arrange to get:

$$\dot{\rho}_{22}^{(2)} + \gamma_{21}\rho_{22}^{(2)} = \frac{1}{\hbar^2}|\mu_{12}|^2\tilde{E}_1^*\tilde{E}_1\left(\frac{-\imath}{\Delta_{21} - \imath\Gamma_{21}} + \frac{\imath}{\Delta_{21} + \imath\Gamma_{21}}\right)$$

$$\dot{\rho}_{22}^{(2)} + \gamma_{21}\rho_{22}^{(2)} = \frac{1}{\hbar^2}|\mu_{12}|^2|\tilde{E}_1|^2\left(\frac{2\Gamma_{21}}{\Delta_{21}^2 + \Gamma_{21}^2}\right)$$

The steady solution is

$$\rho_{22}^{(2)} = \frac{1}{\hbar^2}\frac{|\mu_{12}|^2|\tilde{E}_1|^2}{\gamma_{21}}\left(\frac{2\Gamma_{21}}{\Delta_{21}^2+\Gamma_{21}^2}\right) \tag{C.78}$$

Finally, we solve equation (C.60)

$$\dot{\rho}_{11}^{(2)} = -\frac{\imath}{\hbar}(H_{12}\rho_{21}^{(1)} + H_{14}\rho_{41}^{(1)} - H_{21}\rho_{12}^{(1)} - H_{41}\rho_{14}^{(1)}) + \gamma_{21}\rho_{22}^{(2)} + \gamma_{41}\rho_{44}^{(2)}$$

Rearrange to give:

$$\dot{\rho}_{11}^{(2)} = -\frac{\imath}{\hbar}(H_{12}\rho_{21}^{(1)} - H_{21}\rho_{12}^{(1)} + H_{14}\rho_{41}^{(1)} - H_{41}\rho_{14}^{(1)}) + \gamma_{21}\rho_{22}^{(2)} + \gamma_{41}\rho_{44}^{(2)}$$

$$\dot{\rho}_{11}^{(2)} = -\frac{\imath}{\hbar}(H_{12}\rho_{21}^{(1)} - H_{21}\rho_{12}^{(1)}) + -\frac{\imath}{\hbar}(H_{14}\rho_{41}^{(1)} - H_{41}\rho_{14}^{(1)}) + \gamma_{21}\rho_{22}^{(2)} + \gamma_{41}\rho_{44}^{(2)}$$

The RHS of the above equation is identically zero when we expand and simplify thus giving

$$\dot{\rho}_{11}^{(2)} = 0$$

We can solve for $\rho_{11}^{(2)}$ in another way as follows:

$$\begin{aligned}
\rho_{11}^{(1)} + \rho_{11}^{(2)} + \rho_{22}^{(1)} + \rho_{22}^{(2)} + \rho_{33}^{(1)} + \rho_{33}^{(2)} + \rho_{44}^{(1)} + \rho_{44}^{(2)} &= 1 \\
1 + \rho_{11}^{(2)} + 0 + \rho_{22}^{(2)} + 0 + 0 + 0 + \rho_{44}^{(2)} &= 1 \\
\rho_{11}^{(2)} &= -\rho_{22}^{(2)} - \rho_{44}^{(2)}
\end{aligned}$$

Therefore

$$\rho_{11}^{(2)} = -\left(\frac{1}{\hbar^2}\frac{|\mu_{12}|^2|\tilde{E}_1|^2}{\gamma_{21}}\left(\frac{2\Gamma_{21}}{\Delta_{21}^2+\Gamma_{21}^2}\right)\right) - \left(\frac{1}{\hbar^2}\frac{|\mu_{14}|^2|\tilde{E}_4|^2}{\gamma_{41}}\left(\frac{2\Gamma_{41}}{\Delta_{41}^2+\Gamma_{41}^2}\right)\right) \tag{C.79}$$

C.4.2 Derivation of second order coherence terms

We then solve equations (C.64) - (C.75) where $\dot{\rho}_{21}^{(2)} = \dot{\rho}_{12}^{(2)*}$, $\dot{\rho}_{31}^{(2)} = \dot{\rho}_{13}^{(2)*}$, $\dot{\rho}_{41}^{(2)} = \dot{\rho}_{14}^{(2)*}$, $\dot{\rho}_{32}^{(2)} = \dot{\rho}_{23}^{(2)*}$, $\dot{\rho}_{42}^{(2)} = \dot{\rho}_{24}^{(2)*}$ and $\dot{\rho}_{43}^{(2)} = \dot{\rho}_{34}^{(2)*}$. It is therefore only necessary to solve for one equation in each pair. We start by solving equation (C.64) for $\dot{\rho}_{12}^{(2)}$:

$$\dot{\rho}_{12}^{(2)} = -\Gamma_{12}\rho_{12}^{(2)}$$

The steady state solution is

$$\rho_{12}^{(2)} = 0 \tag{C.80}$$

and therefore

$$\rho_{21}^{(2)} = 0 \tag{C.81}$$

Next we solve equation (C.70) for $\dot{\rho}_{31}^{(2)}$:

$$\dot{\rho}_{31}^{(2)} = -\frac{\imath}{\hbar}(H_{32}\rho_{21}^{(1)} + H_{34}\rho_{41}^{(1)}) - \Gamma_{31}\rho_{31}^{(2)}$$

Re-arranging and expanding the terms gives:

$$\dot{\rho}_{31}^{(2)} + \Gamma_{31}\rho_{31}^{(2)} = -\frac{\imath}{\hbar}(-\mu_{32}E\tilde{\rho}_{21}^{(1)}e^{\imath(\omega_{32}+\omega_{21})t} - \mu_{34}E\tilde{\rho}_{41}^{(1)}e^{\imath(\omega_{34}+\omega_{41})t})$$

resulting in

$$\dot{\rho}_{31}^{(2)}e^{-\imath\omega_{31}t} + \Gamma_{31}\rho_{12}^{(2)}e^{-\imath\omega_{31}t} = -\frac{\imath}{\hbar}\left(-\mu_{32}E\left(\frac{1}{\hbar}\frac{\mu_{21}\tilde{E}_1e^{-\imath\omega_1t}}{\Delta_{21}-\imath\Gamma_{21}}\right) - \mu_{34}E\left(\frac{1}{\hbar}\frac{\mu_{41}\tilde{E}_4e^{-\imath\omega_4t}}{\Delta_{41}-\imath\Gamma_{41}}\right)\right)$$

When expanding E, we take into account only the frequencies that couple the $|3\rangle - |1\rangle$ transition, i.e. $e^{-\imath\omega_2t}$ and $e^{-\imath\omega_3t}$.

$$\dot{\rho}_{31}^{(2)}e^{-\imath\omega_{31}t} + \Gamma_{31}\rho_{12}^{(2)}e^{-\imath\omega_{31}t} = -\frac{\imath}{\hbar}\left(-\mu_{32}\tilde{E}_2e^{-\imath\omega_2t}\left(\frac{1}{\hbar}\frac{\mu_{21}\tilde{E}_1e^{-\imath\omega_1t}}{\Delta_{21}-\imath\Gamma_{21}}\right) - \mu_{34}\tilde{E}_3e^{-\imath\omega_3t}\left(\frac{1}{\hbar}\frac{\mu_{41}\tilde{E}_4e^{-\imath\omega_4t}}{\Delta_{41}-\imath\Gamma_{41}}\right)\right)$$

To get the steady state solution we must split the terms on the RHS as their driving terms are not the same. Let $\tilde{\rho}_{31}^{(2)} = \rho_{31}^{(2)}e^{-\imath\omega_{31}t}$ therefore $\dot{\tilde{\rho}}_{31}^{(2)} = \dot{\rho}_{31}^{(2)}e^{-\imath\omega_{31}t} - \imath\omega_{31}\tilde{\rho}_{31}^{(2)}$ which is substituted into the LHS of the equation. From the first term on the RHS we get:

$$\dot{\tilde{\rho}}_{31}^{(2)} + \imath\omega_{31}\tilde{\rho}_{31}^{(2)} + \Gamma_{31}\tilde{\rho}_{31}^{(2)} = \frac{\imath}{\hbar^2}\mu_{32}\mu_{21}\frac{\tilde{E}_1\tilde{E}_2e^{-\imath(\omega_2+\omega_1)t}}{\Delta_{21}-\imath\Gamma_{21}}$$

Taking the steady state solution to be of the form $\tilde{\rho}^{(2)}_{31(a)} = Ae^{-\imath(\omega_2+\omega_1)t}$ results in

$$\tilde{\rho}^{(2)}_{31(a)} = \frac{1}{\hbar^2}\mu_{32}\mu_{21}\frac{\tilde{E}_1\tilde{E}_2 e^{-\imath(\omega_2+\omega_1)t}}{(\Delta_{21}-\imath\Gamma_{21})(\Delta_{31}-\imath\Gamma_{31})} \tag{C.82}$$

where $\Delta_{31} = \omega_{31} - \omega_2 - \omega_1$. From the second term on the RHS we get:

$$\dot{\tilde{\rho}}^{(2)}_{31} + \imath\omega_{31}\tilde{\rho}^{(2)}_{31} + \Gamma_{31}\tilde{\rho}^{(2)}_{31} = \frac{\imath}{\hbar^2}\mu_{34}\mu_{41}\frac{\tilde{E}_3\tilde{E}_4 e^{-\imath(\omega_3+\omega_4)t}}{\Delta_{41}-\imath\Gamma_{41}}$$

Taking the steady state solution where $\tilde{\rho}^{(2)}_{31(b)} = Ae^{-\imath(\omega_3+\omega_4)t}$ results in

$$\tilde{\rho}^{(2)}_{31(b)} = \frac{1}{\hbar^2}\mu_{34}\mu_{41}\frac{\tilde{E}_3\tilde{E}_4 e^{-\imath(\omega_3+\omega_4)t}}{(\Delta_{41}-\imath\Gamma_{41})(\Delta_{31'}-\imath\Gamma_{31})} \tag{C.83}$$

where $\Delta_{31'} = \omega_{31} - \omega_3 - \omega_4$. Therefore the steady state solution is the sum of (C.82) and (C.83).

$$\tilde{\rho}^{(2)}_{31} = \frac{1}{\hbar^2}\frac{\mu_{21}\mu_{32}\tilde{E}_1\tilde{E}_2 e^{-\imath(\omega_2+\omega_1)t}}{(\Delta_{21}-\imath\Gamma_{21})(\Delta_{31}-\imath\Gamma_{31})} + \frac{1}{\hbar^2}\frac{\mu_{34}\mu_{41}\tilde{E}_3\tilde{E}_4 e^{-\imath(\omega_3+\omega_4)t}}{(\Delta_{41}-\imath\Gamma_{41})(\Delta_{31'}-\imath\Gamma_{31})} \tag{C.84}$$

and therefore

$$\tilde{\rho}^{(2)}_{13} = \frac{1}{\hbar^2}\frac{\mu_{12}\mu_{23}\tilde{E}^*_1\tilde{E}^*_2 e^{\imath(\omega_2+\omega_1)t}}{(\Delta_{21}+\imath\Gamma_{21})(\Delta_{31}+\imath\Gamma_{31})} + \frac{1}{\hbar^2}\frac{\mu_{43}\mu_{14}\tilde{E}^*_3\tilde{E}^*_4 e^{\imath(\omega_3+\omega_4)t}}{(\Delta_{41}+\imath\Gamma_{41})(\Delta_{31'}+\imath\Gamma_{31})} \tag{C.85}$$

We solve equation (C.73) for $\dot{\rho}_{41}^{(2)}$:

$$\dot{\rho}_{41}^{(2)} = -\Gamma_{41}\rho_{41}^{(2)}$$

The steady state solution is

$$\rho_{41}^{(2)} = 0 \tag{C.86}$$

and therefore

$$\rho_{14}^{(2)} = 0 \tag{C.87}$$

We solve equation (C.71) for $\dot{\rho}_{32}^{(2)}$:

$$\dot{\rho}_{32}^{(2)} = -\frac{\imath}{\hbar}(H_{31}\rho_{12}^{(1)}) - \Gamma_{32}\rho_{32}^{(2)}$$

Re-arranging and expanding the terms gives:

$$\dot{\rho}_{32}^{(2)} + \Gamma_{32}\rho_{32}^{(2)} = -\frac{\imath}{\hbar}(-\mu_{31}E\tilde{\rho}_{12}^{(1)}e^{\imath(\omega_{31}+\omega_{12})t})$$

resulting in

$$\dot{\rho}_{32}^{(2)}e^{-\imath\omega_{32}t} + \Gamma_{32}\rho_{32}^{(2)}e^{-\imath\omega_{32}t} = -\frac{\imath}{\hbar}\left(-\mu_{31}E\left(\frac{1}{\hbar}\frac{\mu_{12}\tilde{E}_1^* e^{\imath\omega_1 t}}{\Delta_{21}+\imath\Gamma_{21}}\right)\right)$$

When expanding E, we take into account only the frequencies that couple the $|3\rangle - |2\rangle$ transition. Since

none of the terms in the above equation will do this

$$\rho_{32}^{(2)} = 0 \tag{C.88}$$

and therefore

$$\rho_{23}^{(2)} = 0 \tag{C.89}$$

Next we solve equation (C.74) for $\dot{\rho}_{42}^{(2)}$:

$$\dot{\rho}_{42}^{(2)} = -\frac{\imath}{\hbar}(H_{41}\rho_{12}^{(1)} - H_{12}\rho_{41}^{(1)}) - \Gamma_{42}\rho_{42}^{(2)}$$

Re-arranging and expanding the terms gives:

$$\dot{\rho}_{42}^{(2)} + \Gamma_{42}\rho_{42}^{(2)} = -\frac{\imath}{\hbar}(-\mu_{41}E\tilde{\rho}_{12}^{(1)}e^{\imath(\omega_{41}+\omega_{12})t} + \mu_{12}E\tilde{\rho}_{41}^{(1)}e^{\imath(\omega_{12}+\omega_{41})t})$$

resulting in

$$\dot{\rho}_{42}^{(2)}e^{-\imath\omega_{42}t} + \Gamma_{42}\rho_{42}^{(2)}e^{-\imath\omega_{42}t} = -\frac{\imath}{\hbar}\left(-\mu_{41}E\left(\frac{1}{\hbar}\frac{\mu_{12}\tilde{E}_1^*e^{\imath\omega_1 t}}{\Delta_{21}+\imath\Gamma_{21}}\right) + \mu_{12}E\left(\frac{1}{\hbar}\frac{\mu_{41}\tilde{E}_4e^{-\imath\omega_4 t}}{\Delta_{41}-\imath\Gamma_{41}}\right)\right)$$

When expanding E, we take into account only the frequencies that couple the $|4\rangle - |2\rangle$ transition, i.e. $e^{-\imath\omega_4 t}$

and $e^{\imath\omega_1 t}$.

$$\dot{\rho}_{42}^{(2)} e^{-\imath\omega_{42}t} + \Gamma_{42}\rho_{42}^{(2)} e^{-\imath\omega_{42}t} = -\frac{\imath}{\hbar}\left(-\mu_{41}\tilde{E}_4 e^{-\imath\omega_4 t}\left(\frac{1}{\hbar}\frac{\mu_{12}\tilde{E}_1^* e^{\imath\omega_1 t}}{\Delta_{21}+\imath\Gamma_{21}}\right) + \mu_{12}\tilde{E}_1^* e^{\imath\omega_1 t}\left(\frac{1}{\hbar}\frac{\mu_{41}\tilde{E}_4 e^{-\imath\omega_4 t}}{\Delta_{41}-\imath\Gamma_{41}}\right)\right)$$

Let $\tilde{\rho}_{42}^{(2)} = \rho_{42}^{(2)} e^{-\imath\omega_{42}t}$ therefore $\dot{\tilde{\rho}}_{42}^{(2)} = \dot{\rho}_{42}^{(2)} e^{-\imath\omega_{42}t} - \imath\omega_{42}\tilde{\rho}_{42}^{(2)}$ which is substituted into the LHS of the equation.

$$\dot{\tilde{\rho}}_{42}^{(2)} + \imath\omega_{42}\tilde{\rho}_{42}^{(2)} + \Gamma_{42}\tilde{\rho}_{42}^{(2)} = \frac{\imath}{\hbar^2}\mu_{12}\mu_{41}\tilde{E}_1^*\tilde{E}_4\left(\frac{1}{\Delta_{21}+\imath\Gamma_{21}} - \frac{1}{\Delta_{41}-\imath\Gamma_{41}}\right)e^{-\imath(\omega_4-\omega_1)t}$$

Taking the steady state solution to be of the form $\tilde{\rho}_{42}^{(2)} = Ae^{-\imath(\omega_4-\omega_1)t}$ results in

$$\tilde{\rho}_{42}^{(2)} = \frac{1}{\hbar^2}\frac{\mu_{12}\mu_{41}\tilde{E}_1^*\tilde{E}_4}{\Delta_{42}-\imath\Gamma_{42}}\left(\frac{1}{\Delta_{21}+\imath\Gamma_{21}} - \frac{1}{\Delta_{41}-\imath\Gamma_{41}}\right)e^{-\imath(\omega_4-\omega_1)t} \tag{C.90}$$

and therefore

$$\tilde{\rho}_{24}^{(2)} = \frac{1}{\hbar^2}\frac{\mu_{21}\mu_{14}\tilde{E}_1\tilde{E}_4^*}{\Delta_{42}+\imath\Gamma_{42}}\left(\frac{1}{\Delta_{21}-\imath\Gamma_{21}} - \frac{1}{\Delta_{41}+\imath\Gamma_{41}}\right)e^{\imath(\omega_4-\omega_1)t} \tag{C.91}$$

where $\Delta_{42} = \omega_{42} - \omega_4 + \omega_1$. Lastly, we solve equation (C.75) for $\dot{\rho}_{43}^{(2)}$:

$$\dot{\rho}_{43}^{(2)} = -\frac{\imath}{\hbar}(-H_{13}\rho_{41}^{(1)}) - \Gamma_{43}\rho_{43}^{(2)}$$

Re-arranging and expanding the terms gives:

$$\dot{\rho}_{43}^{(2)} + \Gamma_{43}\rho_{43}^{(2)} = -\frac{\imath}{\hbar}(\mu_{13}E\tilde{\rho}_{41}^{(1)}e^{\imath(\omega_{13}+\omega_{41})t})$$

resulting in

$$\dot{\rho}_{43}^{(2)}e^{-\imath\omega_{43}t} + \Gamma_{43}\rho_{43}^{(2)}e^{-\imath\omega_{43}t} = -\frac{\imath}{\hbar}\left(\mu_{13}E\left(\frac{1}{\hbar}\frac{\mu_{41}\tilde{E}_4 e^{-\imath\omega_4 t}}{\Delta_{41} - \imath\Gamma_{41}}\right)\right)$$

When expanding E, we take into account only the frequencies that couple the $|4\rangle - |3\rangle$ transition. Since none of the terms in the above equation will do this

$$\rho_{43}^{(2)} = 0 \tag{C.92}$$

and therefore

$$\rho_{34}^{(2)} = 0 \tag{C.93}$$

Therefore

$$\rho^{(2)} = \begin{pmatrix} \tilde{\rho}_{11}^{(2)} & 0 & \tilde{\rho}_{13}^{(2)}e^{\imath\omega_{13}t} & 0 \\ 0 & \tilde{\rho}_{22}^{(2)} & 0 & \tilde{\rho}_{24}^{(2)}e^{\imath\omega_{24}t} \\ \tilde{\rho}_{31}^{(2)}e^{\imath\omega_{31}t} & 0 & 0 & 0 \\ 0 & \tilde{\rho}_{42}^{(2)}e^{\imath\omega_{42}t} & 0 & \tilde{\rho}_{44}^{(2)} \end{pmatrix} \tag{C.94}$$

C.5 Third Order Solution

Using equation (C.18) we can solve for the third order by expanding the following commutator:

$$\lambda^3 \dot{\rho}^{(3)} = -\frac{\imath}{\hbar}[\lambda H'_I, \lambda^2 \rho^{(2)}] + relaxation\, terms \tag{C.95}$$

$$\dot{\rho}^{(3)} = -\frac{\imath}{\hbar}\left[\begin{pmatrix} 0 & H_{12} & H_{13} & H_{14} \\ H_{21} & 0 & H_{23} & 0 \\ H_{31} & H_{32} & 0 & H_{34} \\ H_{41} & 0 & H_{43} & 0 \end{pmatrix}, \begin{pmatrix} \rho_{11}^{(2)} & 0 & \rho_{13}^{(2)} & 0 \\ 0 & \rho_{22}^{(2)} & 0 & \rho_{24}^{(2)} \\ \rho_{31}^{(2)} & 0 & 0 & 0 \\ 0 & \rho_{42}^{(2)} & 0 & \rho_{44}^{(2)} \end{pmatrix}\right] + relaxation\, terms \tag{C.96}$$

Note that $H_{ij} = \langle i|H'|j\rangle$. When expanding the commutator we get the following equations:

$$\dot{\rho}_{11}^{(3)} = -\frac{\imath}{\hbar}(H_{13}\rho_{31}^{(2)} - H_{31}\rho_{13}^{(2)}) + \gamma_{21}\rho_{22}^{(3)} + \gamma_{41}\rho_{44}^{(3)} \tag{C.97}$$

$$\dot{\rho}_{22}^{(3)} = \gamma_{32}\rho_{33}^{(3)} - \gamma_{21}\rho_{22}^{(3)} \tag{C.98}$$

$$\dot{\rho}_{33}^{(3)} = -\frac{\imath}{\hbar}(H_{31}\rho_{13}^{(2)} - H_{13}\rho_{31}^{(2)}) - \gamma_{32}\rho_{33}^{(3)} - \gamma_{34}\rho_{33}^{(3)} \tag{C.99}$$

$$\dot{\rho}_{44}^{(3)} = -\gamma_{41}\rho_{44}^{(3)} + \gamma_{34}\rho_{33}^{(3)} \tag{C.100}$$

$$\dot{\rho}_{12}^{(3)} = -\frac{\imath}{\hbar}(H_{12}\rho_{22}^{(2)} + H_{14}\rho_{42}^{(2)} - H_{12}\rho_{11}^{(2)} - H_{32}\rho_{13}^{(2)}) - \Gamma_{12}\rho_{12}^{(3)} \tag{C.101}$$

$$\dot{\rho}_{13}^{(3)} = -\frac{\imath}{\hbar}(-H_{13}\rho_{11}^{(2)}) - \Gamma_{13}\rho_{13}^{(3)} \tag{C.102}$$

$$\dot{\rho}_{14}^{(3)} = -\frac{\imath}{\hbar}(H_{12}\rho_{24}^{(2)} + H_{14}\rho_{44}^{(2)} - H_{14}\rho_{11}^{(2)} - H_{34}\rho_{13}^{(2)}) - \Gamma_{14}\rho_{14}^{(3)} \tag{C.103}$$

$$\dot{\rho}_{21}^{(3)} = -\frac{\imath}{\hbar}(H_{21}\rho_{11}^{(2)} + H_{23}\rho_{31}^{(2)} - H_{21}\rho_{22}^{(2)} - H_{41}\rho_{24}^{(2)}) - \Gamma_{21}\rho_{21}^{(3)} \tag{C.104}$$

$$\dot{\rho}_{23}^{(3)} = -\frac{\imath}{\hbar}(H_{21}\rho_{13}^{(2)} - H_{23}\rho_{22}^{(2)} - H_{43}\rho_{24}^{(2)}) - \Gamma_{23}\rho_{23}^{(3)} \tag{C.105}$$

$$\dot{\rho}_{24}^{(3)} = -\Gamma_{24}\rho_{24}^{(3)} \tag{C.106}$$

$$\dot{\rho}_{31}^{(3)} = -\frac{\imath}{\hbar}(H_{31}\rho_{11}^{(2)}) - \Gamma_{31}\rho_{31}^{(3)} \tag{C.107}$$

$$\dot{\rho}_{32}^{(3)} = -\frac{\imath}{\hbar}(H_{32}\rho_{22}^{(2)} + H_{34}\rho_{42}^{(2)} - H_{12}\rho_{31}^{(2)}) - \Gamma_{32}\rho_{32}^{(3)} \tag{C.108}$$

$$\dot{\rho}_{34}^{(3)} = -\frac{\imath}{\hbar}(H_{32}\rho_{24}^{(2)} + H_{34}\rho_{44}^{(2)} - H_{14}\rho_{31}^{(2)}) - \Gamma_{34}\rho_{34}^{(3)} \tag{C.109}$$

$$\dot{\rho}_{41}^{(3)} = -\frac{\imath}{\hbar}(H_{41}\rho_{11}^{(2)} + H_{43}\rho_{31}^{(2)} - H_{21}\rho_{42}^{(2)} - H_{41}\rho_{44}^{(2)}) - \Gamma_{41}\rho_{41}^{(3)} \tag{C.110}$$

$$\dot{\rho}_{42}^{(3)} = -\Gamma_{42}\rho_{42}^{(3)} \tag{C.111}$$

$$\dot{\rho}_{43}^{(3)} = -\frac{\imath}{\hbar}(H_{41}\rho_{13}^{(2)} - H_{23}\rho_{42}^{(2)} - H_{43}\rho_{44}^{(2)}) - \Gamma_{43}\rho_{43}^{(3)} \tag{C.112}$$

C.5.1 Derivation of third order population terms

Solving for equations (C.97) - (C.100) starting with equation (C.99):

$$\dot{\rho}_{33}^{(3)} = -\frac{\imath}{\hbar}(H_{31}\rho_{13}^{(2)} - H_{13}\rho_{31}^{(2)}) - \gamma_{32}\rho_{33}^{(3)} - \gamma_{34}\rho_{33}^{(3)}$$

We re-arrange and expand the terms:

$$\dot{\rho}_{33}^{(3)} + \gamma_{32}\rho_{33}^{(3)} + \gamma_{34}\rho_{33}^{(3)} = -\frac{\imath}{\hbar}(-\mu_{31}E\tilde{\rho}_{13}^{(2)}e^{\imath(\omega_{31}+\omega_{13})t} + \mu_{13}E\tilde{\rho}_{31}^{(2)}e^{\imath(\omega_{13}+\omega_{31})t})$$

$$\dot{\rho}_{33}^{(3)} + \gamma_{32}\rho_{33}^{(3)} + \gamma_{34}\rho_{33}^{(3)} = -\frac{\imath}{\hbar}\left(-\mu_{31}E\tilde{\rho}_{13}^{(2)} + \mu_{13}E\tilde{\rho}_{31}^{(2)}\right)$$

where

$$\tilde{\rho}_{13}^{(2)} = \left(\frac{1}{\hbar^2}\frac{\mu_{12}\mu_{23}\tilde{E}_1^*\tilde{E}_2^*e^{\imath(\omega_2+\omega_1)t}}{(\Delta_{21}+\imath\Gamma_{21})(\Delta_{31}+\imath\Gamma_{31})} + \frac{1}{\hbar^2}\frac{\mu_{43}\mu_{14}\tilde{E}_3^*\tilde{E}_4^*e^{\imath(\omega_3+\omega_4)t}}{(\Delta_{41}+\imath\Gamma_{41})(\Delta_{31'}+\imath\Gamma_{31})}\right)$$

and

$$\tilde{\rho}_{31}^{(2)} = \left(\frac{1}{\hbar^2}\frac{\mu_{21}\mu_{32}\tilde{E}_1\tilde{E}_2e^{-\imath(\omega_2+\omega_1)t}}{(\Delta_{21}-\imath\Gamma_{21})(\Delta_{31}-\imath\Gamma_{31})} + \frac{1}{\hbar^2}\frac{\mu_{34}\mu_{41}\tilde{E}_3\tilde{E}_4e^{-\imath(\omega_3+\omega_4)t}}{(\Delta_{41}-\imath\Gamma_{41})(\Delta_{31'}-\imath\Gamma_{31})}\right)$$

We now expand E and consider only the terms in $\pm\omega_3$ in the expansion of the above equation. Since none of the frequencies results in $\pm\omega_3$

$$\rho_{33}^{(3)} = 0 \tag{C.113}$$

We solve equation (C.100) for $\dot{\rho}_{44}^{(3)}$:

$$\dot{\rho}_{44}^{(3)} = -\gamma_{41}\rho_{44}^{(3)} + \gamma_{34}\rho_{33}^{(3)}$$

The steady state solution is

$$\rho_{44}^{(3)} = 0 \tag{C.114}$$

Next we solve equation (C.98) for $\dot{\rho}_{22}^{(3)}$:

$$\dot{\rho}_{22}^{(3)} = \gamma_{32}\rho_{33}^{(3)} - \gamma_{21}\rho_{22}^{(3)}$$

The steady state solution is

$$\rho_{22}^{(3)} = 0 \tag{C.115}$$

Finally, we solve equation (C.97) for $\dot{\rho}_{11}^{(3)}$:

$$\dot{\rho}_{11}^{(3)} = -\frac{\imath}{\hbar}(H_{13}\rho_{31}^{(2)} - H_{31}\rho_{13}^{(2)}) + \gamma_{21}\rho_{22}^{(3)} + \gamma_{41}\rho_{44}^{(3)}$$

We re-arrange and expand the terms:

$$\dot{\rho}_{11}^{(3)} = -\frac{\imath}{\hbar}(-\mu_{13}E\tilde{\rho}_{31}^{(2)}e^{\imath(\omega_{13}+\omega_{31})t} + \mu_{31}E\tilde{\rho}_{13}^{(2)}e^{\imath(\omega_{31}+\omega_{13})t})$$

$$\dot{\rho}_{11}^{(3)} = -\frac{\imath}{\hbar}\left(-\mu_{13}E\tilde{\rho}_{31}^{(2)} + \mu_{31}E\tilde{\rho}_{13}^{(2)}\right)$$

where

$$\tilde{\rho}_{13}^{(2)} = \left(\frac{1}{\hbar^2}\frac{\mu_{12}\mu_{23}\tilde{E}_1^*\tilde{E}_2^*e^{\imath(\omega_2+\omega_1)t}}{(\Delta_{21}+\imath\Gamma_{21})(\Delta_{31}+\imath\Gamma_{31})} + \frac{1}{\hbar^2}\frac{\mu_{43}\mu_{14}\tilde{E}_3^*\tilde{E}_4^*e^{\imath(\omega_3+\omega_4)t}}{(\Delta_{41}+\imath\Gamma_{41})(\Delta_{31'}+\imath\Gamma_{31})}\right)$$

and

$$\tilde{\rho}_{31}^{(2)} = \left(\frac{1}{\hbar^2} \frac{\mu_{21}\mu_{32}\tilde{E}_1\tilde{E}_2 e^{-\imath(\omega_2+\omega_1)t}}{(\Delta_{21} - \imath\Gamma_{21})(\Delta_{31} - \imath\Gamma_{31})} + \frac{1}{\hbar^2} \frac{\mu_{34}\mu_{41}\tilde{E}_3\tilde{E}_4 e^{-\imath(\omega_3+\omega_4)t}}{(\Delta_{41} - \imath\Gamma_{41})(\Delta_{31'} - \imath\Gamma_{31})} \right)$$

We now expand E and consider only the terms in $\pm\omega_1$ in the expansion of the above equation. Since none of the frequencies results in $\pm\omega_1$

$$\rho_{11}^{(3)} = 0 \tag{C.116}$$

C.5.2 Derivation of third order coherence terms

We then solve equations (C.101) - (C.112) where $\dot{\rho}_{21}^{(3)} = \dot{\rho}_{12}^{(3)*}$, $\dot{\rho}_{31}^{(3)} = \dot{\rho}_{13}^{(3)*}$, $\dot{\rho}_{41}^{(3)} = \dot{\rho}_{14}^{(3)*}$, $\dot{\rho}_{32}^{(3)} = \dot{\rho}_{23}^{(3)*}$, $\dot{\rho}_{42}^{(3)} = \dot{\rho}_{24}^{(3)*}$ and $\dot{\rho}_{43}^{(3)} = \dot{\rho}_{34}^{(3)*}$. It is therefore only necessary to solve for one equation in each pair. We start by solving equation (C.104) for $\dot{\rho}_{21}^{(3)}$:

$$\dot{\rho}_{21}^{(3)} = -\frac{\imath}{\hbar}(H_{21}\rho_{11}^{(2)} + H_{23}\rho_{31}^{(2)} - H_{21}\rho_{22}^{(2)} - H_{41}\rho_{24}^{(2)}) - \Gamma_{21}\rho_{21}^{(3)}$$

Re-arranging and expanding the terms gives:

$$\dot{\rho}_{21}^{(3)} + \Gamma_{21}\rho_{21}^{(3)} = -\frac{\imath}{\hbar}(-\mu_{21}E(\tilde{\rho}_{11}^{(2)} - \tilde{\rho}_{22}^{(2)})e^{\imath\omega_{21}t} - \mu_{23}E\tilde{\rho}_{31}^{(2)}e^{\imath(\omega_{23}+\omega_{31})t} + \mu_{41}E\tilde{\rho}_{24}^{(2)}e^{\imath(\omega_{41}+\omega_{24})t})$$

resulting in

$$\dot{\rho}_{21}^{(3)}e^{-\imath\omega_{21}t} + \Gamma_{21}\rho_{21}^{(3)}e^{-\imath\omega_{21}t} = \frac{\imath}{\hbar}\left(\mu_{21}E(\tilde{\rho}_{11}^{(2)} - \tilde{\rho}_{22}^{(2)}) + \mu_{23}E\tilde{\rho}_{31}^{(2)} - \mu_{41}E\tilde{\rho}_{24}^{(2)}\right)$$

where

$$\tilde{\rho}_{11}^{(2)} = \left(-\left(\frac{1}{\hbar^2} \frac{|\mu_{12}|^2 |\tilde{E}_1|^2}{\gamma_{21}} \left(\frac{2\Gamma_{21}}{\Delta_{21}^2 + \Gamma_{21}^2} \right) \right) - \left(\frac{1}{\hbar^2} \frac{|\mu_{14}|^2 |\tilde{E}_4|^2}{\gamma_{41}} \left(\frac{2\Gamma_{41}}{\Delta_{41}^2 + \Gamma_{41}^2} \right) \right) \right)$$

$$\tilde{\rho}_{22}^{(2)} = \left(\frac{1}{\hbar^2} \frac{|\mu_{12}|^2 |\tilde{E}_1|^2}{\gamma_{21}} \left(\frac{2\Gamma_{21}}{\Delta_{21}^2 + \Gamma_{21}^2} \right) \right)$$

$$\tilde{\rho}_{31}^{(2)} = \left(\frac{1}{\hbar^2} \frac{\mu_{21}\mu_{32}\tilde{E}_1\tilde{E}_2 e^{-\imath(\omega_2+\omega_1)t}}{(\Delta_{21} - \imath\Gamma_{21})(\Delta_{31} - \imath\Gamma_{31})} + \frac{1}{\hbar^2} \frac{\mu_{34}\mu_{41}\tilde{E}_3\tilde{E}_4 e^{-\imath(\omega_3+\omega_4)t}}{(\Delta_{41} - \imath\Gamma_{41})(\Delta_{31'} - \imath\Gamma_{31})} \right)$$

and

$$\tilde{\rho}_{24}^{(2)} = \left(\frac{1}{\hbar^2} \frac{\mu_{21}\mu_{14}\tilde{E}_1\tilde{E}_4^*}{\Delta_{42} + \imath\Gamma_{42}} \left(\frac{1}{\Delta_{21} - \imath\Gamma_{21}} - \frac{1}{\Delta_{41} + \imath\Gamma_{41}} \right) e^{\imath(\omega_4 - \omega_1)t} \right)$$

We now expand E and consider only the terms that are resonant with the $|2\rangle - |1\rangle$ transition.

$$\dot{\rho}_{21}^{(3)} e^{-\imath\omega_{21}t} + \Gamma_{21}\rho_{21}^{(3)} e^{-\imath\omega_{21}t} = \frac{\imath}{\hbar} \left(\mu_{21}\tilde{E}_1 e^{-\imath\omega_1 t}(\tilde{\rho}_{11}^{(2)} - \tilde{\rho}_{22}^{(2)}) + \mu_{23}\tilde{E}_2 e^{-\imath\omega_2 t}\tilde{\rho}_{31}^{(2)} - \mu_{41}\tilde{E}_4 e^{-\imath\omega_4 t}\tilde{\rho}_{24}^{(2)} \right)$$

The steady state solution is

$$\tilde{\rho}_{21}^{(3)} = \frac{1}{(\Delta_{21} - \imath\Gamma_{21})}\Bigg[-\frac{1}{\hbar^3}\frac{\mu_{21}|\mu_{12}|^2\tilde{E}_1|\tilde{E}_1|^2}{\gamma_{21}}\left(\frac{4\Gamma_{21}}{\Delta_{21}^2+\Gamma_{21}^2}\right) - \frac{1}{\hbar^3}\frac{\mu_{21}|\mu_{14}|^2\tilde{E}_1|\tilde{E}_4|^2}{\gamma_{41}}\left(\frac{2\Gamma_{41}}{\Delta_{41}^2+\Gamma_{41}^2}\right)$$
$$+\frac{1}{\hbar^3}\frac{\mu_{21}|\mu_{23}|^2\tilde{E}_1|\tilde{E}_2|^2}{(\Delta_{21}-\imath\Gamma_{21})(\Delta_{31}-\imath\Gamma_{31})} + \frac{1}{\hbar^3}\frac{\mu_{23}\mu_{34}\mu_{41}\tilde{E}_2\tilde{E}_3\tilde{E}_4}{(\Delta_{41}-\imath\Gamma_{41})(\Delta_{31'}-\imath\Gamma_{31})}$$
$$-\frac{1}{\hbar^3}\frac{\mu_{21}|\mu_{41}|^2\tilde{E}_1|\tilde{E}_4|^2}{(\Delta_{42}+\imath\Gamma_{42})}\left(\frac{1}{(\Delta_{21}-\imath\Gamma_{21})} - \frac{1}{(\Delta_{41}+\imath\Gamma_{41})}\right)\Bigg]e^{-\imath\omega_1 t} \tag{C.117}$$

and therefore

$$\tilde{\rho}_{12}^{(3)} = \frac{1}{(\Delta_{21} + \imath\Gamma_{21})}\Bigg[-\frac{1}{\hbar^3}\frac{\mu_{12}|\mu_{21}|^2\tilde{E}_1^*|\tilde{E}_1|^2}{\gamma_{21}}\left(\frac{4\Gamma_{21}}{\Delta_{21}^2+\Gamma_{21}^2}\right) - \frac{1}{\hbar^3}\frac{\mu_{12}|\mu_{41}|^2\tilde{E}_1^*|\tilde{E}_4|^2}{\gamma_{41}}\left(\frac{2\Gamma_{41}}{\Delta_{41}^2+\Gamma_{41}^2}\right)$$
$$+\frac{1}{\hbar^3}\frac{\mu_{12}|\mu_{32}|^2\tilde{E}_1^*|\tilde{E}_2|^2}{(\Delta_{21}+\imath\Gamma_{21})(\Delta_{31}+\imath\Gamma_{31})} + \frac{1}{\hbar^3}\frac{\mu_{32}\mu_{43}\mu_{14}\tilde{E}_2^*\tilde{E}_3^*\tilde{E}_4^*}{(\Delta_{41}+\imath\Gamma_{41})(\Delta_{31'}+\imath\Gamma_{31})}$$
$$-\frac{1}{\hbar^3}\frac{\mu_{12}|\mu_{14}|^2\tilde{E}_1^*|\tilde{E}_4|^2}{(\Delta_{42}-\imath\Gamma_{42})}\left(\frac{1}{(\Delta_{21}+\imath\Gamma_{21})} - \frac{1}{(\Delta_{41}-\imath\Gamma_{41})}\right)\Bigg]e^{\imath\omega_1 t} \tag{C.118}$$

where $\Delta_{21} = \omega_{21} - \omega_1$. Next we solve equation (C.107) for $\dot{\rho}_{31}^{(3)}$:

$$\dot{\rho}_{31}^{(3)} = -\frac{\imath}{\hbar}(H_{31}\rho_{11}^{(2)}) - \Gamma_{31}\rho_{31}^{(3)}$$

Re-arrange and expand the terms to give

$$\dot{\rho}_{31}^{(3)} + \Gamma_{31}\rho_{31}^{(3)} = -\frac{\imath}{\hbar}(-\mu_{31}E\rho_{11}^{(2)}e^{\imath\omega_{31}t})$$

$$\dot{\rho}_{31}^{(3)}e^{-\imath\omega_{31}t} + \Gamma_{31}\rho_{31}^{(3)}e^{-\imath\omega_{31}t} = \frac{\imath}{\hbar}(\mu_{31}E\rho_{11}^{(2)})$$

where

$$\tilde{\rho}_{11}^{(2)} = \left(-\left(\frac{1}{\hbar^2}\frac{|\mu_{12}|^2|\tilde{E}_1|^2}{\gamma_{21}}\left(\frac{2\Gamma_{21}}{\Delta_{21}^2+\Gamma_{21}^2}\right)\right) - \left(\frac{1}{\hbar^2}\frac{|\mu_{14}|^2|\tilde{E}_4|^2}{\gamma_{41}}\left(\frac{2\Gamma_{41}}{\Delta_{41}^2+\Gamma_{41}^2}\right)\right)\right)$$

We now expand E and consider only the terms that are resonant with the $|3\rangle - |1\rangle$ transition. Since none of the frequencies resonantly couple the transition

$$\rho_{31}^{(3)} = 0 \tag{C.119}$$

and therefore

$$\rho_{13}^{(3)} = 0 \tag{C.120}$$

We now solve equation (C.110) for $\dot{\rho}_{41}^{(3)}$:

$$\dot{\rho}_{41}^{(3)} = -\frac{\imath}{\hbar}(H_{41}\rho_{11}^{(2)} + H_{43}\rho_{31}^{(2)} - H_{21}\rho_{42}^{(2)} - H_{41}\rho_{44}^{(2)}) - \Gamma_{41}\rho_{41}^{(3)}$$

Re-arranging and expanding the terms gives:

$$\dot{\rho}_{41}^{(3)} + \Gamma_{41}\rho_{41}^{(3)} = -\frac{\imath}{\hbar}(-\mu_{41}E(\tilde{\rho}_{11}^{(2)} - \tilde{\rho}_{44}^{(2)})e^{\imath\omega_{41}t} - \mu_{43}E\tilde{\rho}_{31}^{(2)}e^{\imath(\omega_{43}+\omega_{31})t} + \mu_{21}E\tilde{\rho}_{42}^{(2)}e^{\imath(\omega_{21}+\omega_{42})t})$$

resulting in

$$\dot{\rho}_{41}^{(3)}e^{-\imath\omega_{41}t} + \Gamma_{41}\rho_{41}^{(3)}e^{-\imath\omega_{41}t} = \frac{\imath}{\hbar}\left(\mu_{41}E(\tilde{\rho}_{11}^{(2)} - \tilde{\rho}_{44}^{(2)}) + \mu_{43}E\tilde{\rho}_{31}^{(2)} - \mu_{21}E\tilde{\rho}_{42}^{(2)}\right)$$

where

$$\tilde{\rho}_{11}^{(2)} = \left(-\left(\frac{1}{\hbar^2}\frac{|\mu_{12}|^2|\tilde{E}_1|^2}{\gamma_{21}}\left(\frac{2\Gamma_{21}}{\Delta_{21}^2+\Gamma_{21}^2}\right)\right) - \left(\frac{1}{\hbar^2}\frac{|\mu_{14}|^2|\tilde{E}_4|^2}{\gamma_{41}}\left(\frac{2\Gamma_{41}}{\Delta_{41}^2+\Gamma_{41}^2}\right)\right)\right)$$

$$\tilde{\rho}_{44}^{(2)} = \left(\frac{1}{\hbar^2}\frac{|\mu_{14}|^2|\tilde{E}_4|^2}{\gamma_{41}}\left(\frac{2\Gamma_{41}}{\Delta_{41}^2+\Gamma_{41}^2}\right)\right)$$

$$\tilde{\rho}_{31}^{(2)} = \left(\frac{1}{\hbar^2}\frac{\mu_{21}\mu_{32}\tilde{E}_1\tilde{E}_2e^{-\imath(\omega_2+\omega_1)t}}{(\Delta_{21}-\imath\Gamma_{21})(\Delta_{31}-\imath\Gamma_{31})} + \frac{1}{\hbar^2}\frac{\mu_{34}\mu_{41}\tilde{E}_3\tilde{E}_4e^{-\imath(\omega_3+\omega_4)t}}{(\Delta_{41}-\imath\Gamma_{41})(\Delta_{31'}-\imath\Gamma_{31})}\right)$$

and

$$\tilde{\rho}_{42}^{(2)} = \left(\frac{1}{\hbar^2}\frac{\mu_{12}\mu_{41}\tilde{E}_1^*\tilde{E}_4}{\Delta_{42}-\imath\Gamma_{42}}\left(\frac{1}{\Delta_{21}+\imath\Gamma_{21}} - \frac{1}{\Delta_{41}-\imath\Gamma_{41}}\right)e^{-\imath(\omega_4-\omega_1)t}\right)$$

We now expand E and consider only the terms that are resonant with the $|4\rangle - |1\rangle$ transition.

$$\dot{\rho}_{41}^{(3)}e^{-\imath\omega_{41}t} + \Gamma_{41}\rho_{41}^{(3)}e^{-\imath\omega_{41}t} = \frac{\imath}{\hbar}\left(\mu_{41}\tilde{E}_4e^{-\imath\omega_4t}(\tilde{\rho}_{11}^{(2)} - \tilde{\rho}_{44}^{(2)}) + \mu_{43}\tilde{E}_3e^{-\imath\omega_3t}\tilde{\rho}_{31}^{(2)} - \mu_{21}\tilde{E}_1^*e^{\imath\omega_1t}\tilde{\rho}_{42}^{(2)}\right)$$

The steady state solution is

$$\tilde{\rho}_{41}^{(3)} = \frac{1}{(\Delta_{41} - \imath\Gamma_{41})}\Bigg[-\frac{1}{\hbar^3}\frac{|\mu_{12}|^2\mu_{41}|\tilde{E}_1|^2\tilde{E}_4}{\gamma_{21}}\left(\frac{2\Gamma_{21}}{\Delta_{21}^2+\Gamma_{21}^2}\right) - \frac{1}{\hbar^3}\frac{\mu_{41}|\mu_{14}|^2\tilde{E}_4|\tilde{E}_4|^2}{\gamma_{41}}\left(\frac{4\Gamma_{41}}{\Delta_{41}^2+\Gamma_{41}^2}\right)$$
$$+\frac{1}{\hbar^3}\frac{\mu_{21}\mu_{32}\mu_{43}\tilde{E}_1\tilde{E}_2\tilde{E}_3}{(\Delta_{21}-\imath\Gamma_{21})(\Delta_{31}-\imath\Gamma_{31})} + \frac{1}{\hbar^3}\frac{|\mu_{34}|^2\mu_{41}|\tilde{E}_3|^2\tilde{E}_4}{(\Delta_{41}-\imath\Gamma_{41})(\Delta_{31'}-\imath\Gamma_{31})}$$
$$-\frac{1}{\hbar^3}\frac{|\mu_{21}|^2\mu_{41}|\tilde{E}_1|^2\tilde{E}_4}{(\Delta_{42}-\imath\Gamma_{42})}\left(\frac{1}{(\Delta_{21}+\imath\Gamma_{21})} - \frac{1}{(\Delta_{41}-\imath\Gamma_{41})}\right)\Bigg]e^{-\imath\omega_4 t} \tag{C.121}$$

and therefore

$$\tilde{\rho}_{14}^{(3)} = \frac{1}{(\Delta_{41} + \imath\Gamma_{41})}\Bigg[-\frac{1}{\hbar^3}\frac{|\mu_{21}|^2\mu_{14}|\tilde{E}_1|^2\tilde{E}_4^*}{\gamma_{21}}\left(\frac{2\Gamma_{21}}{\Delta_{21}^2+\Gamma_{21}^2}\right) - \frac{1}{\hbar^3}\frac{\mu_{14}|\mu_{41}|^2\tilde{E}_4^*|\tilde{E}_4|^2}{\gamma_{41}}\left(\frac{4\Gamma_{41}}{\Delta_{41}^2+\Gamma_{41}^2}\right)$$
$$+\frac{1}{\hbar^3}\frac{\mu_{12}\mu_{23}\mu_{34}\tilde{E}_1^*\tilde{E}_2^*\tilde{E}_3^*}{(\Delta_{21}+\imath\Gamma_{21})(\Delta_{31}+\imath\Gamma_{31})} + \frac{1}{\hbar^3}\frac{|\mu_{43}|^2\mu_{14}|\tilde{E}_3|^2\tilde{E}_4^*}{(\Delta_{41}+\imath\Gamma_{41})(\Delta_{31'}+\imath\Gamma_{31})}$$
$$-\frac{1}{\hbar^3}\frac{|\mu_{12}|^2\mu_{14}|\tilde{E}_1|^2\tilde{E}_4^*}{(\Delta_{42}+\imath\Gamma_{42})}\left(\frac{1}{(\Delta_{21}-\imath\Gamma_{21})} - \frac{1}{(\Delta_{41}+\imath\Gamma_{41})}\right)\Bigg]e^{\imath\omega_4 t} \tag{C.122}$$

where $\Delta_{41} = \omega_{41} - \omega_4$. We now solve equation (C.108) for $\dot{\rho}_{32}^{(3)}$:

$$\dot{\rho}_{32}^{(3)} = -\frac{\imath}{\hbar}(H_{32}\rho_{22}^{(2)} + H_{34}\rho_{42}^{(2)} - H_{12}\rho_{31}^{(2)}) - \Gamma_{32}\rho_{32}^{(3)}$$

Re-arranging and expanding the terms gives:

$$\dot{\rho}_{32}^{(3)} + \Gamma_{32}\rho_{32}^{(3)} = -\frac{\imath}{\hbar}(-\mu_{32}E\tilde{\rho}_{22}^{(2)}e^{\imath\omega_{32}t} - \mu_{34}E\tilde{\rho}_{42}^{(2)}e^{\imath(\omega_{34}+\omega_{42})t} + \mu_{12}E\tilde{\rho}_{31}^{(2)}e^{\imath(\omega_{12}+\omega_{31})t})$$

resulting in

$$\dot{\rho}_{32}^{(3)}e^{-\imath\omega_{32}t} + \Gamma_{32}\rho_{32}^{(3)}e^{-\imath\omega_{32}t} = \frac{\imath}{\hbar}\left(\mu_{32}E\tilde{\rho}_{22}^{(2)} + \mu_{34}E\tilde{\rho}_{42}^{(2)} - \mu_{12}E\tilde{\rho}_{31}^{(2)}\right)$$

where

$$\tilde{\rho}_{22}^{(2)} = \left(\frac{1}{\hbar^2}\frac{|\mu_{12}|^2|\tilde{E}_1|^2}{\gamma_{21}}\left(\frac{2\Gamma_{21}}{\Delta_{21}^2+\Gamma_{21}^2}\right)\right)$$

$$\tilde{\rho}_{42}^{(2)} = \left(\frac{1}{\hbar^2}\frac{\mu_{12}\mu_{41}\tilde{E}_1^*\tilde{E}_4}{\Delta_{42}-\imath\Gamma_{42}}\left(\frac{1}{\Delta_{21}+\imath\Gamma_{21}} - \frac{1}{\Delta_{41}-\imath\Gamma_{41}}\right)e^{-\imath(\omega_4-\omega_1)t}\right)$$

and

$$\tilde{\rho}_{31}^{(2)} = \left(\frac{1}{\hbar^2}\frac{\mu_{21}\mu_{32}\tilde{E}_1\tilde{E}_2e^{-\imath(\omega_2+\omega_1)t}}{(\Delta_{21}-\imath\Gamma_{21})(\Delta_{31}-\imath\Gamma_{31})} + \frac{1}{\hbar^2}\frac{\mu_{34}\mu_{41}\tilde{E}_3\tilde{E}_4e^{-\imath(\omega_3+\omega_4)t}}{(\Delta_{41}-\imath\Gamma_{41})(\Delta_{31'}-\imath\Gamma_{31})}\right)$$

We now expand E and consider only the terms that are resonant with the $|3\rangle - |2\rangle$ transition.

$$\dot{\rho}_{32}^{(3)}e^{-\imath\omega_{32}t} + \Gamma_{32}\rho_{32}^{(3)}e^{-\imath\omega_{32}t} = \frac{\imath}{\hbar}\left(\mu_{32}\tilde{E}_2e^{-\imath\omega_2t}\tilde{\rho}_{22}^{(2)} + \mu_{34}\tilde{E}_3^*e^{\imath\omega_3t}\tilde{\rho}_{42}^{(2)} - \mu_{12}\tilde{E}_1e^{-\imath\omega_1t}\tilde{\rho}_{31}^{(2)}\right)$$

The steady state solution is

$$\tilde{\rho}_{32}^{(3)} = \frac{1}{(\Delta_{32} - \imath\Gamma_{32})}\left[\frac{1}{\hbar^3}\frac{|\mu_{12}|^2\mu_{32}|\tilde{E}_1|^2\tilde{E}_2}{\gamma_{21}}\left(\frac{2\Gamma_{21}}{\Delta_{21}^2+\Gamma_{21}^2}\right) - \frac{1}{\hbar^3}\frac{|\mu_{12}|^2\mu_{32}|\tilde{E}_1|^2\tilde{E}_2}{(\Delta_{21}-\imath\Gamma_{21})(\Delta_{31}-\imath\Gamma_{31})}\right.$$
$$+ \frac{1}{\hbar^3}\frac{\mu_{12}\mu_{34}\mu_{41}\tilde{E}_1^*\tilde{E}_3^*\tilde{E}_4}{(\Delta_{42}-\imath\Gamma_{42})}\left(\frac{1}{(\Delta_{21}+\imath\Gamma_{21})} - \frac{1}{(\Delta_{41}-\imath\Gamma_{41})}\right) \qquad \text{(C.123)}$$
$$\left. - \frac{1}{\hbar^3}\frac{\mu_{12}\mu_{34}\mu_{14}\tilde{E}_1\tilde{E}_3\tilde{E}_4}{(\Delta_{41}-\imath\Gamma_{41})(\Delta_{31'}-\imath\Gamma_{31})}\right]e^{-\imath\omega_2 t}$$

and therefore

$$\tilde{\rho}_{23}^{(3)} = \frac{1}{(\Delta_{32} + \imath\Gamma_{32})}\left[\frac{1}{\hbar^3}\frac{|\mu_{21}|^2\mu_{23}|\tilde{E}_1|^2\tilde{E}_2^*}{\gamma_{21}}\left(\frac{2\Gamma_{21}}{\Delta_{21}^2+\Gamma_{21}^2}\right) - \frac{1}{\hbar^3}\frac{|\mu_{21}|^2\mu_{23}|\tilde{E}_1|^2\tilde{E}_2^*}{(\Delta_{21}+\imath\Gamma_{21})(\Delta_{31}+\imath\Gamma_{31})}\right.$$
$$+ \frac{1}{\hbar^3}\frac{\mu_{21}\mu_{43}\mu_{14}\tilde{E}_1\tilde{E}_3\tilde{E}_4^*}{(\Delta_{42}+\imath\Gamma_{42})}\left(\frac{1}{(\Delta_{21}-\imath\Gamma_{21})} - \frac{1}{(\Delta_{41}+\imath\Gamma_{41})}\right) \qquad \text{(C.124)}$$
$$\left. - \frac{1}{\hbar^3}\frac{\mu_{21}\mu_{43}\mu_{41}\tilde{E}_1^*\tilde{E}_3^*\tilde{E}_4^*}{(\Delta_{41}+\imath\Gamma_{41})(\Delta_{31'}+\imath\Gamma_{31})}\right]e^{\imath\omega_2 t}$$

where $\Delta_{32} = \omega_{32} - \omega_2$. Next we solve equation (C.111) for $\dot{\rho}_{42}^{(3)}$:

$$\dot{\rho}_{42}^{(3)} = -\Gamma_{42}\rho_{42}^{(3)}$$

The steady state solution is

$$\rho_{42}^{(3)} = 0 \tag{C.125}$$

and therefore

$$\rho_{24}^{(3)} = 0 \tag{C.126}$$

We now solve equation (C.109) for $\dot{\rho}_{34}^{(3)}$:

$$\dot{\rho}_{34}^{(3)} = -\frac{\imath}{\hbar}(H_{32}\rho_{24}^{(2)} + H_{34}\rho_{44}^{(2)} - H_{14}\rho_{31}^{(2)}) - \Gamma_{34}\rho_{34}^{(3)}$$

Re-arranging and expanding the terms gives:

$$\dot{\rho}_{34}^{(3)} + \Gamma_{34}\rho_{34}^{(3)} = -\frac{\imath}{\hbar}(-\mu_{32}E\tilde{\rho}_{24}^{(2)}e^{\imath(\omega_{32}-\omega_{24})t} - \mu_{34}E\tilde{\rho}_{44}^{(2)}e^{\imath\omega_{34}t} + \mu_{14}E\tilde{\rho}_{31}^{(2)}e^{\imath(\omega_{14}+\omega_{31})t})$$

resulting in

$$\dot{\rho}_{34}^{(3)}e^{-\imath\omega_{34}t} + \Gamma_{34}\rho_{34}^{(3)}e^{-\imath\omega_{34}t} = \frac{\imath}{\hbar}\left(\mu_{32}E\tilde{\rho}_{24}^{(2)} + \mu_{34}E\tilde{\rho}_{44}^{(2)} - \mu_{14}E\tilde{\rho}_{31}^{(2)}\right)$$

where

$$\tilde{\rho}_{24}^{(2)} = \left(\frac{1}{\hbar^2}\frac{\mu_{21}\mu_{14}\tilde{E}_1\tilde{E}_4^*}{\Delta_{42}+\imath\Gamma_{42}}\left(\frac{1}{\Delta_{21}-\imath\Gamma_{21}} - \frac{1}{\Delta_{41}+\imath\Gamma_{41}}\right)e^{\imath(\omega_4-\omega_1)t}\right)$$

$$\tilde{\rho}_{44}^{(2)} = \left(\frac{1}{\hbar^2}\frac{|\mu_{14}|^2|\tilde{E}_4|^2}{\gamma_{41}}\left(\frac{2\Gamma_{41}}{\Delta_{41}^2+\Gamma_{41}^2}\right)\right)$$

and

$$\tilde{\rho}_{31}^{(2)} = \left(\frac{1}{\hbar^2} \frac{\mu_{21}\mu_{32}\tilde{E}_1\tilde{E}_2 e^{-\imath(\omega_2+\omega_1)t}}{(\Delta_{21}-\imath\Gamma_{21})(\Delta_{31}-\imath\Gamma_{31})} + \frac{1}{\hbar^2} \frac{\mu_{34}\mu_{41}\tilde{E}_3\tilde{E}_4 e^{-\imath(\omega_3+\omega_4)t}}{(\Delta_{41}-\imath\Gamma_{41})(\Delta_{31'}-\imath\Gamma_{31})} \right)$$

We now expand E and consider only the terms that are resonant with the $|3\rangle - |4\rangle$ transition.

$$\dot{\rho}_{34}^{(3)} e^{-\imath\omega_{34}t} + \Gamma_{34}\rho_{34}^{(3)} e^{-\imath\omega_{34}t} = \frac{\imath}{\hbar}\left(\mu_{32}\tilde{E}_2 e^{-\imath\omega_2 t}\tilde{\rho}_{24}^{(2)} + \mu_{34}\tilde{E}_3 e^{-\imath\omega_3 t}\tilde{\rho}_{44}^{(2)} - \mu_{14}\tilde{E}_4 e^{-\imath\omega_4 t}\tilde{\rho}_{31}^{(2)} \right)$$

The steady state solution results in

$$\begin{aligned}\tilde{\rho}_{34}^{(3)} = \frac{1}{(\Delta_{34}-\imath\Gamma_{34})}\Bigg[& \frac{1}{\hbar^3}\frac{\mu_{21}\mu_{32}\mu_{14}\tilde{E}_1\tilde{E}_2\tilde{E}_4^*}{(\Delta_{42}+\imath\Gamma_{42})}\left(\frac{1}{(\Delta_{21}-\imath\Gamma_{21})} - \frac{1}{(\Delta_{41}+\imath\Gamma_{41})}\right) \\ & + \frac{1}{\hbar^3}\frac{\mu_{34}|\mu_{14}|^2\tilde{E}_3|\tilde{E}_4|^2}{\gamma_{41}}\left(\frac{2\Gamma_{41}}{\Delta_{41}^2+\Gamma_{41}^2}\right) - \frac{1}{\hbar^3}\frac{\mu_{21}\mu_{32}\mu_{14}\tilde{E}_1\tilde{E}_2\tilde{E}_4}{(\Delta_{21}-\imath\Gamma_{21})(\Delta_{31}-\imath\Gamma_{31})} \\ & - \frac{1}{\hbar^3}\frac{\mu_{34}|\mu_{14}|^2\tilde{E}_3|\tilde{E}_4|^2}{(\Delta_{41}-\imath\Gamma_{41})(\Delta_{31'}-\imath\Gamma_{31})}\Bigg] e^{-\imath\omega_3 t}\end{aligned} \tag{C.127}$$

and therefore

$$\tilde{\rho}_{43}^{(3)} = \frac{1}{(\Delta_{34}+\imath\Gamma_{34})}\Bigg[\frac{1}{\hbar^3}\frac{\mu_{12}\mu_{23}\mu_{41}\tilde{E}_1^*\tilde{E}_2^*\tilde{E}_4}{(\Delta_{42}-\imath\Gamma_{42})}\left(\frac{1}{(\Delta_{21}+\imath\Gamma_{21})}-\frac{1}{(\Delta_{41}-\imath\Gamma_{41})}\right) + \frac{1}{\hbar^3}\frac{\mu_{43}|\mu_{41}|^2\tilde{E}_3^*|\tilde{E}_4|^2}{\gamma_{41}}\left(\frac{2\Gamma_{41}}{\Delta_{41}^2+\Gamma_{41}^2}\right) - \frac{1}{\hbar^3}\frac{\mu_{12}\mu_{23}\mu_{41}\tilde{E}_1^*\tilde{E}_2^*\tilde{E}_4^*}{(\Delta_{21}+\imath\Gamma_{21})(\Delta_{31}+\imath\Gamma_{31})} - \frac{1}{\hbar^3}\frac{\mu_{43}|\mu_{41}|^2\tilde{E}_3^*|\tilde{E}_4|^2}{(\Delta_{41}+\imath\Gamma_{41})(\Delta_{31'}+\imath\Gamma_{31})}\Bigg]e^{\imath\omega_3 t} \tag{C.128}$$

where $\Delta_{34} = \omega_{34} - \omega_3$. Therefore

$$\rho^{(3)} = \begin{pmatrix} 0 & \tilde{\rho}_{12}^{(3)}e^{\imath\omega_{12}t} & 0 & \tilde{\rho}_{14}^{(3)}e^{\imath\omega_{14}t} \\ \tilde{\rho}_{21}^{(3)}e^{\imath\omega_{21}t} & 0 & \tilde{\rho}_{23}^{(3)}e^{\imath\omega_{23}t} & 0 \\ 0 & \tilde{\rho}_{32}^{(3)}e^{\imath\omega_{32}t} & 0 & \tilde{\rho}_{34}^{(3)}e^{\imath\omega_{34}t} \\ \tilde{\rho}_{41}^{(3)}e^{\imath\omega_{41}t} & 0 & \tilde{\rho}_{43}^{(3)}e^{\imath\omega_{43}t} & 0 \end{pmatrix} \tag{C.129}$$

C.6 Fourth Order Solution

Using equation (C.19) we can solve for the fourth order by expanding the following commutator:

$$\lambda^4 \dot{\rho}^{(4)} = -\frac{\imath}{\hbar}[\lambda H'_I, \lambda^3 \rho^{(3)}] + relaxation\, terms \tag{C.130}$$

$$\dot{\rho}^{(4)} = -\frac{\imath}{\hbar}\left[\begin{pmatrix} 0 & H_{12} & H_{13} & H_{14} \\ H_{21} & 0 & H_{23} & 0 \\ H_{31} & H_{32} & 0 & H_{34} \\ H_{41} & 0 & H_{43} & 0 \end{pmatrix}, \begin{pmatrix} 0 & \rho^{(3)}_{12} & 0 & \rho^{(3)}_{14} \\ \rho^{(3)}_{21} & 0 & \rho^{(3)}_{23} & 0 \\ 0 & \rho^{(3)}_{32} & 0 & \rho^{(3)}_{34} \\ \rho^{(3)}_{41} & 0 & \rho^{(3)}_{43} & 0 \end{pmatrix}\right] + relaxation\, terms \tag{C.131}$$

Note that $H_{ij} = \langle i|H'|j\rangle$. Expanding the commutator we get the following equations:

$$\dot{\rho}^{(4)}_{11} = -\frac{\imath}{\hbar}(H_{12}\rho^{(3)}_{21} + H_{14}\rho^{(3)}_{41} - H_{21}\rho^{(3)}_{12} - H_{41}\rho^{(3)}_{14}) + \gamma_{21}\rho^{(4)}_{22} + \gamma_{41}\rho^{(4)}_{44} \tag{C.132}$$

$$\dot{\rho}^{(4)}_{22} = -\frac{\imath}{\hbar}(H_{21}\rho^{(3)}_{12} + H_{23}\rho^{(3)}_{32} - H_{12}\rho^{(3)}_{21} - H_{32}\rho^{(3)}_{23}) + \gamma_{32}\rho^{(4)}_{33} - \gamma_{21}\rho^{(4)}_{22} \tag{C.133}$$

$$\dot{\rho}^{(4)}_{33} = -\frac{\imath}{\hbar}(H_{32}\rho^{(3)}_{23} + H_{34}\rho^{(3)}_{43} - H_{23}\rho^{(3)}_{32} - H_{43}\rho^{(3)}_{34}) - \gamma_{32}\rho^{(4)}_{33} - \gamma_{34}\rho^{(4)}_{33} \tag{C.134}$$

$$\dot{\rho}^{(4)}_{44} = -\frac{\imath}{\hbar}(H_{41}\rho^{(3)}_{14} + H_{43}\rho^{(3)}_{34} - H_{14}\rho^{(3)}_{41} - H_{34}\rho^{(3)}_{43}) - \gamma_{41}\rho^{(4)}_{44} + \gamma_{34}\rho^{(4)}_{33} \tag{C.135}$$

Since we are only interested in the populations of this order, we can omit the coherence terms.

C.6.1 Derivation of fourth order population terms

When solving equations (C.132) - (C.135), we let $A = H_{41}\rho_{14}^{(3)} - H_{14}\rho_{41}^{(3)}$ where

$$\tilde{\rho}_{14}^{(3)} = \frac{1}{(\Delta_{41} + \imath\Gamma_{41})}\Bigg[-\frac{1}{\hbar^3}\frac{|\mu_{21}|^2\mu_{14}|\tilde{E}_1|^2\tilde{E}_4^*}{\gamma_{21}}\left(\frac{2\Gamma_{21}}{\Delta_{21}^2+\Gamma_{21}^2}\right) - \frac{1}{\hbar^3}\frac{\mu_{14}|\mu_{41}|^2\tilde{E}_4^*|\tilde{E}_4|^2}{\gamma_{41}}\left(\frac{4\Gamma_{41}}{\Delta_{41}^2+\Gamma_{41}^2}\right)$$
$$+ \frac{1}{\hbar^3}\frac{\mu_{12}\mu_{23}\mu_{34}\tilde{E}_1^*\tilde{E}_2^*\tilde{E}_3^*}{(\Delta_{21}+\imath\Gamma_{21})(\Delta_{31}+\imath\Gamma_{31})} + \frac{1}{\hbar^3}\frac{|\mu_{43}|^2\mu_{14}|\tilde{E}_3|^2\tilde{E}_4^*}{(\Delta_{41}+\imath\Gamma_{41})(\Delta_{31'}+\imath\Gamma_{31})}$$
$$- \frac{1}{\hbar^3}\frac{|\mu_{12}|^2\mu_{14}|\tilde{E}_1|^2\tilde{E}_4^*}{(\Delta_{42}+\imath\Gamma_{42})}\left(\frac{1}{(\Delta_{21}-\imath\Gamma_{21})} - \frac{1}{(\Delta_{41}+\imath\Gamma_{41})}\right)\Bigg]e^{\imath\omega_4 t}$$

and

$$\tilde{\rho}_{41}^{(3)} = \frac{1}{(\Delta_{41} - \imath\Gamma_{41})}\Bigg[-\frac{1}{\hbar^3}\frac{|\mu_{12}|^2\mu_{41}|\tilde{E}_1|^2\tilde{E}_4}{\gamma_{21}}\left(\frac{2\Gamma_{21}}{\Delta_{21}^2+\Gamma_{21}^2}\right) - \frac{1}{\hbar^3}\frac{\mu_{41}|\mu_{14}|^2\tilde{E}_4|\tilde{E}_4|^2}{\gamma_{41}}\left(\frac{4\Gamma_{41}}{\Delta_{41}^2+\Gamma_{41}^2}\right)$$
$$+ \frac{1}{\hbar^3}\frac{\mu_{21}\mu_{32}\mu_{43}\tilde{E}_1\tilde{E}_2\tilde{E}_3}{(\Delta_{21}-\imath\Gamma_{21})(\Delta_{31}-\imath\Gamma_{31})} + \frac{1}{\hbar^3}\frac{|\mu_{34}|^2\mu_{41}|\tilde{E}_3|^2\tilde{E}_4}{(\Delta_{41}-\imath\Gamma_{41})(\Delta_{31'}-\imath\Gamma_{31})}$$
$$- \frac{1}{\hbar^3}\frac{|\mu_{21}|^2\mu_{41}|\tilde{E}_1|^2\tilde{E}_4}{(\Delta_{42}-\imath\Gamma_{42})}\left(\frac{1}{(\Delta_{21}+\imath\Gamma_{21})} - \frac{1}{(\Delta_{41}-\imath\Gamma_{41})}\right)\Bigg]e^{-\imath\omega_4 t}$$

resulting in

$$
\begin{aligned}
A = &-2\imath\Bigg[\frac{\Gamma_{41}}{\Delta_{41}^2+\Gamma_{41}^2}\left(\frac{1}{\hbar^3}\frac{|\mu_{21}|^2|\mu_{14}|^2|\tilde{E}_1|^2|\tilde{E}_4|^2}{\gamma_{21}}\left(\frac{2\Gamma_{21}}{\Delta_{21}^2+\Gamma_{21}^2}\right)+\frac{1}{\hbar^3}\frac{|\mu_{41}|^2|\mu_{14}|^2|\tilde{E}_4|^2|\tilde{E}_4|^2}{\gamma_{41}}\left(\frac{4\Gamma_{41}}{\Delta_{41}^2+\Gamma_{41}^2}\right)\right)\\
&-\frac{1}{\hbar^3}\mu_{12}\mu_{23}\mu_{34}\mu_{41}\tilde{E}_1\tilde{E}_2\tilde{E}_3\tilde{E}_4\frac{[\Delta_{41}(\Gamma_{21}\Delta_{31}+\Gamma_{31}\Delta_{21})+\Gamma_{41}(\Delta_{21}\Delta_{31}-\Gamma_{21}\Gamma_{31})]}{(\Delta_{41}^2+\Gamma_{41}^2)(\Delta_{21}^2+\Gamma_{21}^2)(\Delta_{31}^2+\Gamma_{31}^2)}\\
&-\frac{1}{\hbar^3}|\mu_{43}|^2|\mu_{14}|^2|\tilde{E}_3|^2|\tilde{E}_4|^2\frac{[\Delta_{41}(\Gamma_{41}\Delta_{31'}+\Gamma_{31}\Delta_{41})+\Gamma_{41}(\Delta_{41}\Delta_{31'}-\Gamma_{41}\Gamma_{31})]}{(\Delta_{41}^2+\Gamma_{41}^2)(\Delta_{31'}^2+\Gamma_{31}^2)}\\
&+\frac{1}{\hbar^3}|\mu_{21}|^2|\mu_{14}|^2|\tilde{E}_1|^2|\tilde{E}_4|^2\frac{[\Delta_{41}(\Gamma_{42}\Delta_{21}-\Gamma_{21}\Delta_{42})+\Gamma_{41}(\Delta_{42}\Delta_{21}+\Gamma_{42}\Gamma_{21})]}{(\Delta_{41}^2+\Gamma_{41}^2)(\Delta_{42}^2+\Gamma_{42}^2)(\Delta_{21}^2+\Gamma_{21}^2)}\\
&-\frac{1}{\hbar^3}|\mu_{21}|^2|\mu_{14}|^2|\tilde{E}_1|^2|\tilde{E}_4|^2\frac{[\Delta_{41}(\Gamma_{42}\Delta_{41}+\Gamma_{41}\Delta_{42})+\Gamma_{41}(\Delta_{42}\Delta_{41}-\Gamma_{42}\Gamma_{41})]}{(\Delta_{41}^2+\Gamma_{41}^2)(\Delta_{42}^2+\Gamma_{42}^2)(\Delta_{41}^2+\Gamma_{41}^2)}\Bigg]
\end{aligned}
\tag{C.136}
$$

We let $B = H_{43}\rho_{34}^{(3)} - H_{34}\rho_{43}^{(3)}$ where

$$
\begin{aligned}
\tilde{\rho}_{34}^{(3)} = \frac{1}{(\Delta_{34}-\imath\Gamma_{34})}\Bigg[&\frac{1}{\hbar^3}\frac{\mu_{21}\mu_{32}\mu_{14}\tilde{E}_1\tilde{E}_2\tilde{E}_4^*}{(\Delta_{42}+\imath\Gamma_{42})}\left(\frac{1}{(\Delta_{21}-\imath\Gamma_{21})}-\frac{1}{(\Delta_{41}+\imath\Gamma_{41})}\right)\\
&+\frac{1}{\hbar^3}\frac{\mu_{34}|\mu_{14}|^2\tilde{E}_3|\tilde{E}_4|^2}{\gamma_{41}}\left(\frac{2\Gamma_{41}}{\Delta_{41}^2+\Gamma_{41}^2}\right)-\frac{1}{\hbar^3}\frac{\mu_{21}\mu_{32}\mu_{14}\tilde{E}_1\tilde{E}_2\tilde{E}_4}{(\Delta_{21}-\imath\Gamma_{21})(\Delta_{31}-\imath\Gamma_{31})}\\
&-\frac{1}{\hbar^3}\frac{\mu_{34}|\mu_{14}|^2\tilde{E}_3|\tilde{E}_4|^2}{(\Delta_{41}-\imath\Gamma_{41})(\Delta_{31'}-\imath\Gamma_{31})}\Bigg]e^{-\imath\omega_3 t}
\end{aligned}
$$

and

$$\tilde{\rho}_{43}^{(3)} = \frac{1}{(\Delta_{34}+\imath\Gamma_{34})}\Bigg[\frac{1}{\hbar^3}\frac{\mu_{12}\mu_{23}\mu_{41}\tilde{E}_1^*\tilde{E}_2^*\tilde{E}_4}{(\Delta_{42}-\imath\Gamma_{42})}\left(\frac{1}{(\Delta_{21}+\imath\Gamma_{21})}-\frac{1}{(\Delta_{41}-\imath\Gamma_{41})}\right) + \frac{1}{\hbar^3}\frac{\mu_{43}|\mu_{41}|^2\tilde{E}_3^*|\tilde{E}_4|^2}{\gamma_{41}}\left(\frac{2\Gamma_{41}}{\Delta_{41}^2+\Gamma_{41}^2}\right) - \frac{1}{\hbar^3}\frac{\mu_{12}\mu_{23}\mu_{41}\tilde{E}_1^*\tilde{E}_2^*\tilde{E}_4^*}{(\Delta_{21}+\imath\Gamma_{21})(\Delta_{31}+\imath\Gamma_{31})} - \frac{1}{\hbar^3}\frac{\mu_{43}|\mu_{41}|^2\tilde{E}_3^*|\tilde{E}_4|^2}{(\Delta_{41}+\imath\Gamma_{41})(\Delta_{31'}+\imath\Gamma_{31})}\Bigg]e^{\imath\omega_3 t}$$

resulting in

$$\begin{aligned}
B =& 2\imath\Bigg[-\frac{\Gamma_{34}}{\Delta_{34}^2+\Gamma_{34}^2}\left(\frac{1}{\hbar^3}\frac{|\mu_{34}|^2|\mu_{14}|^2|\tilde{E}_3|^2|\tilde{E}_4|^2}{\gamma_{41}}\left(\frac{2\Gamma_{41}}{\Delta_{41}^2+\Gamma_{41}^2}\right)\right) \\
&+ \frac{1}{\hbar^3}\mu_{21}\mu_{32}\mu_{34}\mu_{41}\tilde{E}_1\tilde{E}_2\tilde{E}_3^*\tilde{E}_4\frac{[\Delta_{34}(\Gamma_{42}\Delta_{21}-\Gamma_{21}\Delta_{42})-\Gamma_{34}(\Delta_{42}\Delta_{21}+\Gamma_{42}\Gamma_{21})]}{(\Delta_{34}^2+\Gamma_{34}^2)(\Delta_{21}^2+\Gamma_{21}^2)(\Delta_{42}^2+\Gamma_{42}^2)} \\
&- \frac{1}{\hbar^3}\mu_{21}\mu_{32}\mu_{34}\mu_{41}\tilde{E}_1\tilde{E}_2\tilde{E}_3^*\tilde{E}_4\frac{[\Delta_{34}(\Gamma_{42}\Delta_{41}-\Gamma_{41}\Delta_{42})-\Gamma_{34}(\Delta_{42}\Delta_{41}+\Gamma_{42}\Gamma_{41})]}{(\Delta_{34}^2+\Gamma_{34}^2)(\Delta_{41}^2+\Gamma_{41}^2)(\Delta_{42}^2+\Gamma_{42}^2)} \\
&+ \frac{1}{\hbar^3}\mu_{21}\mu_{32}\mu_{43}\mu_{41}\tilde{E}_1\tilde{E}_2\tilde{E}_3\tilde{E}_4\frac{[\Delta_{34}(\Gamma_{21}\Delta_{31}+\Gamma_{31}\Delta_{21})+\Gamma_{34}(\Delta_{21}\Delta_{31}-\Gamma_{21}\Gamma_{31})]}{(\Delta_{34}^2+\Gamma_{34}^2)(\Delta_{21}^2+\Gamma_{21}^2)(\Delta_{31}^2+\Gamma_{31}^2)} \\
&+ \frac{1}{\hbar^3}|\mu_{43}|^2|\mu_{41}|^2|\tilde{E}_3|^2|\tilde{E}_4|^2\frac{[\Delta_{34}(\Gamma_{41}\Delta_{31'}+\Gamma_{31}\Delta_{41})+\Gamma_{34}(\Delta_{41}\Delta_{31'}-\Gamma_{41}\Gamma_{31})]}{(\Delta_{41}^2+\Gamma_{41}^2)(\Delta_{34}^2+\Gamma_{34}^2)(\Delta_{31'}^2+\Gamma_{31}^2)}\Bigg]
\end{aligned} \tag{C.137}$$

Next we let $C = H_{32}\rho_{23}^{(3)} - H_{23}\rho_{32}^{(3)}$ where

$$\tilde{\rho}_{23}^{(3)} = \frac{1}{(\Delta_{32} + \imath\Gamma_{32})}\left[\frac{1}{\hbar^3}\frac{|\mu_{21}|^2\mu_{23}|\tilde{E}_1|^2\tilde{E}_2^*}{\gamma_{21}}\left(\frac{2\Gamma_{21}}{\Delta_{21}^2+\Gamma_{21}^2}\right) - \frac{1}{\hbar^3}\frac{|\mu_{21}|^2\mu_{23}|\tilde{E}_1|^2\tilde{E}_2^*}{(\Delta_{21}+\imath\Gamma_{21})(\Delta_{31}+\imath\Gamma_{31})}\right.$$
$$+ \frac{1}{\hbar^3}\frac{\mu_{21}\mu_{43}\mu_{14}\tilde{E}_1\tilde{E}_3\tilde{E}_4^*}{(\Delta_{42}+\imath\Gamma_{42})}\left(\frac{1}{(\Delta_{21}-\imath\Gamma_{21})} - \frac{1}{(\Delta_{41}+\imath\Gamma_{41})}\right)$$
$$\left. - \frac{1}{\hbar^3}\frac{\mu_{21}\mu_{43}\mu_{41}\tilde{E}_1^*\tilde{E}_3^*\tilde{E}_4^*}{(\Delta_{41}+\imath\Gamma_{41})(\Delta_{31'}+\imath\Gamma_{31})}\right]e^{\imath\omega_2 t}$$

and

$$\tilde{\rho}_{32}^{(3)} = \frac{1}{(\Delta_{32} - \imath\Gamma_{32})}\left[\frac{1}{\hbar^3}\frac{|\mu_{12}|^2\mu_{32}|\tilde{E}_1|^2\tilde{E}_2}{\gamma_{21}}\left(\frac{2\Gamma_{21}}{\Delta_{21}^2+\Gamma_{21}^2}\right) - \frac{1}{\hbar^3}\frac{|\mu_{12}|^2\mu_{32}|\tilde{E}_1|^2\tilde{E}_2}{(\Delta_{21}-\imath\Gamma_{21})(\Delta_{31}-\imath\Gamma_{31})}\right.$$
$$+ \frac{1}{\hbar^3}\frac{\mu_{12}\mu_{34}\mu_{41}\tilde{E}_1^*\tilde{E}_3^*\tilde{E}_4}{(\Delta_{42}-\imath\Gamma_{42})}\left(\frac{1}{(\Delta_{21}+\imath\Gamma_{21})} - \frac{1}{(\Delta_{41}-\imath\Gamma_{41})}\right)$$
$$\left. - \frac{1}{\hbar^3}\frac{\mu_{12}\mu_{34}\mu_{14}\tilde{E}_1\tilde{E}_3\tilde{E}_4}{(\Delta_{41}-\imath\Gamma_{41})(\Delta_{31'}-\imath\Gamma_{31})}\right]e^{-\imath\omega_2 t}$$

resulting in

$$
\begin{aligned}
C =& 2\imath\Bigg[\frac{\Gamma_{32}}{\Delta_{32}^2+\Gamma_{32}^2}\left(\frac{1}{\hbar^3}\frac{|\mu_{21}|^2|\mu_{23}|^2|\tilde{E}_1|^2|\tilde{E}_2|^2}{\gamma_{21}}\left(\frac{2\Gamma_{21}}{\Delta_{21}^2+\Gamma_{21}^2}\right)\right)\\
&+\frac{1}{\hbar^3}\mu_{21}\mu_{32}\mu_{43}\mu_{14}\tilde{E}_1\tilde{E}_2\tilde{E}_3\tilde{E}_4^*\frac{[\Delta_{32}(\Gamma_{42}\Delta_{21}-\Gamma_{21}\Delta_{42})+\Gamma_{32}(\Delta_{42}\Delta_{21}+\Gamma_{42}\Gamma_{21})]}{(\Delta_{32}^2+\Gamma_{32}^2)(\Delta_{21}^2+\Gamma_{21}^2)(\Delta_{42}^2+\Gamma_{42}^2)}\\
&-\frac{1}{\hbar^3}\mu_{21}\mu_{32}\mu_{43}\mu_{14}\tilde{E}_1\tilde{E}_2\tilde{E}_3\tilde{E}_4^*\frac{[\Delta_{32}(\Gamma_{42}\Delta_{41}+\Gamma_{41}\Delta_{42})+\Gamma_{32}(\Delta_{42}\Delta_{41}-\Gamma_{42}\Gamma_{41})]}{(\Delta_{32}^2+\Gamma_{32}^2)(\Delta_{41}^2+\Gamma_{41}^2)(\Delta_{42}^2+\Gamma_{42}^2)}\\
&-\frac{1}{\hbar^3}\mu_{12}\mu_{32}\mu_{34}\mu_{41}\tilde{E}_1^*\tilde{E}_2\tilde{E}_3^*\tilde{E}_4\frac{[\Delta_{32}(\Gamma_{41}\Delta_{31'}+\Gamma_{31}\Delta_{41})+\Gamma_{32}(\Delta_{41}\Delta_{31'}-\Gamma_{41}\Gamma_{31})]}{(\Delta_{32}^2+\Gamma_{32}^2)(\Delta_{41}^2+\Gamma_{41}^2)(\Delta_{31'}^2+\Gamma_{31}^2)}\\
&-\frac{1}{\hbar^3}|\mu_{12}|^2|\mu_{32}|^2|\tilde{E}_1|^2|\tilde{E}_2|^2\frac{[\Delta_{32}(\Gamma_{21}\Delta_{31}+\Gamma_{31}\Delta_{21})+\Gamma_{32}(\Delta_{21}\Delta_{31}-\Gamma_{21}\Gamma_{31})]}{(\Delta_{32}^2+\Gamma_{32}^2)(\Delta_{21}^2+\Gamma_{21}^2)(\Delta_{31}^2+\Gamma_{31}^2)}\Bigg]
\end{aligned}
\tag{C.138}
$$

And finally we let $D = H_{21}\rho_{12}^{(3)} - H_{12}\rho_{21}^{(3)}$ where

$$
\begin{aligned}
\tilde{\rho}_{12}^{(3)} = \frac{1}{(\Delta_{21}+\imath\Gamma_{21})}\Bigg[&-\frac{1}{\hbar^3}\frac{\mu_{12}|\mu_{21}|^2\tilde{E}_1^*|\tilde{E}_1|^2}{\gamma_{21}}\left(\frac{4\Gamma_{21}}{\Delta_{21}^2+\Gamma_{21}^2}\right)-\frac{1}{\hbar^3}\frac{\mu_{12}|\mu_{41}|^2\tilde{E}_1^*|\tilde{E}_4|^2}{\gamma_{41}}\left(\frac{2\Gamma_{41}}{\Delta_{41}^2+\Gamma_{41}^2}\right)\\
&+\frac{1}{\hbar^3}\frac{\mu_{12}|\mu_{32}|^2\tilde{E}_1^*|\tilde{E}_2|^2}{(\Delta_{21}+\imath\Gamma_{21})(\Delta_{31}+\imath\Gamma_{31})}+\frac{1}{\hbar^3}\frac{\mu_{32}\mu_{43}\mu_{14}\tilde{E}_2^*\tilde{E}_3^*\tilde{E}_4^*}{(\Delta_{41}+\imath\Gamma_{41})(\Delta_{31'}+\imath\Gamma_{31})}\\
&-\frac{1}{\hbar^3}\frac{\mu_{12}|\mu_{14}|^2\tilde{E}_1^*|\tilde{E}_4|^2}{(\Delta_{42}-\imath\Gamma_{42})}\left(\frac{1}{(\Delta_{21}+\imath\Gamma_{21})}-\frac{1}{(\Delta_{41}-\imath\Gamma_{41})}\right)\Bigg]e^{\imath\omega_1 t}
\end{aligned}
$$

and

$$\tilde{\rho}_{21}^{(3)} = \frac{1}{(\Delta_{21} - \imath\Gamma_{21})}\Bigg[-\frac{1}{\hbar^3}\frac{\mu_{21}|\mu_{12}|^2\tilde{E}_1|\tilde{E}_1|^2}{\gamma_{21}}\left(\frac{4\Gamma_{21}}{\Delta_{21}^2+\Gamma_{21}^2}\right) - \frac{1}{\hbar^3}\frac{\mu_{21}|\mu_{14}|^2\tilde{E}_1|\tilde{E}_4|^2}{\gamma_{41}}\left(\frac{2\Gamma_{41}}{\Delta_{41}^2+\Gamma_{41}^2}\right)$$
$$+\frac{1}{\hbar^3}\frac{\mu_{21}|\mu_{23}|^2\tilde{E}_1|\tilde{E}_2|^2}{(\Delta_{21}-\imath\Gamma_{21})(\Delta_{31}-\imath\Gamma_{31})} + \frac{1}{\hbar^3}\frac{\mu_{23}\mu_{34}\mu_{41}\tilde{E}_2\tilde{E}_3\tilde{E}_4}{(\Delta_{41}-\imath\Gamma_{41})(\Delta_{31'}-\imath\Gamma_{31})}$$
$$-\frac{1}{\hbar^3}\frac{\mu_{21}|\mu_{41}|^2\tilde{E}_1|\tilde{E}_4|^2}{(\Delta_{42}+\imath\Gamma_{42})}\left(\frac{1}{(\Delta_{21}-\imath\Gamma_{21})} - \frac{1}{(\Delta_{41}+\imath\Gamma_{41})}\right)\Bigg]e^{-\imath\omega_1 t}$$

resulting in

$$\begin{aligned}
D = &-2\imath\Bigg[\frac{\Gamma_{21}}{\Delta_{21}^2+\Gamma_{21}^2}\left(\frac{1}{\hbar^3}\frac{|\mu_{21}|^2|\mu_{21}|^2|\tilde{E}_1|^2|\tilde{E}_1|^2}{\gamma_{21}}\left(\frac{4\Gamma_{21}}{\Delta_{21}^2+\Gamma_{21}^2}\right) + \frac{1}{\hbar^3}\frac{|\mu_{21}|^2|\mu_{41}|^2|\tilde{E}_1|^2|\tilde{E}_4|^2}{\gamma_{41}}\left(\frac{2\Gamma_{41}}{\Delta_{41}^2+\Gamma_{41}^2}\right)\right)\\
&-\frac{1}{\hbar^3}\mu_{21}\mu_{32}\mu_{43}\mu_{41}\tilde{E}_1\tilde{E}_2\tilde{E}_3\tilde{E}_4\frac{[\Delta_{21}(\Gamma_{41}\Delta_{31'}+\Gamma_{31}\Delta_{41})+\Gamma_{21}(\Delta_{41}\Delta_{31'}-\Gamma_{41}\Gamma_{31})]}{(\Delta_{41}^2+\Gamma_{41}^2)(\Delta_{21}^2+\Gamma_{21}^2)(\Delta_{31'}^2+\Gamma_{31}^2)}\\
&-\frac{1}{\hbar^3}|\mu_{21}|^2|\mu_{32}|^2|\tilde{E}_1|^2|\tilde{E}_2|^2\frac{[\Delta_{21}(\Gamma_{21}\Delta_{31}+\Gamma_{31}\Delta_{21})+\Gamma_{21}(\Delta_{21}\Delta_{31}-\Gamma_{21}\Gamma_{31})]}{(\Delta_{21}^2+\Gamma_{21}^2)^2(\Delta_{31}^2+\Gamma_{31}^2)}\\
&-\frac{1}{\hbar^3}|\mu_{21}|^2|\mu_{41}|^2|\tilde{E}_1|^2|\tilde{E}_4|^2\frac{[\Delta_{21}(\Gamma_{42}\Delta_{21}-\Gamma_{21}\Delta_{42})-\Gamma_{21}(\Delta_{42}\Delta_{21}+\Gamma_{42}\Gamma_{21})]}{(\Delta_{42}^2+\Gamma_{42}^2)(\Delta_{21}^2+\Gamma_{21}^2)^2}\\
&+\frac{1}{\hbar^3}|\mu_{21}|^2|\mu_{41}|^2|\tilde{E}_1|^2|\tilde{E}_4|^2\frac{[\Delta_{21}(\Gamma_{42}\Delta_{41}+\Gamma_{41}\Delta_{42})-\Gamma_{21}(\Delta_{42}\Delta_{41}-\Gamma_{42}\Gamma_{41})]}{(\Delta_{41}^2+\Gamma_{41}^2)(\Delta_{42}^2+\Gamma_{42}^2)(\Delta_{21}^2+\Gamma_{21}^2)}\Bigg]
\end{aligned} \tag{C.139}$$

Starting with equation (C.134) for $\dot{\rho}_{33}^{(4)}$:

$$\dot{\rho}_{33}^{(4)} = -\frac{\imath}{\hbar}(H_{32}\rho_{23}^{(3)} + H_{34}\rho_{43}^{(3)} - H_{23}\rho_{32}^{(3)} - H_{43}\rho_{34}^{(3)}) - \gamma_{32}\rho_{33}^{(4)} - \gamma_{34}\rho_{33}^{(4)}$$

$$\dot{\rho}_{33}^{(4)} = -\frac{\imath}{\hbar}(C - B) - \gamma_{32}\rho_{33}^{(4)} - \gamma_{34}\rho_{33}^{(4)}$$

The steady state solution is

$$\rho_{33}^{(4)} = -\frac{\imath}{\hbar}\frac{(C - B)}{\gamma_{32} + \gamma_{34}} \tag{C.140}$$

Next we solve equation (C.135) for $\dot{\rho}_{44}^{(4)}$:

$$\dot{\rho}_{44}^{(4)} = -\frac{\imath}{\hbar}(H_{41}\rho_{14}^{(3)} + H_{43}\rho_{34}^{(3)} - H_{14}\rho_{41}^{(3)} - H_{34}\rho_{43}^{(3)}) - \gamma_{41}\rho_{44}^{(4)} + \gamma_{34}\rho_{33}^{(4)}$$

$$\dot{\rho}_{44}^{(4)} = -\frac{\imath}{\hbar}(A + B) - \gamma_{41}\rho_{44}^{(4)} + \gamma_{34}\rho_{33}^{(4)}$$

The steady state solution is

$$\rho_{44}^{(4)} = -\frac{\imath}{\hbar}\frac{(A + B)}{\gamma_{41}} + \frac{\gamma_{34}\rho_{33}^{(4)}}{\gamma_{41}} \tag{C.141}$$

Next we solve equation (C.133) for $\dot{\rho}_{22}^{(4)}$:

$$\dot{\rho}_{22}^{(4)} = -\frac{\imath}{\hbar}(H_{21}\rho_{12}^{(3)} + H_{23}\rho_{32}^{(3)} - H_{12}\rho_{21}^{(3)} - H_{32}\rho_{23}^{(3)}) + \gamma_{32}\rho_{33}^{(4)} - \gamma_{21}\rho_{22}^{(4)}$$

$$\dot{\rho}_{22}^{(4)} = -\frac{\imath}{\hbar}(D - C) + \gamma_{32}\rho_{33}^{(4)} - \gamma_{21}\rho_{22}^{(4)}$$

The steady state solution is

$$\rho_{22}^{(4)} = -\frac{\imath}{\hbar}\frac{(D - C)}{\gamma_{21}} + \frac{\gamma_{32}\rho_{33}^{(4)}}{\gamma_{21}} \tag{C.142}$$

Finally, we solve equation (C.132) for $\dot{\rho}_{11}^{(4)}$:

$$\dot{\rho}_{11}^{(4)} = -\frac{\imath}{\hbar}(H_{12}\rho_{21}^{(3)} + H_{14}\rho_{41}^{(3)} - H_{21}\rho_{12}^{(3)} - H_{41}\rho_{14}^{(3)}) + \gamma_{21}\rho_{22}^{(4)} + \gamma_{41}\rho_{44}^{(4)}$$

$$\dot{\rho}_{11}^{(4)} = -\frac{\imath}{\hbar}(-D - A) + \gamma_{21}\rho_{22}^{(4)} + \gamma_{41}\rho_{44}^{(4)}$$

The steady state solution is

$$\rho_{11}^{(4)} = -\frac{\imath}{\hbar}(-D - A) + \gamma_{21}\rho_{22}^{(4)} + \gamma_{41}\rho_{44}^{(4)} \tag{C.143}$$

But we can solve for equation (C.132) by noting that the sum of all $\rho = 1$, therefore the sum of all

non-zero terms is:

$$\begin{aligned}\rho_{11}^{(0)}+\rho_{11}^{(2)}+\rho_{11}^{(4)}+\rho_{22}^{(2)}+\rho_{22}^{(4)}+\rho_{33}^{(4)}+\rho_{44}^{(2)}+\rho_{44}^{(4)}&=1\\ 1+\rho_{11}^{(2)}+\rho_{11}^{(4)}+\rho_{22}^{(2)}+\rho_{22}^{(4)}+\rho_{33}^{(4)}+\rho_{44}^{(2)}+\rho_{44}^{(4)}&=1\\ \rho_{11}^{(4)}&=-\rho_{11}^{(2)}-\rho_{22}^{(2)}-\rho_{22}^{(4)}-\rho_{33}^{(4)}-\rho_{44}^{(2)}-\rho_{44}^{(4)}\end{aligned}$$

Therefore

$$\rho_{11}^{(4)}=-\rho_{11}^{(2)}-\rho_{22}^{(2)}-\rho_{22}^{(4)}-\rho_{33}^{(4)}-\rho_{44}^{(2)}-\rho_{44}^{(4)} \tag{C.144}$$

C.7 Summary

We have provided a full derivation of the equations required to solve four-wave mixing. Results of the analysis can be seen in Chapter 6.

References

Arya, A. P. 1986. *Elementary Modern Physics*. Addison-Wesley Publishing Company.

Becerra, F. E., Willis, R. T., Rolston, S. L., and Orozco, L. A. 2011. Quantum beats from four-wave mixing in rubidium 87. *Revista Mexicana de Física* 57, pp. 23–28.

Bloch, I. 2005. Ultracold quantum gases in optical lattices. *Nature Physics* 1.1, pp. 23–30.

Boyd, R. W., Malcuit, M. S., Gauthier, D. J., and Rzaewski, K. Feb 1987. Competition between amplified spontaneous emission and the four-wave-mixing process. *Phys. Rev. A* 35(4), pp. 1648–1658.

Brekke, E., Day, J. O., and Walker, T. G. Dec 2008. Four-wave mixing in ultracold atoms using intermediate rydberg states. *Phys. Rev. A* 78(6), p. 063830.

Chen, J. F., Zhang, S., Yan, H., Loy, M. M. T., Wong, G. K. L., and Du, S. May 2010. Shaping biphoton temporal waveforms with modulated classical fields. *Phys. Rev. Lett.* 104(18), p. 183604.

Coffey, V. Mar 2013. Next-gen quantum networks. *Opt. Photon. News* 24.3, pp. 34–41.

Dabrowski, M., Parniak, M., Pecak, D., Chrapkiewicz, R., and Wasilewski, W. December 2014. Spontaneuos and parametric processes in warm rubidium vapours. *Latvian Journal of Physics and Technical Sciences* 51.5, pp. 21–34.

de Melo, N. R. and Vianna, S. S. 2014. Two-photon resonant forward four-wave mixing in rubidium vapor involving rydberg states. *J. Opt. Soc. Am. B* 31.7, pp. 1735–1740.

DiVincenzo, D. 2000. The physical implementation of quantum computation. *Fortschritte der Physik* 48.9-11, pp. 771–783.

Du, S., Wen, J., and Rubin, M. H. Dec 2008. Narrowband biphoton generation near atomic resonance. *J. Opt. Soc. Am. B* 25.12, pp. C98–C108.

Gisin, N., Ribordy, G., Tittel, W., and Zbinden, H. Mar 2002. Quantum cryptography. *Rev. Mod. Phys.* 74(1), pp. 145–195.

Glushkov, A. V. 2014. Spectroscopy of atom and nucleus in a strong laser field: Stark effect and multiphoton resonances. *JPCS* 548.1, p. 012020.

Glushkov, A. V., Khetselius, O. Y., Svinarenko, A. A., and Prepelitsa, G. P. 2011. *Coherence and Ultrashort Pulse Laser Emission*. CroatiaM Intech.

Grynberg, G., Aspect, A., and Fabre, C. 2010. *Introduction to Quantum Optics: From the Semi-classical Approach to Quantized Light*. Cambridge University Press.

Gulati, G. K., Srivathsan, B., Chng, B., Cerè, A., Matsukevich, D., and Kurtsiefer, C. Sep 2014. Generation of an exponentially rising single-photon field from parametric conversion in atoms. *Phys. Rev. A* 90(3), p. 033819.

Gulati, G. K., Srivathsan, B., Chng, B., Cerè, A., and Kurtsiefer, C. 2015. Polarization entanglement and quantum beats of photon pairs from four-wave mixing in a cold 87 rb ensemble. *New Journal of Physics* 17.9, p. 093034.

Han, Z., Qian, P., Zhou, L., Chen, J. F., and Zhang, W. 2015. Coherence time limit of the biphotons generated in a dense cold atom cloud. *Scientific Reports* 5, p. 9126.

Jakowski, J. and Morokuma, K. 2009. Liouville–von neumann molecular dynamics. *J. Chem. Phys.* 130.22, p. 224106.

Jen, H. H. and Chen, Y. C. 2016. Spectral shaping of cascade emissions from multiplexed cold atomic ensembles. *Phys. Rev. A* 93(1), p. 013811.

Kolchin, P., Belthangady, C., Du, S., Yin, G. Y., and Harris, S. E. Sep 2008. Electro-optic modulation of single photons. *Phys. Rev. Lett.* 101 (10), p. 103601.

Kölle, A. Coherent phenomena in four-wave mixing via a rydberg state in thermal vapor of rubidium 2014.

Lambropoulos, P. and Petrosyan, D. 2006. *Fundamentals of Quantum Optics and Quantum Information.* Springer Berlin Heidelberg. ISBN 9783540345718.

Levenson, M. 1982. *Introduction to Nonlinear Laser Spectroscopy.* New YorkM Academic Press.

Liao, K., Yan, H., He, J., Du, S., Zhang, Z., and Zhu, S. Jun 2014. Subnatural-linewidth polarization-entangled photon pairs with controllable temporal length. *Phys. Rev. Lett.* 112(24), p. 243602.

Liboff, R. 2002. *Introductory Quantum Mechanics.* Addison-Wesley Publishing Company. ISBN 9780805387145.

Loudon, R. 2000. *The Quantum Theory of Light*. OUP Oxford. ISBN 9780191589782.

Meystre, P. and Sargent, M. 2007. *Elements of Quantum Optics*. Springer-Link: Springer e-Books. Springer Berlin Heidelberg. ISBN 9783540742111.

Parniak, M. and Wasilewski, W. Feb 2015. Interference and nonlinear properties of four-wave-mixing resonances in thermal vapor: Analytical results and experimental verification. *Phys. Rev. A* 91(2), p. 023418.

Patel, M., De Jager, G., Nkosi, Z., Wyngaard, A., and Govender, K. 2017. On the non-linear spectroscopy including saturated absorption and four-wave mixing in two and multi-level atoms: a computational study. *Journal of Physics: Conference Series* 905(1), p. 012005. URL `http://stacks.iop.org/1742-6596/905/i=1/a=012005`.

Pisipati, U., Almakrami, I. M., Joshi, A., and Serna, J. D. July 2012. Cavity quantum electrodynamics of a two-level atom with modulated fields. *American Journal of Physics* 80.7, pp. 612–620.

Quantum Physics Research Group. Quantum physics research group - cput 2016. URL `http://www.cput.ac.za/academic/faculties/engineering/research/quantum_physics`.

Srivathsan, B., Gulati, G. K., Chng, B., Maslennikov, G., Matsukevich, D., and Kurtsiefer, C. Sep 2013. Narrow band source of transform-limited photon pairs via four-wave mixing in a cold atomic ensemble. *Phys. Rev. Lett.* 111(12), p. 123602.

Steck, D. Rubidium 85 d line data. 2013.

Steck, D. Rubidium 87 d line data. 2015.

Wyngaard, A. L. Saturated absorption spectroscopy of rubidium and feedback control of laser frequency for doppler cooling. 2017.

Zhao, L., Guo, X., Liu, C., Sun, Y., Loy, M. M. T., and Du, S. Aug 2014. Photon pairs with coherence time exceeding 1μ s. *Optica* 1.2, pp. 84–88.